Dependence of the Stress Field on Plate-Mantle Coupling and Lithospheric Structure

by

John Benjamin Naliboff

A dissertation submitted in partial fulfillment
of the requirements for the degree of
Doctor of Philosophy
(Geology)
in The University of Michigan
2010

Doctoral Committee:

Professor Carolina R. Lithgow-Bertelloni, Co-Chair
Professor Larry J. Ruff, Co-Chair
Professor Rebecca A. Lange
Professor Sherif El-Tawil

ACKNOWLEDGEMENTS

First and foremost, I wish to sincerely thank my advisor Carolina Lithgow-Bertelloni. Throughout the course of my time at Michigan she selflessly and patiently provided constant guidance, wisdom, encouragement and advice. I benefited greatly from her willinglessly to afford me the freedom to me explore and expand my scientific interestests, which were largely inspired by her passion towards science. It was a tremendous honor to work with Carolina and I wish her continued happiness and success in London.

I am very grateful to my co-advisor Larry Ruff, who graciously worked closely with me on many of the most difficult topics of my thesis. Throughout our many discussions, I never ceased to be impressed by his enthusiasm and approach towards science.

I benefited greatly from discussions and input from committee members Becky Lange and Sherif El-Tawil, and I deeply appreciate their time and efforts. I also received valuable input and key insights from Marin Clark while she served on my committee. The geophysics group at Michigan was a consistent source of input and thoughtful discussions, and I can only hope my future peers will be as much of a pleasure to work with.

Last, I would have undoubtedly not succeeded at finishing my thesis without the support and encouragement of David, Karen, Lesley and Susan.

TABLE OF CONTENTS

LIST OF FIGURES

Figure

CHAPTER I

Introduction

The state of stress in the lithosphere reflects both the weight of overlying material (lithostatic pressure) and non-lithostatic (tectonic) stresses related to global mantle convection and the subsequent motion of lithospheric plates (e.g. Turcotte & Oxburgh 1972). As all deformation is inherently tied directly to the state of stress, determining the origin of stresses within the lithosphere is a fundamental aspect of understanding processes at multiple scales, including global tectonic patterns, intra-plate deformation, regional faulting behavior and grain-scale seismic anisotropy. Although the origin of the lithospheric stress field has been the subject of considerable research even prior to the advent of plate tectonics, active debate still continues regarding the relative influence of different sources of stress (e.g. Steinberger 2001; Lithgow-Bertelloni and Guynn 2004; Ghosh et al. 2008, 2009). The high degree of uncertainty regarding the origins of the lithospheric stress field largely arises from a relatively poor understanding of the lithosphere and convecting mantle's density and rheological structure, which inherently govern how stresses are generated and distributed. Consistent advances in multiple fields (Gung et al. 2003; Mitrovica & Forte 2004; Li et al. 2007; for example), however, have greatly improved our understanding of the Earth's structure in the past decade, allowing a reexamination of the forces acting on and within the lithosphere. The primary goal of

this thesis is to reexamine how the forces acting on and within the lithosphere contribute to the total lithospheric stress field, in the light of recent advances in our knowledge of lithospheric structure, mantle rheology and mantle flow modeling. This thesis also aims to critically evaluate whether specific numerical approximations are appropriate for studying the lithosphere's state of stress and provide guidance for future studies if the numerical approximations do indeed neglect key processes.

From a broad perspective, the tectonic stress state arises from the action of gravity on lateral variations in density. At any given point in the lithosphere we can separate contributions from edge forces at plate boundaries, basal stresses related to mantle flow and variations in topography and density within the lithosphere (internal loads). Edge forces, for example the thickening of the oceanic lithosphere as it ages, commonly referred to as ridge push, are a necessary approximation because of our incomplete knowledge of the rheology of plate boundaries and of the density structure of lithosphere and mantle. The lithosphere's response to different sources of stress is represented in part by the world stress map (Zoback 1992), which displays variations in stress regime (extension, compression, strike-slip) and orientation across tectonic provinces. The information contained within the world stress map reflects a compilation of diverse data sets including but not limited to seismic observations from earthquakes, large-scale faulting patterns, regional tectonic structures and borehole data. Although the world stress map contains no direct information regarding stress magnitude, large-scale stress patterns that remain coherent across long-wavelengths provide a potential benchmark for modeling the lithospheric stress field. The long-wavelength of many observed stress patterns (1000's of km) compared to the thickness of the lithosphere (< ~ 200-300 km)

may also indicate these stress patterns are coherent throughout the thickness of the lithosphere, in contrast to a scenario where the lithospheric stress field is strongly depth-dependent. The assumption that the lithosphere behaves in a mechanically coherent fashion is a controversial subject as this depends directly on the rheological structure of the lithosphere (e.g. Kohlstedt et al. 1995), which at present is the focus of intense research (Jackson 2003; Burov and Watts 2006; Regenauer-Lieb et al. 2006; Thatcher & Pollitz 2008; Bürgmann & Dresen 2008). Multiple studies have shown how variations in lithospheric strength as a function of depth and time can lead to depth-dependent stress and strain distributions (e.g. Kusznir & Bott 1997; Liu et al. 2000). The hypothesized presence of a weak lower crust and subsequent localized channel flow in the Tibetan Plateau (e.g. Royden et al. 1997; Clark & Royden 2000) illustrates how variations in lithospheric strength may lead to partially decoupled regions of deformation. Nonetheless, the idea of a mechanically coherent lithosphere has served as the basis for the vast majority of numerical studies modeling the lithospheric stress field.

By considering the lithosphere as a mechanically coherent body and neglecting any variations in the stress field as a function of depth, the lithosphere can be treated as thin shell (global) or sheet (regional) based on its thickness relative to the radius of the earth. To determine the relative influence of different sources of stress in different regions, lithospheric stress studies first independently calculate each source of stress and then apply them to the lithospheric numerical model. Stresses related to variations in topography and density within the lithosphere are determined by constructing a lithospheric density model (based on geophysical or geologic observations) (e.g. Bassin et al. 2000) and then solving for the non-lithostatic stress field balancing gradients in

lithostatic pressure (Artyushkov 1973). The influence of plate-boundary interactions is often represented as a force applied to the corresponding plate boundary regions within the lithospheric model. Shear stresses at the base of the lithosphere related to mantle flow are typically modeled by solving numerically for global viscous convection patterns based on the rheological structure of the mantle and applied surface plate motions (Hager & O'Connell 1979) or internal body forces relate to density heterogeneity (Hager & O'Connell 1981). The resulting viscous shear stresses are then extracted at the base of the lithosphere (defined by a viscosity contour or fixed depth) and applied to the independent lithospheric model. Inherently, improved understanding of these sources of stress is the key to understanding the origins of the lithospheric stress field.

Prior to the compilation of the world stress map as a reference guide, early studies treating the lithosphere as a thin elastic shell (Solomon et al. 1975; Richardson et al. 1979) explored the relative influence of edge forces and basal tractions on global stress patterns and attempted to asses their relative influence based on limited documented stress patterns, namely in North America and Europe. Although these studies were able to reproduce certain observed stress patterns, large uncertainties associated with the magnitude of basal shear stresses, taken as proportional to plate velocities, prevented a robust analysis of the relative contributions of edge forces and basal shear to the stress patterns in lithospheric plate interiors. Similarly, these global studies lacked the effects of intra-continental variations in topography and density on stress patterns (Artyushkov 1973), which early on were hypothesized to play a potentially large in role in large orogenies such as Tibet (Molnar & Tapponier 1978).

Subsequent global lithospheric stress studies using forms of the thin sheet or shell approximation (e.g. Bai et al. 1992; Richardson 1992; Bird 1998; Steinberger et al. 2001; Lithgow-Bertelloni & Guynn 2004; Ghosh et al. 2008, 2009) sequentially reexamined estimates of the relative contribution of different sources of stress, as models of lithospheric and mantle density structure improved. Similarly, studies focusing on individual lithospheric plates (e.g. Richardson & Redding 1991; Humphreys & Coblentz 2007) or tectonic provinces (e.g. Jones et al. 1996; Flesch et al. 1999; Flesch et al. 2001; Ghosh et al. 2006; Dyksterhuis et al. 2005; Flesch et al. 2007; Klein et al. 2009) allowed direct comparison to regions with relatively well-documented stress and/or strain rate distributions. Despite the significant advances provided by these studies with respect to understanding the origins of the lithospheric stress field, a great deal of uncertainty still remains about the relative influence different sources of stress. One source of this uncertainty relates to the simplified lithospheric structures assumed when calculating stresses related to variations in topography and density.

Inherently, changes in lithostatic pressure related to variations in topography and density vary as a function of depth, although the use of a thin sheet or shell approximation to model the lithosphere implies that the stress field remains constant as a function of depth. To account for this lack of stress depth-dependence the lithostatic pressure is integrated over the thickness of the lithosphere at each point, which allows one to solve for the stresses balancing gradients in the integrated pressure as originally described by Artyushkov (1973). Although solving for stresses balancing variations in integrated pressure permits use of thin sheet or shell models, this method requires integration from a uniform lithospheric base depth in order to remain consistent with the

numerical approximation. The assumption of a uniform lithospheric base depth is highly problematic as continental lithosphere may extend below 200 km depth in cratonic regions (e.g. Jordan 1975; Gung et al. 2003) and as low as 50-60 km in parts of young, tectonically active regions such as the Western USA (Li et al. 2007). Similarly, the thickness of oceanic lithosphere increases from effectively 0 km at a mid-ocean ridge to roughly a maximum depth of 100 km based on a half-space cooling model (Turcotte & Schubert 2002). The majority of previous studies have commonly selected 100 km as a models base depth, which is meant to reflect an average lithospheric thickness value. The question remains, however, to what degree will global or plate-scale estimates of the lithospheric stress field change if one considers a wide range of model base depths that reflect the minimum and maximum end-members of lithospheric thickness estimates or even shallower base depths above the base of the lithosphere?

Aside from the assumption of model base depth, Lithgow-Bertelloni & Guynn (2004) found that for a constant mantle density and a 100 km base depth, enforcing isostasy (constant pressure at model base depth) through lower crustal density adjustments leads to significantly different stress distributions than a model with no isostatic enforcement. Moving the base depth significantly deeper than 100 km increases the influence of the assumed mantle density structure, although different assumptions about the composition and isostatic state of the mantle lithosphere can lead to different conclusions regarding the stress state of deep lithospheric roots (Zoback & Mooney 2003; Pascal 2006). Given this range of possibilities for constructing the lithospheric density model, Chapter II explores the dependence of the lithospheric stress field on a multiple parameters including model base depth, isostatic enforcement and mantle density

structure. The goal of Chapter II is to both determine the relative influence of these parameters and given the resulting variability of the stress field, critically analyze whether a depth-independent analysis is a reasonable approximation for the stress field solution.

The lithospheric structures and resulting stress distributions in Chapter II make no assumptions regarding the origins of topography, although early convection studies established that mantle flow contributes to surface topography (e.g. Hager et al. 1985). Independent isostatic analysis of lithospheric structure also suggests that sub-lithospheric density variations contribute to observed topography, which Panasyuk & Hager (2000) estimated to be on the order of +/- 1 km expanded to a degree 6 wavelength. Dynamic topography on the order of +/- 1 km roughly coincides with estimates from convection studies, although the amplitude of dynamic topography in different locations largely depends on the assumed mantle density structure. For example, Cenozoic dynamic subsidence in Southeast Asia may be on the order of 2 km or more due to prolonged subduction (Lithgow-Bertelloni & Gurnis 1997; Lithgow-Bertelloni & Guynn 2004), while 0.5 - 1.0 km of dynamic uplift in Eastern and Southern Africa reflects a low density anomaly originating in the deep lower mantle (Lithgow-Bertelloni & Silver 1998). While calibrating estimates of dynamic topography using both predictive convection models and surface observations remains a highly active field of research (e.g. Steinberger 2007; Spasojevic 2008), comparatively little work has focused on the contribution of dynamic topography to the lithospheric stress field.

The contribution of dynamic topography to the lithospheric stress field is commonly assessed by subtracting an estimate of dynamic topography from observed

topography and then calculating the stress patterns associated with the adjusted lithospheric structure using the GPE approximation (Lithgow-Bertelloni & Guynn 2004; Ghosh et al. 2009). Lithgow-Bertelloni & Guynn (2004) also considered the effects of instantaneous radial displacement of the lithosphere, which combined with dynamically supported GPE variations strongly influenced regional stress patterns, particularly in areas of long-lived subduction. Although the afore mentioned studies provide a qualitative comparison between stress patterns with or without the contribution of dynamic topography estimated from mantle flow models (Steinberger et al. 2001; Lithgow-Bertelloni & Guynn 2004) or isostatic analysis of lithospheric structure (Ghosh et al. 2009), no comprehensive quantitative comparisons exist. The goal of Chapter III is to provide a quantitative estimate of the contribution of dynamic topography to the global lithospheric stress field. In providing such quantitative estimates, dynamic topography determined from both convective flow models and isostatic analysis is considered. The sensitivity of dynamic topography and the resulting stress patterns to lithosphere-asthenosphere viscosity contrasts and mantle density structure is explored. Finally, the magnitude of membrane stresses associated with dynamic vertical deflection of the lithosphere is discussed and compared to the magnitude of stresses associated with variations in gravitational potential energy.

While Chapter III focuses on the influence of radial stresses at the base of the lithosphere, Chapter IV addresses the effects of lateral variations in horizontal shear on lithospheric stress patterns. Lateral variations in horizontal shear largely reflect changes in the viscosity or thickness of the asthenosphere, and as a result the lithosphere-asthenosphere viscosity structure prescribed in convection studies plays a first order role

in controlling the magnitude of horizontal shear at the base of the lithosphere. In comparison to convection models with layered (radially symmetric) viscosity structures, convection models containing lateral variations in lithospheric thickness (and hence viscosity) show a factor of 2-4 increase in horizontal shear magnitudes beneath thick continental roots where the asthenosphere is significantly thinner (Conrad & Lithgow-Bertelloni 2006; Cooper & Conrad 2007). Although the influence of variations in lithosphere-asthenosphere viscosity contrasts on horizontal shear and subsequent lithospheric stress patterns has been examined (Lithgow-Bertelloni & Guynn 2004; Ghosh et al. 2008), at present no study has explored the role thick continental roots play on controlling lithospheric stress patterns related to horizontal shear. Chapter IV compares lithospheric stress patterns related to horizontal shear derived from convection models with either layered or laterally-varying viscosity structures, and assesses whether taking into account more realistic lithospheric viscosity structures is likely to improve fits between calculated and observed stress patterns as hypothesized by Lithgow-Bertelloni & Guynn (2004).

Chapter IV has been accepted for publication in Geophysical Research Letters, while Chapters II and III, respectively, will be submitted shortly for publication in Geophysical Journal International and Earth and Planetary Science Letters.

1.1 References

Artyushkov, E.V., 1973. Stresses in the lithosphere caused by crustal thickness inhomogeneities, *J. Geophys. Res.*, **78**, 7675-7708.

Bai, W., Vigny, C., Ricard, Y. & Froidevaux, C., 1992. On the origin of deviatoric stresses in the lithospheres, *J. Geophys. Res.*, **97**(B8), 11,729–11,737.

Bassin, C., Laske, G. & Masters, G., 2000. The Current Limits of Resolution for Surface Wave Tomography in North America, *EOS Trans. AGU*, **81**, F897.

Bird, P., 1998. Testing hypotheses on plate-driving mechanisms with global lithospheric models including topography, thermal structure and faults, *J. Geophys. Res.*, **103**, 10,115-10,129.

Bürgmann, R. & Dresen, G., 2008. Rheology of the lower crust and upper mantle: Evidence from rock mechanics, geodesy and field observations, *Ann. Rev. Earth Plan. Sci.*, **36**, 531-567, doi:10.1146/annurev.earth.36.031207.124326.

Burov, E.B. & Watts, A.B., 2006. The long-term strength of continental lithosphere: ”jelly sandwhich” or ”creme brulee”?, *GSA Today*, **16**(1), 4-10.

Clark, M. K. & Royden, L. H., 2000. Topographic ooze: Building the eastern margin of Tibet by lower crustal flow, *Geology*, **28**, 703–706.

Conrad, C.P. & Lithgow-Bertelloni, C., 2006. Influence of continental roots and asthenosphere on plate-mantle coupling. *Geophys. Res. Lett.*, **33**(5), doi:10.1029/2005GL025621.

Cooper, C.M. & Conrad, C.P., 2009. Does the mantle control the maximum thickness of cratons? Lithosphere, **1**(2), 67-72.

Dyksterhuis, S., Muller, R. & Albert, R., 2005. Paleostress field evolution of the australian continent since the eocene, *J. Geophys. Res.*, **110**, B05102, doi:10.1029/2003JB002728.

Flesch, L.M., Haines, A.J. & Holt, E.W., 2001. Dynamics of the India-Eurasia collision zone, *J. Geophys. Res.*, **106**(B8), 16435-16460.

Flesch, L.M., Holt, E.W, Haines, A.J., Wen, L.X. & Shen-Tu, B.M. 2007. The dynamics of western North America: stress magnitudes and the relative role of gravitational potential energy, plate interaction at the boundary and basal tractions, *Geophys. J. Int.*, **169**, 866-896.

Ghosh, A., Holt, E.W., Flesch, L.M. & Haines, A.J., 2006. Gravitational potential energy of the Tibetan Plateau and the forces driving the Indian plate, *Geology*, **34**(5), 321-324.

Ghosh, A., Holt, E.W., Wen, L., Haines, A.J. & Flesch, L.M., 2008. Joint modeling of lithosphere and mantle dynamics elucidating lithosphere-mantle coupling, *Geophys. Res. Lett.*, **35**, L16309, doi:10.1029/2008GL034365.

Ghosh, A., Holt, E.W., Flesch, L.M. & Haines, A.J., 2009. Contribution of gravitational potential energy differences to the global stress field, *Geophys. J. Int.*, **179**, 787-812.

Gung, Y.C., Panning, M. & Romanowicz, B., 2003. Global anisotropy and the thickness of continents, *Nature*, **422**, 707-711.

Hager, B.H. & O'Connell, R.J., 1979. Kinematic models of large-scale flow in the Earth's mantle, *J. Geophys. Res.*, **84**, 1031-1048.

Hager, B.H. & O'Connell, R.J., 1981. A simple global model of plate dynamics and mantle convecton, *J. Geophys. Res.*, **86**, 4843-4867.

Hager, H.B., Clayton, R.W., Richards, M.A., Comer, R.P. & Dziewonski, A.M., 1985. Lower mantle heterogeneity, dynamic topography and the geoid. *Nature*, **313**, 541-545.

Humphreys, E.D. & Coblentz, D., 2007. North American dynamics and Western US Tectonics, *Rev. Geophys.*, **45**, RG3001, doi:10.1029/2005RG000181.

Jackson, J., 2002. Strength of the continental lithosphere: Time to abandon the jelly sandwhich?, *GSA Today*, **12**, 1-4.

Jones, C.H., Unruh, J.R. & Sonder, L.J., 1996. The role of gravitational potential energy in active deformation in the southwestern United States, *Nature*, **381**, 37-41.

Jordan, T.H., 1975. The Continental Tectosphere, *Rev. Geophys.*, **13**(3), 1-12.

Klein, E.C., Flesch, L.M., Holt, E.W. & Haines, A.J., 2009. Evidence of long-term weakness on seismogenic faults in western North America from dynamic modeling, *J. Geophys. Res.*, **114**, B03402, doi:10.1029/2007JB005201.

Kohlstedt, D.L., Evans, B. & Mackwell, D.J., 1995. Strength of the lithosphere – constraints imposed by laboratory experiments, *J. Geophys. Res.*, **100**(B9), 17587-17602.

Kusznir, N.J. & Bott, M.H.P., 1977. Stress concentrations in the upper lithosphere caused by underlying visco- elastic creep, *Tectonophysics*, **43**, 247-256.

Lenardic, A., Moresi, L.-N. & Mulhaus, H., 2003. Longevity and stability of cratonic lithosphere: Insights from numerical simulations of coupled mantle convection and continental tectonics, *J. Geophys. Res.*, **108**(B6), doi:10.1029/2002JB001859.

Li, X., Yuan, X. & Kind, R., 2007. The lithosphere-asthenosphere boundary beneath the western United States, *Geophys. J. Int.*, **170**(2), 700-710.

Lithgow-Bertelloni, C. & Guynn, J.H., 2004. Origin of the lithospheric stress field, *J. Geophys. Res.*, **109**, B01408, doi:10.1029/2003JB002467.

Liu, M., Shen, Y. & Yang, Y., 2000. Gravitational collapse of orogenic crust: A preliminary three- dimensional finite element study, *J. Geophys. Res.*, **105**(B2), 3159-3173.

Mitrovica, J.X. & Forte, A.M., 2004. A new inference on mantle viscosity based on joint inversion of convection glacial isostatic adjustment data, *Earth Planet. Sci. Letts.*, **225**, 177-189.

Molnar, P. & Tapponier, P., 1978. Active Tectonics of Tibet, *J. Geophys. Res.*, **83**(B11), 5361-5375.

Molnar, P. & Lyon-Caen, H., 1988. Some simple physical aspects of the support, structure, and evolution of mountain belts, *Geol. Soc. Amer. Spec. Paper.*, **218**, 179-207.

Panasyuk, S.V. & Hager, B.H., 2000. Models of isostatic and dynamic topography, geoid anomalies, and their uncertainties, *J. Geophys. Res.*, **105**(B12), 28,199-28,209.

Pascal, C., 2006. On the role of heat flow, lithosphere thickness and lithosphere density on gravitational potential stresses, *Tectonophysics*, **425**(1-4), 83-99.

Regenauer-Lieb, KL., Weinberg, R. & Rosenbaum, G., 2006. The effect of energy feedbacks on continental strength, *Nature*, **442**, 67-70.

Richardson, R.M., Solomon, S.C. & Sleep, N.H., 1976. Intraplate stress as an indicator of plate tectonic driving forces, *J. Geophys. Res.*, **81**, 1847-1856.

Richardson, R.M., Solomon, S.C. & Sleep, N.H., 1979. Tectonic Stress in the Plates, *Rev. Geophys.*, **17**(5), 981-1019.

Richardson, R.M. & Redding, L.M., 1991. North-American plate dynamics, *J. Geophys. Res.*, **96**(B7), 12,201-12,223.

Richardson, R.M., 1992. Ridge Forces, Absolute Plate Motions, and the Intraplate Stress Field, *J. Geophys. Res.*, **97**(B8), 11,739-11,748.

Royden, L.H., Burchfiel, B.C., King, R.W., Wang, E., Chen, Z., Shen, F. & Liu, Y., 1997. Surface Deformation and Lower Crustal Flow in Eastern Tibet, *Science*, **276**, 788-790.

Solomon, S.C., Sleep, N.H. & Richardson, R.M., 1975. On the forces driving plate tectonics: Inferences from absolute plate velocities and intraplate stress, *Geophys. J. R. Astron. Soc.*, **42**, 769-801.

Spasojevic, S., Liu, L., Gurnis, M. & Muller, R.D., 2008. The case for dynamic subsidence of the U.S. east coast since the Eocene, *Geophys. Res. Lett.*, **35**, L08305, doi:10.1029/2008GL033511.

Steinberger, B., Schmeling., H. & Marquart, G., 2001. Large-scale lithospheric stress field and topography induced by global mantle circulation, *Earth Planet. Sci. Letts.*, **186**(1), 75-91.

Steinberger, B., 2007. Effects of latent heat release at phase boundaries on flow in the Earth's mantle, phase boundary topography and dynamic topography at the Earth's surface, *Phys. Earth Planet. Inter.*, **164**, 2-20.

Thatcher, W. & Pollitz, F.F. 2008. Temporal evolution of continental lithospheric strength in actively deforming regions, *GSA Today*, **18**(4/5), 4-11, doi:10.1130/GSAT01804-5A.1

Turcotte, D.L. & Oxburgh, E.R., 1972. Mantle Convection and the New Global Tectonics., *Ann. Rev. Fluid Mech.*, **4**, 33-66.

Turcotte, D.L. & Schubert, G. 2002. Geodynamics, Copy-editing:, 2nd edn, Cambride Univ. Press, Cambridge.

Zoback, M.L., 1992. 1st-Order and 2nd-Order Patterns of Stress in the Lithosphere - The World Stress Map Project, *J. Geophys. Res.*, **97**(B8), 11,703-11,728.

Zoback, M.L. & Mooney, W.D. 2003. Lithospheric Buoyancy and Continental Intraplate Stresses, *Int. Geol. Rev.*, **45**, 95-118.

CHAPTER II

The Effects of Lithospheric Thickness and Density Structure on Earth's Stress Field

2.1 Abstract

The details of lithospheric structure, i.e., variations in lithospheric thickness and density contribute strongly to Earth's stress field. The relationship between the lithosphere's isostatic state, sub-crustal structure and stress field, however, remains unresolved due to the poor constraints on its thickness, composition and rheology. Here, we present calculations that systematically explore variations in a vertically-averaged lithospheric stress field over wavelengths of ~200 km, as a function of mantle density structure, lithospheric thickness (base depth) and lateral boundary conditions to study the influence of lithospheric strength variations on intraplate stresses. We compute the mean outward stress (integrated pressure / base depth) of 2^o x 2^o lithospheric columns and then solve for the resulting global vertically averaged stress field in an elastic finite element model. The results are discussed in the context of both global and regional stress patterns. For a 100 km base depth, a conventional value for average lithospheric thickness, stress patterns are fairly insensitive to mantle density structure, regardless of whether the mantle density is independently determined by tectonic and petrologic considerations or by enforcing isostasy. Increasing the base depth up to 250 km to account for continental roots, however, leads to strong differences in the stress patterns

associated with the two mantle density structures due to the progressively larger component of mantle lithosphere in each column. Decreasing the model base depth, a proxy for vertical decoupling due to low viscosity channels within the crust or lithosphere as a whole, strongly alters stress patterns and magnitudes, because the influence of topographic variations increases. For example, in the Western USA, systematically decreasing the base depth from 100 km to 25 km leads to ~ 50% increases in the extensional stress magnitudes. We find that restricting mean outward stress variations to specific areas, mimicking lateral variations in strength has a large effect on regional stress patterns, because stress transmission is then restricted to shorter distances. The lack of stress transmission over large distances is most prevalent for models with shallower base depths. We may summarize our findings simply as follows: A realistic lithospheric structure (density and rheology) is the controlling factor in the stress patterns determined from it. The choice of mantle density structures, assumptions about average lithospheric thickness and the extent of vertical and lateral decoupling all affect stress patterns and magnitudes significantly. In our view, it is not possible to assess the relative contribution of topography, density variations, basal shear and plate boundary forces to the lithospheric stress field of any given region using depth-integrated approximations. Our results highlight the need for future studies to incorporate the full 3-D variations in density and rheology to elucidate the origin of stress distributions within the lithosphere.

2.2 Introduction

Variations in lithospheric thickness and density produce tectonically significant stresses in the Earth's lithosphere (Artyushkov 1973; Molnar and Tapponnier 1978; Dahlen 1981; Fleitout & Froidevaux 1982; Fleitout & Froidevaux 1983). Such variations

play a particularly significant role in regions with large topographic gradients including mid-ocean ridges (Richardson *et al.* 1978; Dahlen 1981; Turcotte 1983; Richardson & Redding 1991; Richardson *et al.* 1992; Zoback 1992), Tibet (Molnar & Tapponnier 1978; England & Houseman 1986; England & Houseman 1988; England & Houseman 1989; Houseman & England 1993; Molnar *et al.* 1993; England & Molnar 1997; Flesch *et al.* 2001; Liu & Yang 2003; Ghosh *et al.* 2006) and Western North America (Jones *et al.* 1996; Jones *et al.* 1998; Flesch *et al.* 2000; Flesch *et al.* 2007; Humphreys & Coblentz 2007; Klein *et al.* 2009). The stresses arising from such variations are often quantified in terms of the lithosphere's gravitational potential energy (GPE) (e.g., Artyushkov 1973; Molnar & Lyon-Caen 1988; Coblentz *et al.* 1994), which refers to the integrated lithostatic pressure of an isostatically compensated lithospheric column. Stresses related to GPE gradients represent a depth-independent (or vertically-averaged) state of stress balancing variations in topography and density. At first glance, the world stress map shows a great deal of short wavelength variations, which seem to indicate a strong local dependence on topography and structure. An in-depth look reveals a number of coherent, long-wavelength stress patterns (Zoback 1992) which may accurately reflect the state of stress throughout the thickness of the lithosphere. If the latter holds true then using the GPE approximation is perfectly valid as a key to detangling the origins of the observed stress and deformation field.

This method is particularly attractive because of its elegance and simplicity. However, it requires a number of important assumptions including the model base depth and lithospheric density structure. GPE studies commonly use a 100 km base depth as a compromise average lithospheric thickness, although continental roots may extend down

to 200-250 km depth (Gung & Romanowicz 2003). Recent studies also suggest the lithospheric thickness in the tectonically active Western US lies well below 100 km in many places (Zandt *et al.* 1995; Li *et al.* 2007; Levander *et al.* 2008). Consequently, selecting a 100 km base depth includes large sections of asthenospheric material in regions with thinner lithosphere or potentially neglects important GPE contributions from thick continental roots (Zoback & Mooney 2003; Pascal 2006). Considering the GPE contribution of thick continental roots, however, requires assumptions about the density structure of the deep lithosphere and its role in the isostatic support of topography. Alternatively, one can also choose to asses the GPE contribution from only shallow base depths in the strong crustal lithosphere (Klein *et al.* 2009), where topography dominates the GPE signal. Restricting the lateral extent of the model to a specific region with a relatively uniform lithosphere-asthenosphere boundary partially resolves the issue of where to place a model base depth, although regional modeling imposes lateral boundary conditions that may dominate the calculated stress patterns. The presence or absence of a dynamic component to Earth's topography related to large-scale mantle flow (Hager *et al.* 1985; Gurnis 1993; Lithgow-Bertelloni & Silver 1998) may also be crucial as it can have a strong influence on intraplate stress patterns in regions of long-lived subduction (Lithgow-Bertelloni and Guynn, 2004).

The strong effect of these assumptions and approximations are clearly illustrated by the large differences between two end-member models in our previous work (Lithgow-Bertelloni and Guynn, 2004). While we kept the model base depth constant to 100 km, one end-member model enforced isostatic compensation by varying the density of the lower crust, and the other did not. The patterns of stress so derived (Figure 16 in

Lithgow-Bertelloni and Guynn, 2004) bore little resemblance to each other, although the average and maximum stress magnitudes were comparable. In this study, we take our previous results as the initial point of departure to explore how the lithospheric stress field varies as a function of the density structure of the mantle lithosphere, its average thickness and proxies for vertical and lateral variations in strength.

First, we present the formulation for the integrated lithostatic stress (ILS) and outline an array of diverse lithospheric structures for which the integrated lithostatic stress is calculated. Our designed array of lithospheric structures contains both compensated and uncompensated end members, with a focus on variations in mantle density structure, model base depth and lateral stress boundary conditions. Using this series of lithospheric structures we demonstrate how these variables affect depth-integrated lithospheric stress patterns. The implications of the results are discussed in the context of both the validity of the GPE method and the direction of future lithospheric stress studies.

2.3 Theory

The equation of mechanical equilibrium is

$$\frac{\partial \sigma_{ij}}{\partial x_j} = \rho g \hat{z} \tag{2.1}$$

where ρ is the density, g is the acceleration due to gravity, z is a unit vector in the vertical direction, and the stress contains deviatoric (τ_{ij}) and isotropic (p the pressure) contributions

$$\sigma_{ij} = \tau_{ij} - p\delta_{ij} \tag{2.2}$$

If we assume that 1) the upper and lower surfaces of the lithosphere are free of tractions and 2) that the lateral distance over which the loads vary is large compared with the thickness of the lithosphere then the bending stresses vanish $\tau_{xz}= \tau_{yz}=0$. If we further assume that all gradients in lithostatic pressure are balanced by deviatoric stresses then by substituting (2.2) into (2.1) we may write

$$\frac{\partial \bar{\tau}}{\partial x_j} = \frac{\partial \bar{\tau}_{zz}}{\partial x_i} - \frac{\partial \Omega}{\partial x_i} \tag{2.3}$$

where i,j run over the horizontal coordinates only (x,y), the over-bar denotes vertically averaged quantities and the vertically averaged zz-component of the stress is

$$\Omega = \sigma_{zz} = -\frac{1}{L}\int_{-L}^{h} \sigma_{zz} dz = -\frac{1}{L}\int_{-L}^{h} dz \int_{z}^{h} g\rho\left(z'\right) dz' \tag{2.4}$$

where h is the topography above sea level and z is defined positive upwards and zero at sea level. The quantity L is typically taken as the base of the lithosphere and we discuss the choice of L further below.

In this study, because we wish to consider both isostatically compensated and uncompensated models of the lithosphere, we refer to Ω as the mean outward stress (MOS), rather than the terminology used in many previous studies in which Ω is referred to as the gravitational potential energy (GPE) divided by the reference level (L)

$$GPE = \int_{-L}^{h} \rho g z dz \tag{2.5}$$

Indeed, one can show that Ω is simply related to GPE divided by the reference level (L), but only in the special case of isostatic compensation

$$\frac{\partial (L * \Omega)}{\partial x_i} = \frac{\partial (GPE)}{\partial x_i} \quad \text{(isostatic)} \tag{6}$$

The gravitational potential energy (2.5) is therefore properly defined in terms of the body force, which, unlike the pressure, does not depend on the load above (Houseman and England, 1986). The analysis of Molnar and Lyon-Caen (1988) defines GPE in terms of Equation (2.4), which is valid in the context of their study since they also assumed isostatic equilibrium.

Lateral variations in Ω are a source of horizontal deviatoric stress in the lithosphere (Equation 2.3), although unless directly specified variations in Ω may be balanced by both isotropic and deviatoric stresses. The quantity Ω represents the mean outward stress exerted by a column at x,y on surrounding lithosphere. In regions of isostatically compensated high topography or thick crust, the resulting stress state is tensional, whereas in regions of low topography of thin crust, the stress regime tends to be compressional. In detail, lateral variations in Ω and their influence on the lithospheric stress state depend sensitively on whether the lithosphere is in isostatic equilibrium.

Deviations from isostasy in the lithosphere, however are substantial and have an important influence on its state of stress (Lithgow-Bertelloni and Guynn, 2004) as we explore in Chapter III. At long wavelengths lateral variations in mantle properties at the lithosphere-asthenosphere boundary or deflections generated by mantle flow (dynamic topography) are two such examples. Dynamic topography is a determining contribution to Earth's gravitational potential (Hager et al., 1985), explains anomalously high topography and bathymetry (Lithgow-Bertelloni and Silver, 1998) and might be crucial for the state of stress in the lithosphere in regions of long-lived subduction (Lithgow-Bertelloni and Guynn, 2004).

We have found that the choice of L is important and has a significant effect on the computed stress field, and this dependence is the focus of subsequent sections. Most previous studies have generally assumed L to be a constant and equal to some convenient value, e.g. L=100 km, independent of geographic location. This is an approximation since the base of the lithosphere and the depth of compensation vary considerably with tectonic province, or with the age of the ocean floor. As the density contrast across the base of the lithosphere is small compared with that at the base of the crust, or at the free surface, one might expect computed stresses to be insensitive to the choice of L. However, lateral variations in L are very large and similar to the value of L itself, and this means that the choice of L is of comparable importance to the specification of topography or crustal thickness.

The strength of the lithosphere is likely to vary considerably laterally and with depth and the effect of these variations can be explored by varying the value of L. There are two issues: 1) the lithosphere may have weak layers (Kohlstedt *et al.* 1995) within it that do not transmit stresses effectively. We explore the limit of a layer of no strength within the lithosphere at depth S by setting L=S. This is akin to trying to separate the GPE contributions to the stress field from different parts of the lithosphere (Klein *et al.* 2009). 2) By setting the lithospheric thickness to a constant value, independent of location, in many regions large thicknesses of weak asthenospheric mantle will be captured in the integral (Equation 4), which should not be included because they do not effectively support deviatoric stress.

The depth of compensation is often assumed to coincide with the base of the lithosphere, but this is unlikely to be a good approximation in all tectonic provinces. The

depth of compensation may be defined as the depth D for which the lithostatic pressure is uniform across the globe. Setting D equal to the depth of the base of the thickest lithosphere is not a good approximation because lateral variations in the density of the asthenosphere can be substantial.

For example, Figure 2.1 shows a highly simplified scenario where the compensation depth of the deepest lithospheric column includes large sections of asthenospheric material in the neighboring thinner lithospheric columns. Although the change in rheology between the lithosphere and asthenosphere will certainly affect the distribution of stresses, using GPE makes no distinction between regions with different rheologies and the assumption of global isostatic compensation requires the asthenospheric material be included in the force balance between columns. Placing the model base depth above the global compensation depth removes the amount of asthenospheric material in selected columns, although unaccounted for pressure gradients now exist at the base of the model.

2.4 Lithospheric Structure

2.4.1 Crustal Lithosphere

Crustal thickness and density values are taken from the Crust 2.0 model (Bassin *et al.* 2000). Specifically, the models include Crust 2.0 density and thickness values for ice, sediment and crustal layers. Layers representing the upper, middle and lower crust are combined into a single layer with an average density (Figure 2.2c-d). The same is done for unconsolidated and consolidated sediment layers. Crust 2.0 elevations and bathymetry are taken from ETOPO5 (Figure 2.2a).

2.4.2 Mantle Lithosphere

The thickness of the lithosphere can vary geographically by hundreds of kilometers (see Figure 1 from Conrad & Lithgow-Bertelloni, 2006). In oceanic regions, crustal thickness is nearly constant, but lithospheric thickness depends on the age of the ocean floor and ranges from 0 at the ridge to as much as 100 km for the oldest ocean floor. Estimates of the maximum thickness of the continental thermal lithosphere range anywhere between < 200 to > 300 km (e.g. Jordan 1975; Rudnick *et al.* 1998; Artemieva & Mooney 2001; Gung & Romanowicz 2003) and vary strongly as a function of tectonic province. However, these measures are uncertain, and in comparison to the crustal portion of the continental lithosphere, fewer constraints exist on the thickness and composition of the lithospheric mantle. The composition of the lithospheric mantle is also less certain than the overall bulk composition of the crust. For the oceans, petrological models for the origin of basalt provide a basis for constructing a model of the lithospheric mantle. An undepleted peridotitic source that partially melts to produce MORB, leaves behind a depleted residue (a harzburgite), whose thickness depends on the degree of partial melt. As the oceanic lithosphere cools undepleted mantle also becomes part of the lithospheric column, and its thickness increases with age. For continents, the picture is less clear and the composition of the continental mantle lithosphere likely varies strongly as a function of tectonic province and age (e.g., Rudnick *et al.* 1998; Artemieva & Mooney 2001; Kaban *et al.* 2003; Artemieva 2006). In the thickest cratonic portions of very fast seismic velocity (e.g. Jordan 1975; Gung and Romanowicz 2003), the lithospheric mantle may be cold and buoyant (to survive for billions of years), which requires the presence of a depleted layer overlying an undepleted upper mantle layer.

We choose to define the base of the lithosphere thermally rather than mechanically, and do not at first worry about vertical variations in lithospheric strength, in which case the relative density and thickness of the depleted and undepleted lithospheric mantle layers control Ω.

We examine two end-member models to determine the density of both continental and oceanic mantle lithosphere. In the first model, the density of the lithospheric mantle is adjusted so that each lithospheric column is isostatically balanced relative to a reference mid-ocean ridge column. In the second model, described in detail in section 3.2.2, we make use of a new model for Earth's lithospheric thickness and composition (de Koker *et al.* 2005), which incorporates a layered lithospheric mantle. The relative thickness an density of the depleted and undepleted layers varies with the age of the ocean floor and tectonic province in the continents , described in section 2.4.2.2.

2.4.2.1 Isostatically Adjusted Mantle Density

Earth's topography results not only from inhomogeneities in the thickness and density of the crust and mantle lithosphere, but also from lateral variations in density in the asthenosphere and mantle flow. Ascertaining all these components is difficult because it requires information we do not presently have for the globe, such as extremely high resolution images of the lithosphere-asthenosphere boundary, like USArray has provided for parts of North America (Li et al. 2007; Levander et al. 2008) and a full understanding of dynamic topography. The latter remains uncertain because amplitudes generated by most flow models (e.g. Lithgow-Bertelloni & Richards 1998) needed to match Earth's geoid are nearly 3000 m peak to peak and vary as a function of mantle heterogeneity

assumed, viscosity structure and the degree of mass transfer between upper and lower mantle. A complete examination of the role of dynamic topography or a representation of lateral variations in density at the lithosphere-asthenosphere boundary are beyond the scope of this paper. Therefore we adopt a different strategy that is also in keeping with previous studies (Ghosh et al. 2006; Humphreys & Coblentz 2007; Ghosh et al. 2009; other earlier ones) that use the GPE formulation: we examine as one end member lithospheric structures that are fully compensated and adjust the mantle density to accomplish compensation.

The mantle density of isostatically compensated models is adjusted relative to an Atlantic mid-ocean ridge column (29^{o}N,43^{o}W) taken from the thermodynamic lithosphere model of de Koker *et al.* (2005). The bathymetric and crustal structure of this reference column is as follows: 3.028 km of water at 1020 kg m^{-3}, 0.07 km of sediment at 1700 kg m^{-3} and 6.5 km of crust at 2861 kg m^{-3}. The mantle portion of the column contains both a chemically depleted and undepleted section, whose density is a function of both temperature, pressure and composition (see below). The thickness and resulting average density of each layer is determined by the model base depth, which is our primary motive for constructing the reference column in this manner as the average mantle density should vary depending on the assumed base depth.

Adjusting the mantle to enforce isostatic compensation does not remove the contribution of dynamically supported topography to the lithospheric stress field as we show in Chapter III. An alternative is to remove this contribution by first subtracting positive or negative dynamic topography (computed from a mantle flow model) from observed topography, and then adjusting the density of the crust or mantle to enforce

isostatic compensation (e.g. Lithgow-Bertelloni & Guynn 2004). One may also calculate the residual topography of each lithospheric column relative to a reference column and then remove the non-isostatic component of topography from each column, as done by Ghosh et al. (2009). We chose not explore these approaches because of the uncertainties in the origin and magnitude of dynamic topography already mentioned and because in this study we are not interested in separating mantle from lithospheric contributions to stresses.

2.4.2.2 Thermodynamically Calculated Mantle Density

As an alternative end-member to enforced isostatic compensation we examine a model where we make no assumptions about how surface topography is compensated. To do so we use a previously constructed model for lithospheric thickness and density (de Koker et al., 2005). Starting from the crustal data of CRUST 2.0 the lithospheric thickness and density is determined by first performing a tectonic regionalization of oceans and continents. Oceanic regions are regionalized by the age of the ocean floor and continental ones are divided into four tectonic provinces: cratons, platforms, active margins (including previous orogenies and passive margins). These provinces are obtained by grouping the finer division in CRUST2.0. The model aims to determine the optimal thickness and density of the lithospheric mantle, with crustal thicknesses and densities are taken directly from CRUST2.0.

The lithospheric mantle itself is divided into two layers, 1) the depleted (harzburgite) complement to MORB that originates from partial melting of 2) an underlying enriched pyrolitic source. In oceanic lithosphere, the thickness of the depleted

layer is determined by multiplying crustal thickness by a factor (in this case 6.5) proportional to the expected melt fraction needed to produce 6 km of MORB crust (Asimow et al. 1995; Klein and Langmuir 1987). Because CRUST2.0 does not have variations in oceanic crustal thickness, the thickness of this layer is fixed at 39 km. The remainder oceanic lithospheric mantle is assumed to be pyrolitic. In continental regions the thickness of the depleted layer varies by tectonic province, its thickness obtained also by multiplying the thickness of the mafic lower crust as found in CRUST2.0 (Figure 2.2d) by a factor, which varies by tectonic province. The total thickness of the lithosphere is given by the depth at which the conductive part of the geotherm joins the adiabat (Tc = 1600 K), which defines $T(r)$ down to the base of the model.

With the strategy outlined above, de Koker et al. (2005) made two important innovations to determine the density of the mantle lithosphere: 1) Compute the density of depleted and undepleted mantle layers as a function of depth using a self-consistent thermodynamic model for mantle petrology and physical properties (Stixrude and Lithgow-Bertelloni 2005a), which matches existing petrological and mineral physics experimental constraints; 2) Determine the best multiplicative factor to obtain depleted mantle thickness, by requiring that the spherically averaged pressure at the base of the model match PREM and its narrow error bounds (Masters and Gubbins 2002).

We will refer to this model henceforth as TDL (thermodynamically determined lithosphere). The compositions for harzburgite and for pyrolite are taken from Workman and Hart (2005); oceanic geotherms are computed as a function of age using half-space cooling and the Müller et al. (1997) data supplemented as in Xu et al (2006) for regions with no data; continental geotherms (different for each tectonic province) are taken from

the literature (Pollack & Chapman 1977; Jaupart & Mareschal 1999; Michaut & Jaupart 2004). The base of the model is chosen at a depth of 350 km below sea-level because 1) the depleted layer is not expected to be thicker than this, and 2) there are no major phase transitions close to this depth. The base of the model is therefore assumed to be chemically and lithologically homogeneous.

Because isostasy is not enforced in the TDL model, lateral pressure gradients exist at the base of the model, which should reflect the dynamic support of elevation from large-scale mantle flow. From this assumption de Koker *et al.* (2005) estimated global magnitudes of dynamic topography, which showed global swells on the order 1-2 km. In the context of this study, this lithospheric structure implies that at any selected base depth there are lateral gradients in basal pressure. The TDL lithospheric structure, however, allows us to examine the influence of thick continental roots on the global stress field, of lateral variations in lithospheric thickness, without making initial assumptions regarding extent and nature of the isostatic compensation.

2.4.3 Approximated Regional Analysis

To examine the differences between global and regional models and approximate lateral variations in strength, we use an end-member proxy, which should capture the extreme case in which each lithospheric region is completely decoupled from surrounding areas. This extreme is unlikely to be present in the Earth, as even across rheological boundaries a portion of the stress normal to the boundary will be transmitted. Besides allowing a crude first-order examination of lateral variations in strength, it also yields a baseline with which to assess differences between global and regional analyses.

In selected models, we modify the lithospheric structure of each column outside the region of interest and set it equal to the lithospheric structure of the reference oceanic column used for isostatic adjustments. In other words, the entire world is assumed to be a mid-ocean ridge, except in the specified region. This provides a lateral 'stress' boundary condition for the region of interest, although the model is still global geometrically and no lateral displacement boundary conditions are imposed.

2.5 Numerical Method

2.5.1 Model Geometry and Governing Equations

We follow the method of Lithgow-Bertelloni and Guynn (2004) to compute the global stress field from the mean outward stress values calculated for each lithospheric structure (Equation 2.4). The global stress field is calculated by applying the mean outward stress values to a 3D numerical model that solves the equations of conservation of mass and momentum via the finite element method.

The mean outward stress calculated for each lithospheric column is applied to the horizontal faces of a corresponding element in the upper layer of elements following Richardson & Redding (1991) to avoid numerical instabilities related to compression and relaxation of the material. We use the finite element package ABAQUS (Hibbit & Sorenson 2002) to solve for the resulting elastic stress field balancing the variations in mean outward stress. To obtain the global elastic stress field, ABAQUS solves the fundamental equations elasticity, or more specifically conservation of mass and momentum (Equation 2.3) together with the following constitutive equation that relates stress and strain for a linearly elastic solid

$$\varepsilon_{ij} = \frac{1+\nu}{E}\sigma_{ij} - \frac{\nu}{E}\sigma_{kk}\delta_{ij} \tag{2.7}$$

where E is the Young's Modulus, and ν is Poisson's ratio.

Our numerical models consists of two vertically and laterally homogeneous spherical layers divided into 2^o x 2^o equal area 8-node quadrilateral continuum shell elements, which are geometrically 3D but formulated similarly to shell elements (Hibbit & Sorenson 2002). Interestingly, the stress state obtained by using continuum shell elements is nearly identical to the stress state obtained by using 3D continuum elements (Lithgow-Bertelloni & Guynn 2004). This is not surprising, because given the lateral distance over which lithospheric loads change we expect bending moments to be small, which indeed was the case for our previous study (the median value of σ_{zx} and σ_{zy} was two orders of magnitude smaller than the normal stresses). The thickness of the top layer corresponds with the base depth of each model while the lower base layer thickness remains fixed at 100 km. The bottom nodes of the lower layer are pinned in all three directions and since our model is global no artificial lateral displacement or stress boundary conditions exist.

We assign laterally homogenous elastic properties to both layers of elements with the top layer and bottom layers having, respectively, Young's Modulus values of 10^{11} Pa and 10^6 Pa and a Poisson's ratio of 0.3. The upper layer's Young's modulus is meant to represent those of crustal rocks and thus serve as a mean value for the lithosphere. The low Young's modulus value of the basal layer prevents transmission of stresses associated with the pinned basal nodes into the upper layer of elements. Since the elastic properties remain constant throughout each layer, their values only influence the calculated strains and not the stress itself.

2.5.2 Non-Lithostatic vs. Deviatoric Stress Representation

The calculated stress field σ_{ij} balancing mean outward stress variations is equivalent to a depth-integrated non-lithostatic stress field. Due to our choice of continuum shell elements, the calculated planar stress state reduces the 3D stress tensor in spherical coordinates to a 2D stress tensor,

$$\sigma_{ij} = \begin{bmatrix} \sigma_{nn} & \sigma_{ne} & \sigma_{nr} \\ \sigma_{en} & \sigma_{ee} & \sigma_{er} \\ \sigma_{rn} & \sigma_{re} & \sigma_{rr} \end{bmatrix} = \begin{bmatrix} \sigma_{nn} & \sigma_{ne} & 0 \\ \sigma_{en} & \sigma_{ee} & 0 \\ 0 & 0 & 0 \end{bmatrix} \tag{2.8}$$

which is defined in terms of a north(n)-east(e)-radial(r) coordinate system. As discussed above, this planar stress state is very similar to the planar stress state obtained by using full 3D continuum elements and then extracting the in-plane components (σ_{nn}, σ_{ee}, σ_{ne}) as done in Lithgow-Bertelloni & Guynn (2004). The similarity of the planar stress states obtained by using either element reflects that using the full 3D equation should produce very small out of plane compared to in-plane stress components (σ_{rr}, σ_{re}, $\sigma_{rn} << \sigma_{nn}$, σ_{ee}, σ_{ne}) as long as the loads are oriented parallel to the plane of the shell or sheet structure. If this is not the case, the orientation of the principal stress axis will be at an oblique angle to the plane of the shell.

The calculated non-lithostatic stress tensor (σ_{ij}) contains both a deviatoric (τ_{ij}) and a non-lithostatic hydrostatic component (P_{nl}), where

$$\sigma_{ij} = \tau_{ij} + P = \tau_{ij} + \delta_{kk} \frac{\sigma_{nn} + \sigma_{ee} + \sigma_{rr}}{3} \tag{2.9}$$

which becomes

$$\sigma_{ij} = \tau_{ij} + \delta_{kk} \frac{\sigma_{nn} + \sigma_{ee}}{3} \tag{2.10}$$

because the non-lithostatic vertical stress (σ_{rr}) is effectively zero in this case. For the example of all out-of-plane stress components (σ_{rr}, σ_{re}, σ_{rn}) taken as 0, the non-lithostatic isotropic pressure and deviatoric stress tensor in matrix form are

$$P_{nl} = \begin{bmatrix} \frac{\sigma_{nn} + \sigma_{ee}}{3} & 0 & 0 \\ 0 & \frac{\sigma_{nn} + \sigma_{ee}}{3} & 0 \\ 0 & 0 & \frac{\sigma_{nn} + \sigma_{ee}}{3} \end{bmatrix} \tag{2.11}$$

and

$$\tau_{ij} = \begin{bmatrix} \frac{2\sigma_{nn} - \sigma_{ee}}{3} & \sigma_{ne} & 0 \\ \sigma_{en} & \frac{2\sigma_{ee} - \sigma_{nn}}{3} & 0 \\ 0 & 0 & \frac{-\sigma_{nn} - \sigma_{ee}}{3} \end{bmatrix} \tag{2.12}$$

Following Lithgow-Bertelloni and Guynn (2004) we present the full stress tensor determined in our numerical calculations. We present the stress tensor in this form as horizontal deviatoric stresses alone do not accurately represent the stress magnitudes needed to balance mean outward stress variations in our elastic calculations, which do not assume incompressibility.

2.6 Global and Regional Stress Patterns

2.6.1 Reference Models

Our goal is to examine the separate effects of 1) using a more realistic lithospheric thickness and structure and 2) spatial gradients in lithospheric thickness. We start with two models containing a commonly assumed 100 km base depth and either an isostatically adjusted (Figure 2.3a) or thermodynamically determined (Figure 2.3b)

mantle density. The mean outward stress and stress patterns in these models are designed to serve as a reference point for the proceeding models with different base depths or lateral stress boundary conditions. Significantly, although noticeable differences exist between the average density of the isostatically compensated (Figure 2.4a) and TDL mantle structures (Figure 2.4b), especially near continental margins, the mean outward stress distribution and resulting stress patterns are quite similar. This in part reflects the strong influence of topography and crustal density for a 100 km base depth, which limits the potential influence of mantle density variations compared to deeper base depths. As a general trend, however, enforcing isostasy by adjusting the mantle density minimizes gradients in the mean outward stress and consequently slightly lowers stress magnitudes in many regions compared to the TDL mantle density model. The largest deviations in the stress patterns between the two models occur in the polar regions and near continental margins where the largest density variations also exist (Figure 2.4a-b).

The stress patterns in general strongly resemble previously published stress models for a 100 km base depth (Steinberger *et al.* 2001; Lithgow-Bertelloni & Guynn 2004; Ghosh *et al.* 2009). Stress magnitudes (Figure 2.3) range from < 10 MPa to 10's of MPa, with the largest stress magnitudes occurring in regions with large topographic gradients (e.g., pacific margin of North and South America, Tibet and Eastern Africa). The maximum stress magnitudes reach ~ 75 MPa in Tibet for the TDL mantle density (Figure 2.3b).

2.6.2 Thick Continental Roots

Moving the model base to deeper depths increases the mantle thickness and places the center of gravity lower in the lithospheric column, thereby reducing the influence of topographic gradients on stress patterns. For the case of the isostatically adjusted mantle structure with a 175 km base depth (Figures 2.5a), global stress patterns are similar to those for the 100 km base depth model. The similarity of the patterns reflects that the mean outward stress variations remain strictly related to surface and moho topography, while the deeper base depth simply changes the mantle density required to enforce isostasy. The increase in base depth decreases mean outward stress gradients in continental regions, thereby reducing the resulting stress magnitudes throughout the majority of topographically high continental areas. Reduced mantle density variations between columns required to satisfy isostatic constraints (Figure 2.4c) partially explain this pattern. Averaging the mean outward stress variations over thicker columns also reduces the mean outward stress gradients and stress magnitudes in continental regions. Mean outward stress gradients in the ocean basins remain essentially unaffected compared to the continental regions, resulting in higher oceanic stress magnitudes. Increasing the base depth to 250 km (Figure 2.6a) largely reproduces these trends.

In contrast to isostatically adjusted mantle structures, increasing the base depth for the TDL mantle structure incorporates additional mantle density variations that have no assigned role in enforcing isostatic balance. As a result, the additional mantle in each column may drive the models towards or away from regional isostatic compensation, and increase or decrease regional mean outward stress gradients. The mantle incorporated by increasing the base depth from 100 km to 175 km leads to larger gradients in the mean outward stress distribution (Figure 2.5b), particularly across tectonic provinces where

different mantle geotherms influence the density structure. The new mean outward stress distribution often magnifies the stress magnitudes in certain areas while the orientations remain similar (i.e. Antartica, Mediterranean, Ural Mountains, Western Australia, ...), while in other regions the stress orientation is strongly modified as well (i.e. Western North America and Andes). Increasing the base depth to 250 km (Figure 2.6b) generates the largest mean outward stress gradients and resulting stress magnitudes despite the lowest averaged mantle density variations (Figure 2.4f), where the stress field in many regions strongly deviates from the 100 km reference model. In many regions, the stress magnitudes are more than a factor of 2 larger than those in the isostatically compensated model with a 250 km base depth (Figure 2.6). This suggests a key role for either dynamically supported topography or the inadequacy of the integrated lithostatic stress formulation for capturing realistic variations in L.

2.6.3 Effects of Strength Variations Within the Lithosphere

We now assess the possibility that the observed lithospheric stress field reflects pressure variations from base depths shallower than 100 km. For us this is a proxy, within a homogeneous model, for vertical strength variations within the lithosphere. In other words, an end member representation of how complete vertical decoupling within the lithosphere would alter stress patterns and affect deformation. Put a different way, the hypothesis is that deeper parts of the lithosphere will not be able to effectively transmit the stress upward, leading to vertical decoupling within the lithosphere and a strong depth-dependence of the lithospheric stress. We illustrate the general pattern and physical effects globally (Figure 2.7) and then focus in on a few regions, to illustrate the

physics that control the emerging patterns, including possible lateral variations in strength between tectonic provinces.

Decreasing the base depth from 100 km to 50 km for the TDL mantle density structure (Figure 2.7) illustrates the development of large-scale stress patterns related to regions of high topography. As the base depth decreases the relative contribution of topography to the mean outward stress increases, as shown in Tibet, the Western US and the Andes. The larger influence of the topographically highest regions at a 50 km base depths reveals a long-wavelength stress pattern where compressional stresses run parallel to a large percentage of the Pacific plate boundary (Figure 2.7b). This pattern is actually slightly developed in the 100 km base depth model (Figure 2.7a), but not highly apparent without the example of the 50 km base depth case where the compressional stress magnitudes increase up to a factor of 2 in some areas. The ability of the global model to develop long-wavelength trends across multiple plates is due to both the long wavelength of the loads along the pacific plate-boundary as well as the homogenous elastic lithosphere, which allows for efficient transmission of stresses. In this case, one may think of the stress response of the lithosphere to the loading of each column as a Green's function. The stress resultant in each column is the sum of all the Green's functions resulting from the load on each lithospheric column on the rest of the globe. The lack of these stress patterns in the world stress map reflects a number of factors, but most importantly variable lithospheric thickness across tectonic provinces and the presence or large lateral and vertical rheological variations in the lithosphere.

To take a closer look at the effects of complete vertical decoupling on regional stress patterns without the presence of the large global elastic stress patterns, we assign

the mean outward stress of the reference column to elements outside of either a region encompassing roughly North America or the Continental US as in section 3.3. The compressional stress pattern running parallel to the North American plate boundary for a 100 km base depth and isostatically adjusted mantle density (Figures 2.3a and 2.8a) is largely eliminated by assigning a fixed mean outward stress value outside the North American continent (Figure 2.8b). The assigned fixed mean outward stress value changes long-wavelength mean outward stress gradients, which in turn alters the resulting stress patterns within North America. Extensional stresses in Western North American oriented perpendicular to the plate boundary remain largely unaffected by the stress boundary conditions, although in Alaska and the Western Continental US a component of plate-boundary perpendicular extension is translated into plate boundary parallel extension. Extensional stress magnitudes in Greenland and the North Atlantic increase due to a decrease in mean outward stress to the East. Restricting the mean outward stress variations further to within the Continental US and neighboring Atlantic (Figure 2.8c) reduces extensional stress magnitudes in the western US, which decrease significantly due to the smaller mean outward stress variations across neighboring Western Pacific regions. Extensional stress magnitudes along the mid-Atlantic ridge also decrease due to the reduced local mean outward stress variations.

Maintaining the regional stress boundary conditions and decreasing the model base depth from 100 km (Figure 2.9a and 2.10a) to 50 km (Figure 2.9b and 2.10b) and 25 km (Figure 2.9c and 2.10c) increases extensional stress magnitudes in the topographically high Western US as integrated pressure gradients related to topography are averaged over a smaller column thickness. For a 100 km base depth, the extensional stress magnitudes

in the Western US range on average between 5-15 MPa, which for a 50 km and 25 km base depth increase, respectively, to 10-20 MPa and 15-25 MPa. Compressional and extensional stress magnitudes in the continental interior (Figure 2.9) also increase between ~ 50-100% as the base depth decreases by a factor 2, which is a response to both larger E-W and N-S mean outward stress gradients. At base depths of 50 km and 25 km a strike-slip state of stress dominates the majority of the continental USA interior and Western Atlantic basin, which contrasts sharply with the 100 km base depth stress patterns and observed regional stress patterns (Zoback 1992). Notably, for a 100 km base depth the non-lithostatic extensional stress magnitude range of 5-15 MPa in the Western USA is very close to the deviatoric extensional stress magnitude ranges of 5-10 MPa (Flesch *et al.* 2007; Humphreys & Coblentz 2007) reported in previous regional modeling studies for a 100 km base depth. The remaining difference in stress magnitude between this study and the previously studies is likely that we do not remove the non-lithostatic isotropic stress component from the stress tensor.

2.7 Implications of a Shallow Uncompensated Model Base Depth or Full Vertical Decoupling

The end result of assuming full vertical decoupling between deeper layers of the lithosphere by decreasing the model base depth to shallow lithospheric depths is to concentrate integrated stress differences related to topography into thinner lithospheric columns, thereby increasing the magnitude of the lithospheric stress response. This trend has been noted by previous studies examining depth-dependent stress distributions as a function of time (Kusznir & Bott 1977; Bott & Kusznir 1979; Liu *et al.* 2000, for

example) or other depth-independent stress studies varying the model base depth (Molnar *et al.* 1993; Klein *et al.* 2009). In the case of this study and Klein *et al.* (2009) the model base depth is uncompensated and therefore unaccounted for basal tractions exist at the model base. As a result, the stresses calculated for a shallow model base depth are only reasonable estimates under the following conditions: horizontal stress (σ_{nn}, σ_{ee}) gradients across the model base depth are small; a rheologically weak layer at the model base leads to sharp stress gradients and weak coupling between layers above and below the base depth. Based on these conditions, the validity of isolating stress fields from different sections of an isostatically balanced column largely depends on the lithospheric rheological structure or the distribution of pressure gradients as a function of depth.

As an example, consider the stress state between two isostatically balanced lithospheric columns extending to a depth of 100 km and containing a 2 km elevation difference (Figure 2.11). The crustal density and moho depth are equal in both columns, while the mantle density in the topographically high column is adjusted to enforce isostatic compensation relative to the mantle density of 3300 kg m^{-3} in the reference column. The difference in mean outward stress between the topographically high column (MOS_{top}) and reference column (MOS_{ref}) serves as a proxy for the magnitude of extension in the topographically high column. Placing the model base depth at the isostatic compensation depth generates ~ 36 MPa of extension in the topographically high column (Figure 2.12). Moving the base depth above the isostatic compensation depth implies two distinct horizontal stress states exist above the base depth and between the base depth and isostatic compensation depth (Figure 2.11). Systematically decreasing the

base depth increases the magnitude of extension in both column layers, with the stress difference across the layers staying ranging between ~ 36 MPa to 26 MPa (Figure 2.12).

Although these vertical gradients in horizontal stress are likely much larger than those in the lithosphere due to the simplifications in this example, the results clearly demonstrate why placing the base depth at uncompensated shallow depths requires significant assumptions about the rheological structure of the lithosphere. In the case of the Western US, Klein *et al.* (2009) argued that a shallow base depth (20 km) was reasonable based on the magnitude of shear stresses related to mantle flow in the region. This analysis, however, excludes vertical gradients of horizontal stress across the shallow model base depth that result from pressure gradients between the model base depth and the base of the lithosphere. If these gradients are large, then the calculated stress state in the shallow lithosphere may not be accurate unless a weak decoupling layer exists at the base of the seismogenic lithosphere. The relative strength contrast across the base depth determines the validity of the uncompensated shallow base depth approximation. Rather than assume a full horizontal stress decoupling across an uncompensated model base depth, it is strongly preferable to use either expanded thin-viscous sheet approximations (Bird 1989; Medvedev & Podladchikov1999) or full 3D depth-dependent models that account for the rheological coupling between different lithospheric layers.

2.8 Discussion and Conclusions

Determining the stresses required to balance topography and density variations with the integrated lithostatic stress method provides an eloquent procedure for studying the lithosphere under the assumption of full mechanical coupling. Indeed, numerous

studies have successfully used the integrated lithostatic stress approximation to gain insight into first-order lithospheric processes. Using this method to model the lithospheric stress field for a wide range of mantle density structures, model base depths and lateral stress boundary conditions, however, demonstrates the large variability in calculated stress patterns and especially magnitudes, depending on the assumed parameters. For the commonly assumed 100 km base depth the density structure of the mantle lithosphere has a minor impact on global stress magnitudes and orientations. Increasing or decreasing the global model base depth to account for deep continental roots, thin lithosphere or sharp variations in lithospheric strength strongly modifies global and regional stress patterns as the relative contributions of topography and mantle density structure vary. Modeling a specific region in part removes the complication of variable lithospheric thickness, although the lateral stress boundary conditions imposed on the region exert a first-order control on the regional stress patterns.

Overall, the composition of the deep lithosphere, dynamic support vs. isostatic support of topography and the role of lateral and vertical variations in rheology in modifying stress distributions stand out as the largest unresolved issues and variables. Of these issues, the role of density structure and lithospheric rheology is certainly the most important in the context of the integrated lithostatic stress approximation, although the strength of the lithosphere remains actively debated (Kohlstedt *et al.*1995; Jackson 2002; Burov & Diamont 2006; Regenauer-Leib *et al.* 2006; Hartz & Podloadchikov 2008; Thatcher & Pollitz 2008; Burgmann and Dresen 2008). Solving for the full three dimensional lithospheric stress field with depth-dependent strength variations self-consistently determines the extent of mechanical coupling between shallow and deep

lithospheric regions, and removes the need to choose a single base depth that may not properly capture the dynamics of a given region. The effect of variable lithospheric strength on stress distributions has in fact been extensively studied (e.g. Kusznir & Bott 1977; Bott & Kusznir 1979; Liu *et al.* 2000; Regenauer-Leib *et al.* 2006), although, again the rheological structure of the lithosphere remains highly debated. As demonstrated by Beaumont *et al.* (2004), regions such as the Tibet-Himalayan orogen that potentially experience channel flow (e.g. Royden et al. 1997, Clark and Royden 2000) may contain multiple layers that are weakly coupled and exhibit different deformation patterns and rates. Aside from the debate of different proposed lithospheric rheological structures, it is clear that first-order variations in lithospheric strength (i.e. weak lower crust, strength contrast across crust-mantle boundary, etc) can lead to stress and deformation patterns that strongly deviate from the solutions obtained by depth-independent calculations. Incorporating lateral variations in lithospheric strength across tectonic provinces potentially defined by elastic thickness data (Bechtel *et al.* 1990; Lowry & Smith 1995, Lowry *et al.* 2000, in North America for example) will also help determine the length-scales over which stresses transmit and the validity of regional boundary conditions.

Our results show that the integrated lithostatic stress approximation does not capture the depth-dependence of the lithospheric stress field related to strength variations and the effects of realistic variations in lithospheric thickness. The above has major implications for interpreting the origins of the observed stress and deformation patterns. The issue of a depth-dependent stress field is particularly important for studies that assess the relative contribution of basal shear, plate boundary forces and topography and density variations to the lithospheric stress field on a global (Steinberger et al; 2001; Lithgow-

Bertelloni & Guynn 2004; Ghosh *et al.* 2008), plate (Humphreys & Coblentz 2007) or regional (Flesch *et al.* 2007) scale. As pointed out by Steinberger *et al.* (2001), variations in lithospheric strength are likely to reduce the stress magnitudes related to basal shear between the top and bottom of the lithosphere. For certain rheological structures, coupling between the mantle lithosphere and upper crust may be significantly restricted as demonstrated by multiple studies (Pysklewec *et al.* 2002, Beaumont *et al.* 2004). Combined with rheological controls on the depth-dependence of stresses related to topography and density variations, it seems likely that the relative contribution of these different sources of stress may vary strongly as a function of depth. If this is indeed the case, it is essential for future studies to focus on the effects of 3D density and rheology variations in controlling stress distributions within the lithosphere.

The future, however is bright because of more extensive and more detailed in situ pictures of lithospheric structure from seismology. Large scale deployments such as USArray and observational networks such as NIRIES and EPOS enabled by ORFEUS (Observatories and Research Facilities for European Seismology) are already producing substantial advances in our knowledge of the continental lithosphere. Coupled with state-of-the-art thermodynamic methods for determining geophysically active and observable properties such as density from seismic velocity (Stixrude & Lithgow-Bertelloni 2005) we are not far from having the information necessary to study the effects of 3D variations in density and rheology on Earth's surface deformation.

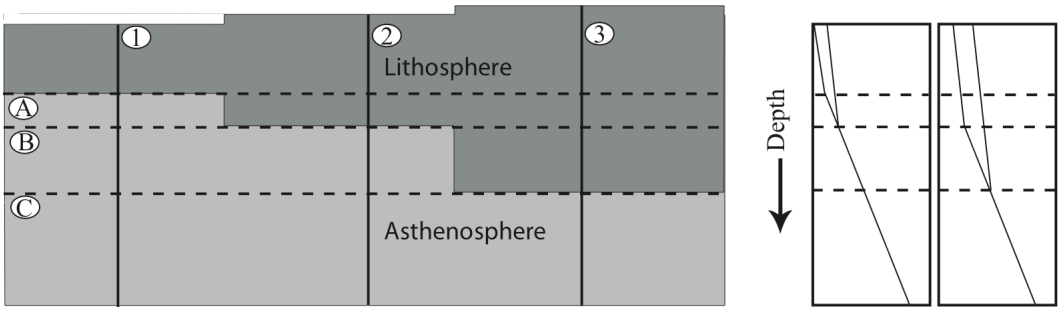

Figure 2.1: Schematic diagram illustrating the concepts of base depth for simplified lithospheric structures. Left: three lithospheric columns of varying thickness floating in a liquid mantle. All three columns are isostatically compensated at line C. Lines A and B mark the base of columns one and two and represent potential choices for integration depths. Right: Hypothetical pressure vs. depth profiles with superimposed base depths.

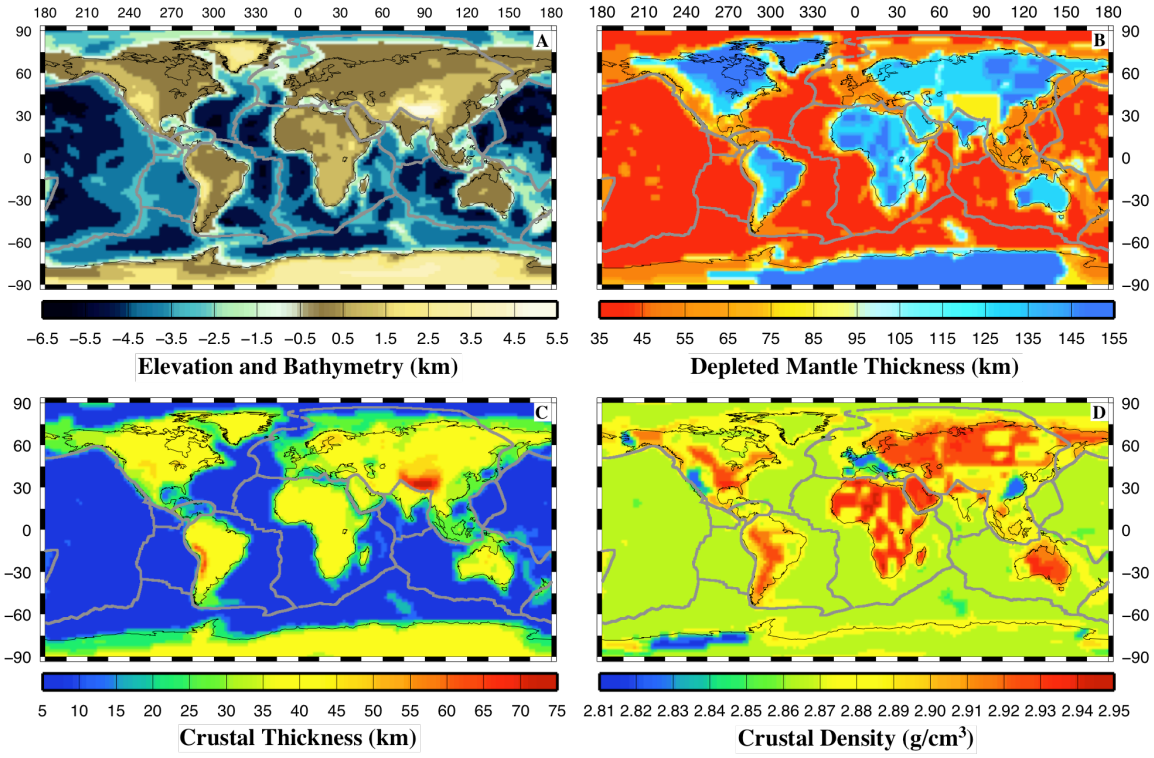

Figure 2.2: Global Lithospheric Structure. The crustal data is taken from the Crust 2.0 model, which includes elevation and bathymetry (a) and the thickness and density of ice, sediment and crust (c-d) layers. Displayed crustal thickness and density values are averages of the upper, middle and lower crust layers. The depleted mantle thickness (b) is taken from the TDL model of de Koker *et al.* (2005).

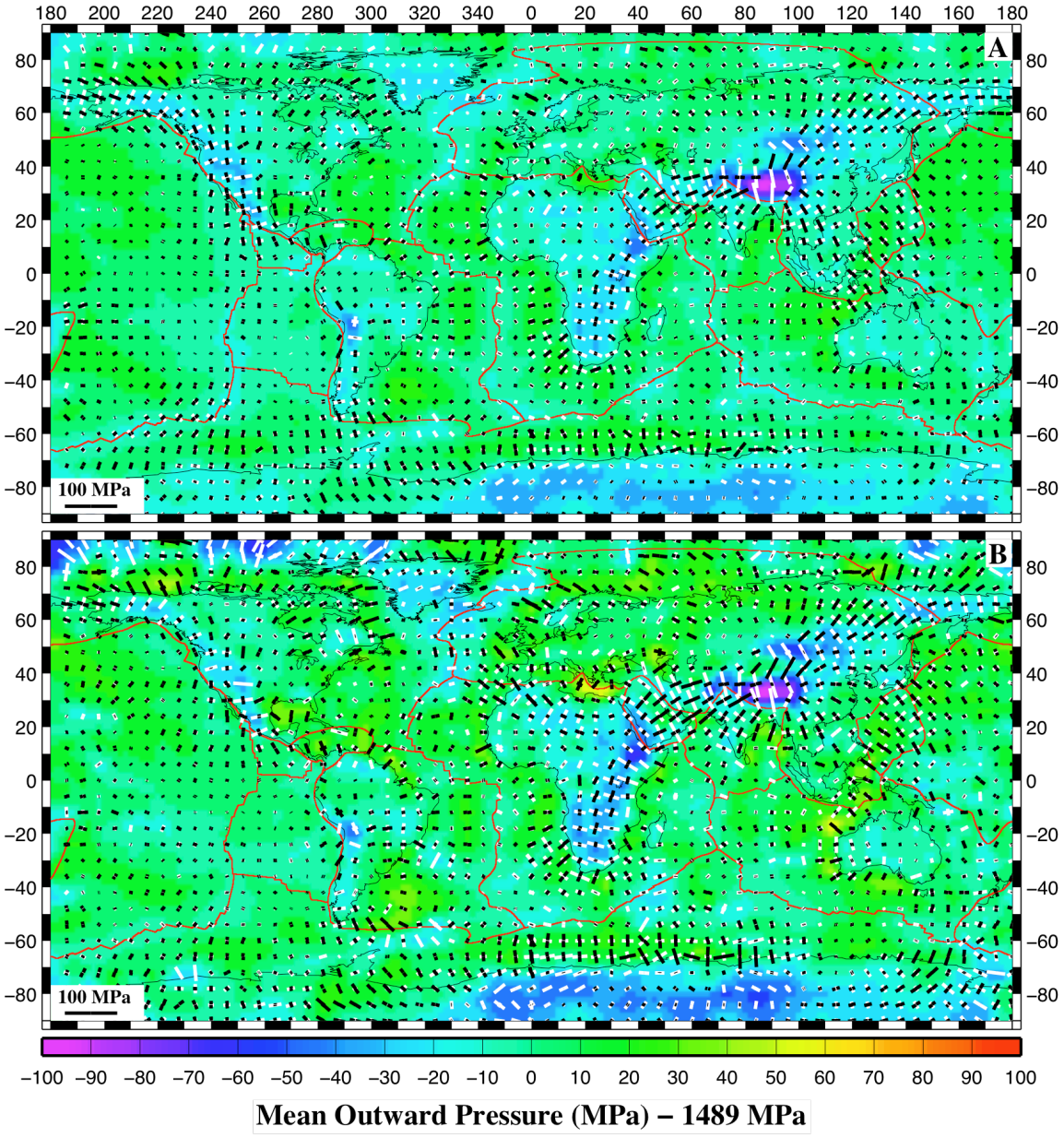

Figure 2.3: Variations in global mean outward stress and the principal stresses balancing these variations for a 100 km base depth. Regions with large negative outward pressures often correspond with topographically high regions and are characterized by extensional principal stresses (white bars, compression ~ black bars). Mean outward stress and stress patterns are shown for models with isostatically adjusted (a) and TDL (b) mantle density structures.

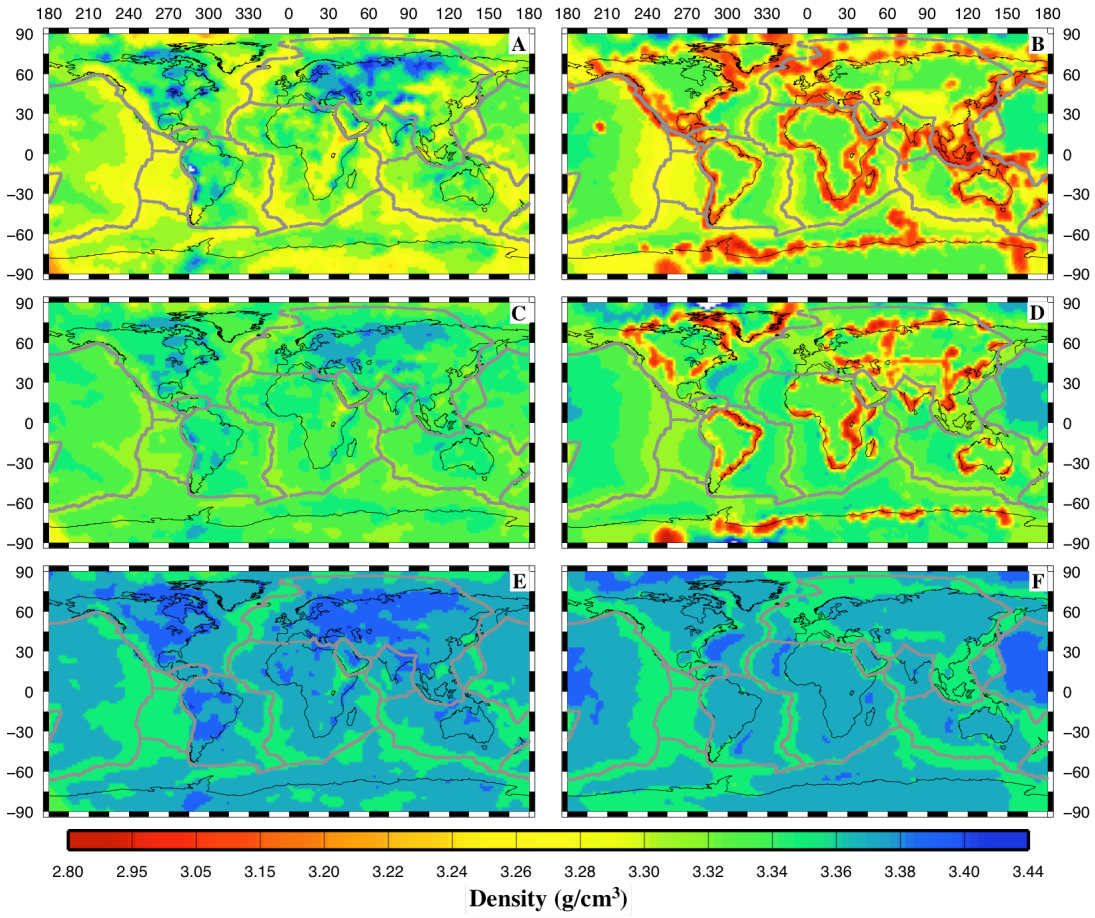

Figure 2.4: Isostatically adjusted (a-c-e) and TDL (b-d-f) mantle densities for model base depths of 100 (a-b) km, 175 km (c-d) and 250 km (e-f). The density in the isostatically compensated models remains constant throughout the thickness of the mantle portion of each column. The TDL mantle densities are the thickness-weighted average of the depleted and undepleted mantle densities in each column.

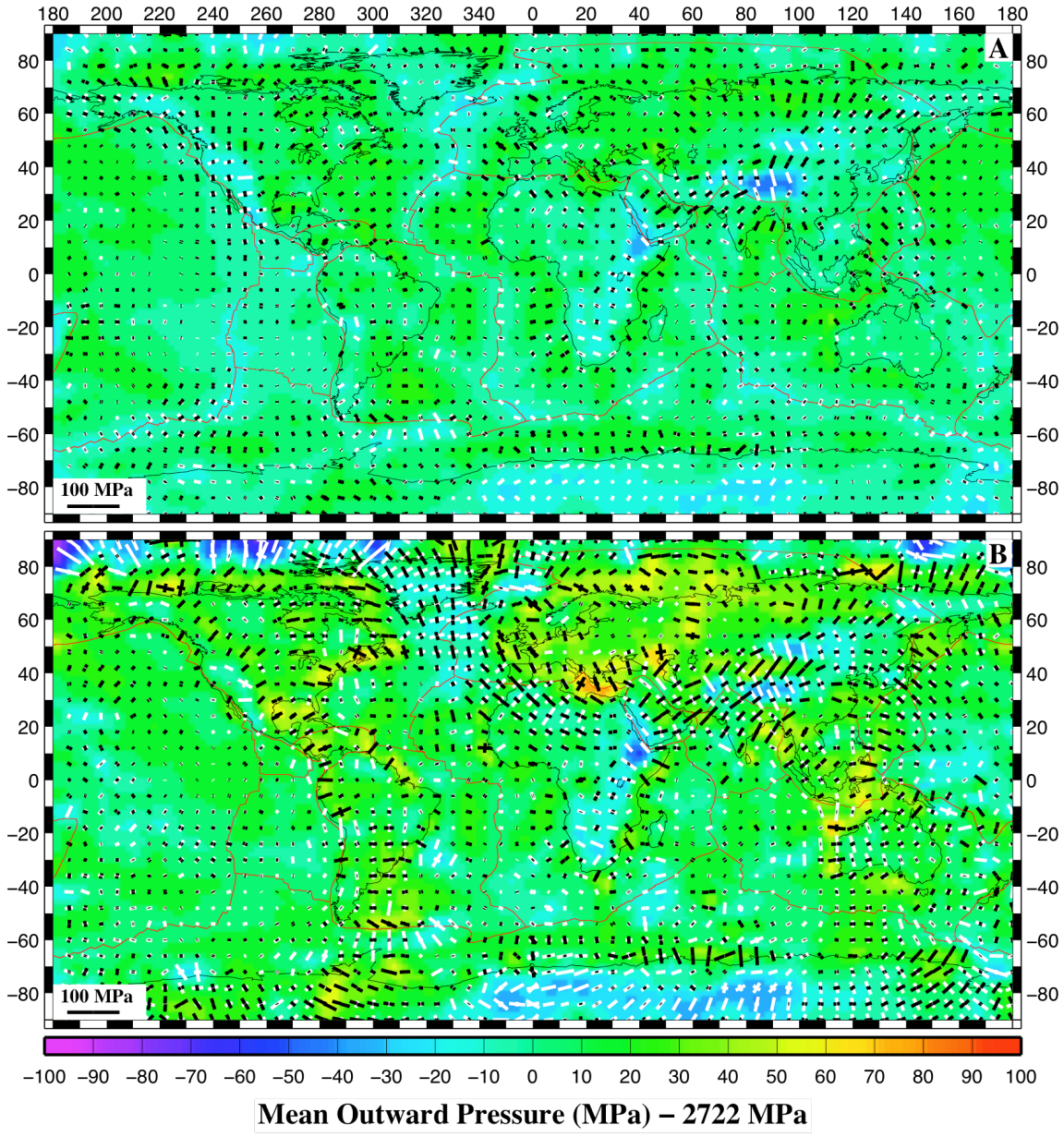

Figure 2.5: Mean outward stress variations and resulting principal stresses for a 175 km model base depth and isostatically adjusted (a) or TDL (b) mantle density structures.

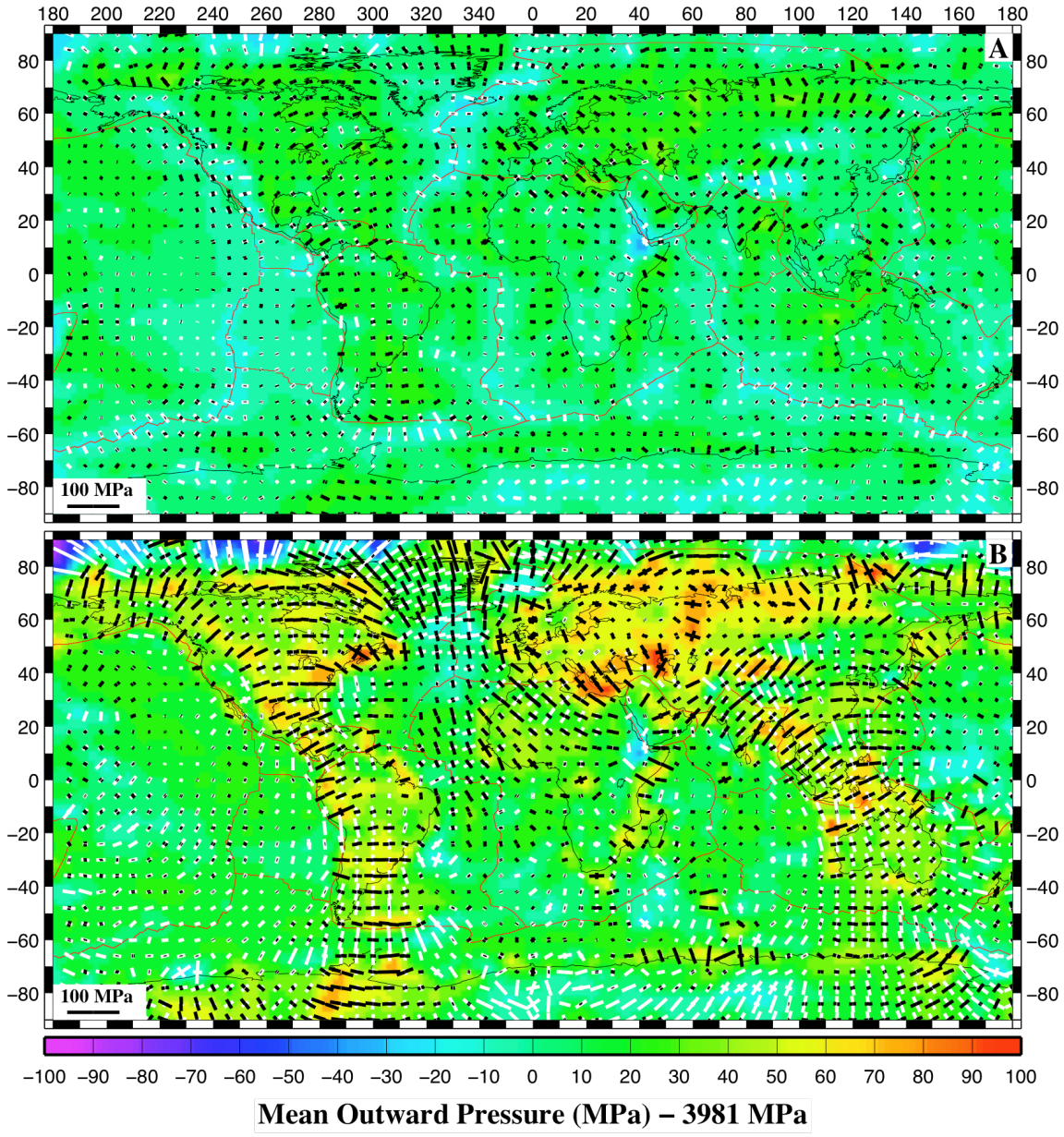

Figure 2.6: Mean outward stress variations and resulting principal stresses for a 250 km model base depth and isostatically adjusted (a) or TDL (b) mantle density structures.

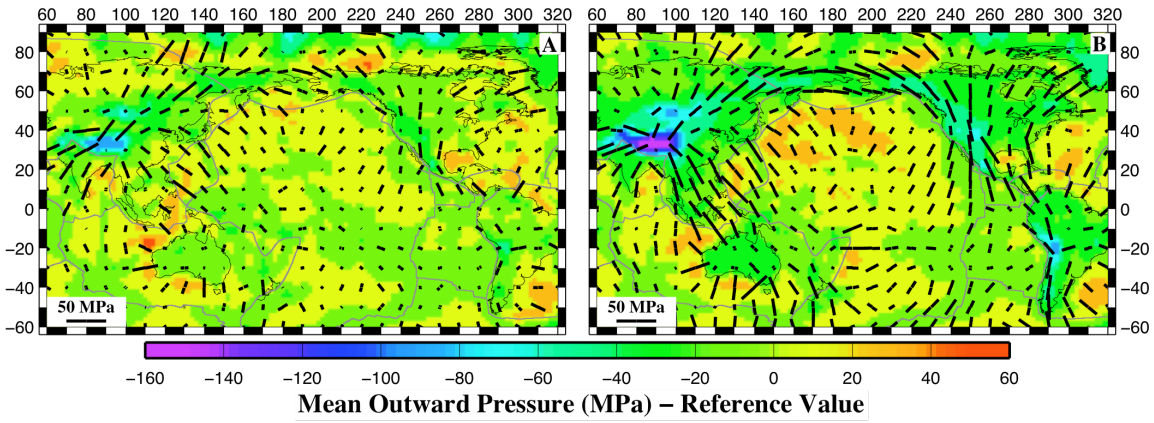

Figure 2.7: Mean outward stress variations and resulting compressional principal stresses for a TDL mantle density structure and a 100 km (a) or 50 km (b) model base depth. The reference values subtracted from the mean outward stresss are 1482 MPa (a) and 678 MPa (b).

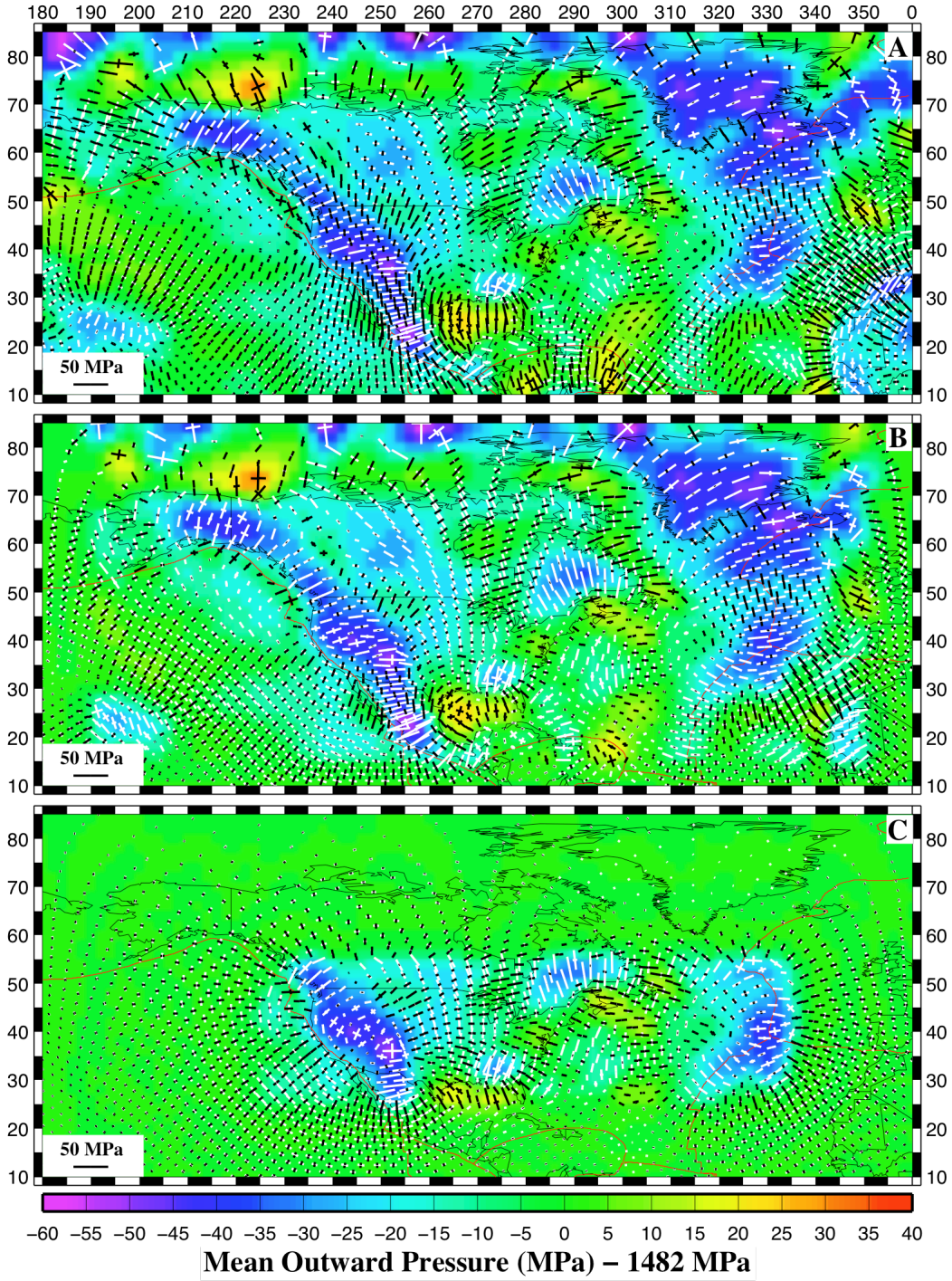

Figure 2.8: Global (a), plate (b) or regional (c) mean outward stress variations and resulting principal stresses for a 100 km model base depth and TDL mantle density structure. The global model (a) contains no lateral stress boundary conditions. Mean outward stress values are assigned the same value as the reference column outside of (15^{o}N-85^{o}N-170^{o}W-10^{o}W) for the plate model (b) and (25^{o}N-55^{o}N-135^{o}W-25^{o}W) for the regional model (c).

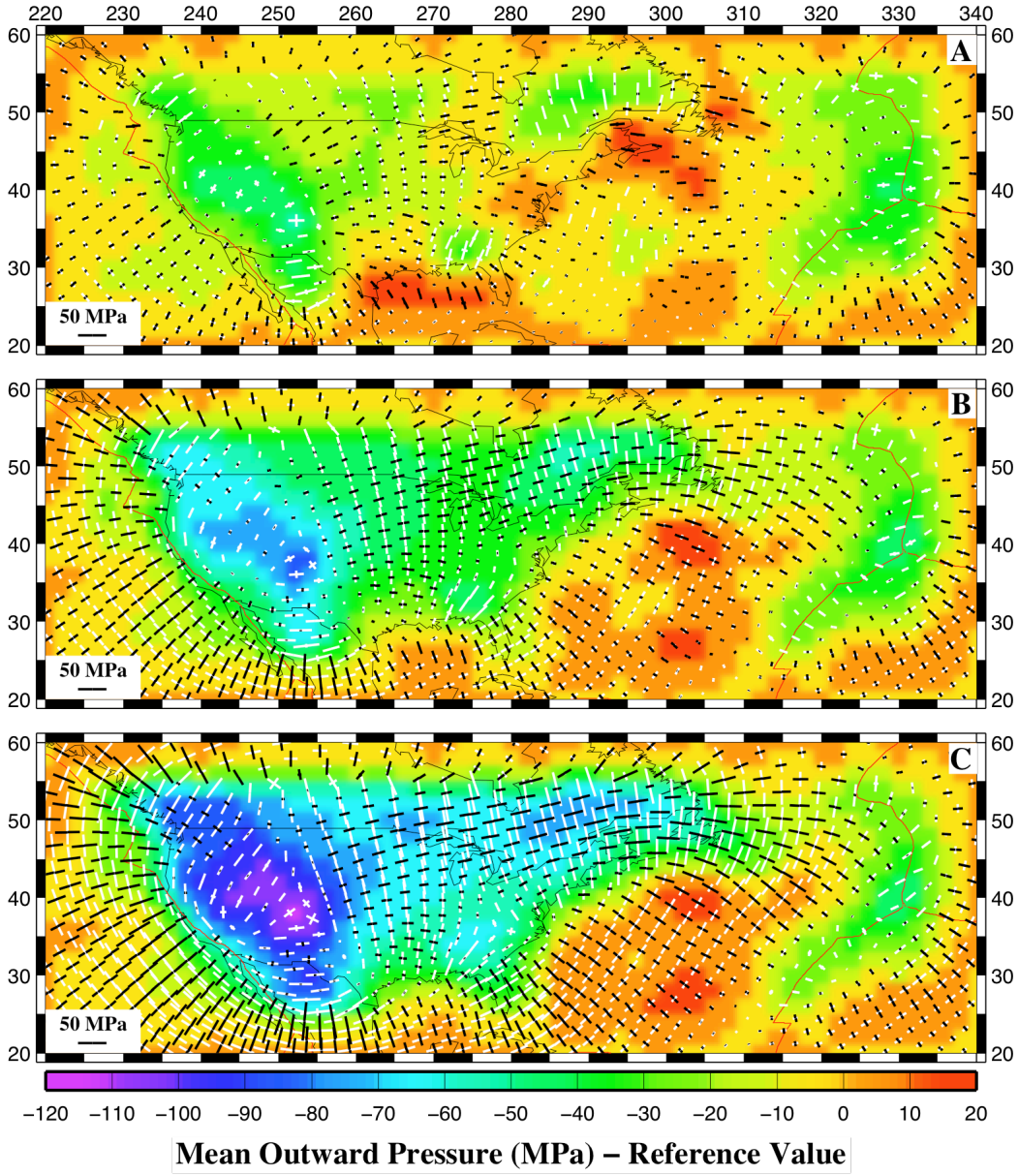

Figure 2.9: Mean outward stress and resulting principal stresses for a TDL mantle density structure, regional stress boundary conditions (25°N-55°N-135°W-25°W) and 100 km (a), 50 km (b) and 25 km (c) model base depths. The reference mean outward stress values for each model are 1482 MPa (a), 678 MPa (b) and 286 MPa (c).

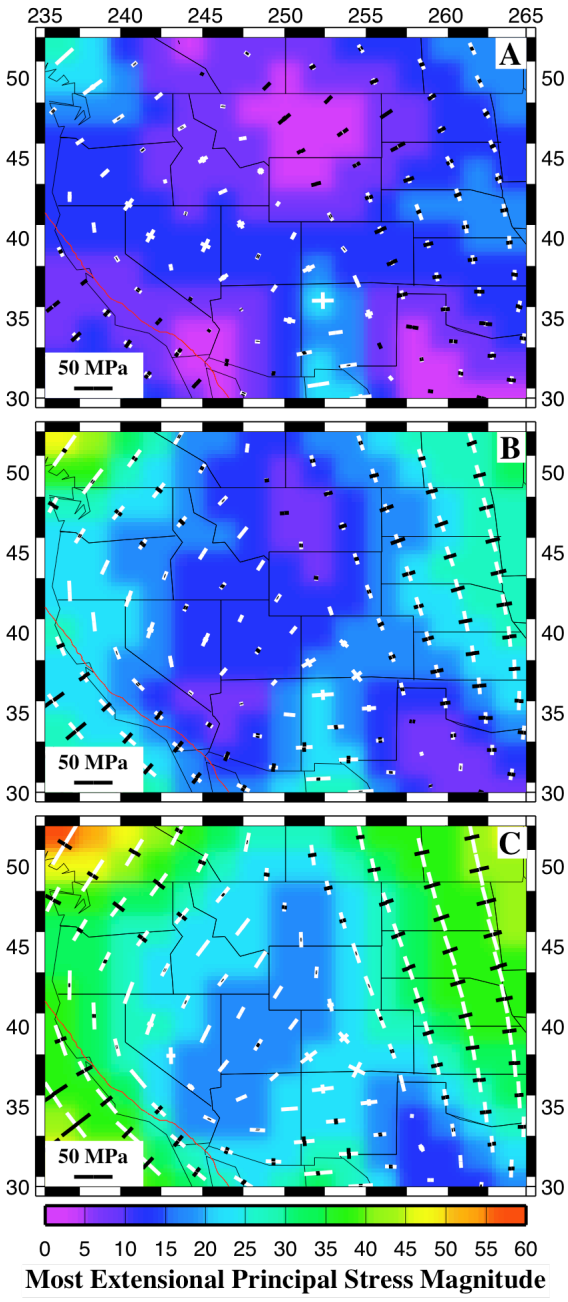

Figure 2.10: Western U.S. principal stresses and most extensional principal stress magnitude for a TDL mantle density structure, regional stress boundary conditions (25°N-55°N-135°W-25°W) and 100 km (a), 50 km (b) and 25 km (c) model base depths.

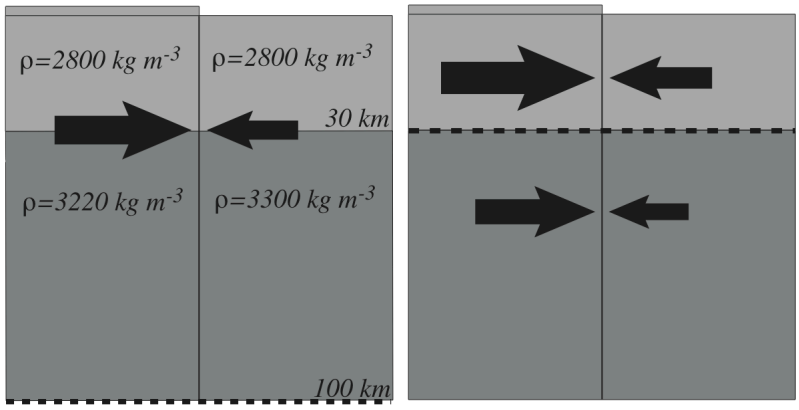

Figure 2.11: Density structure of two simplified lithospheric columns (left). The moho depth and crustal density are constant, while a 2 km elevation difference exists between the two columns. The mantle density in the topographically lower column (reference column) is 3300 kg m^{-3} and the mantle density of the topographically high column is adjusted to enforce isostatic compensation at 100 km depth. The arrows represent the total mean outward stress of each column, when the base depth is placed at the compensation depth. Moving the base depth to the moho (right) implies a horizontal stress gradient with depth, as the mean outward stress differences between the two columns varies above and below the base depth.

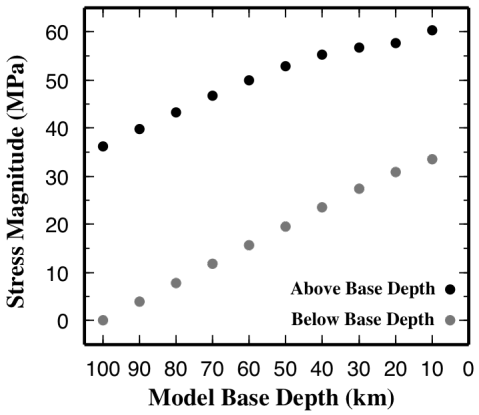

Figure 2.12: State of stress in the topographically high column illustrated in Figure 2.11. The state of stress is defined as the difference in mean outward stress between the topographically high and reference column. When the model base depth is placed above the compensation depth, distinct states of horizontal stress state exist above the base depth and between the base depth and isostatic compensation depth. The state of stress in any part of the topographically high column is extensional regardless of where the model base depth is placed.

2.9 References

Artemieva, I.M., 2006. Global $1^{o}x1^{o}$ thermal model TC1 for the continental lithosphere: Implications for lithosphere secular evolution, *Tectonophysics*, **416**, 245-277.

Artemieva, I.M. & Mooney, W.D., 2001. Thermal thickness and evolution of Precambrian lithosphere: A global study, *J. Geophys. Res.*, **106**(B8), 16837-16414.

Asimow, P., Hirschmann, M., Ghiorso, M., Ohara, M. & Stolper, E., 1995. The effect of pressure-induced solid-solid phase-transitions on decompression melting of the mantle, *Geochim. Cosmochim. Acta*, **59**(21), 2289–4506.

Artyushkov, E.V., 1973. Stresses in the lithosphere caused by crustal thickness inhomogeneities, *J. Geophys. Res.*, **78**, 7675-7708.

Bassin, C., Laske, G. & Masters, G. 2000. The Current Limits of Resolution for Surface Wave Tomography in North America, *EOS Trans. AGU*, **81**, F897.

Beaumont, C., Jamieson, R.A., Nguyen, M.H. & Medvedev, S. 2004. Crustal channel flows: 1. Numerical models with applications to the tectonics of the Himalayan-Tibetan orogen, *J. Geophys. Res.*, **109**(B06406), doi:10.1029/2003JB002809.

Bechtel, T.D., Forsyth, D.W., Sharpotn, V.L. & Grieve, R.A.F., 1990. Variations in effective elastic thickness of the North American lithosphere, *Nature*, **343**, 636-638.

Bendick, R. & Flesch, L., 2007. Reconciling lithospheric deformation and lower crustal flow beneath central Tibet, *Geology*, **35**(10), 895-898, doi:10.1130/G23714A.1.

Bird, P., 1989. New Finite Element Techniques for Modeling Deformation Histories of Continents with Stratified Temperature-Dependent Rheology, *J. Geophys. Res.*, **94**(B4), 3967-3990.

Bott, M.H.P. & Kusznir, N.J., 1979. Stress distributions associated with compensated plateau uplift structures with application to the continental splitting mechanism, *Geophys. J. R. Astr. Soc.*, **56**, 451-459.

Burov, E.B. & Watts, A.B., 2006. The long-term strength of continental lithosphere: ”jelly sandwhich” or ”creme brulee”?, *GSA Today*, **16**(1), 4-10.

Clark, M. K. & Royden, L. H., 2000. Topographic ooze: Building the eastern margin of Tibet by lower crustal flow, *Geology*, **28**, 703–706.

Coblentz, D.D., Richardson, R.M. & Sandiford, M., 1994. On The Gravitational Potential of the Earth’s Lithosphere, *Tectonics*, **13**(4), 929-945.

Dahlen, F. A., 1981. Isostasy and the ambient state of stress in the oceanic lithosphere, *J. Geophys. Res.*, **86**, 7801-7807.

England, P. & Houseman, G., 1986. Finite Strain Calculations of Continental Deformation. 2. Comparison with the India-Asia collision zone, *J. Geophys. Res.*, **91**(B3), 3664-3676.

England, P. & Houseman, G., 1988. The Mechanics of the Tibetan Plateau, *Philos. Trans. Roy. Soc. Lon.*, **326**(1589), 301-319.

England, P. & Houseman, G., 1989. Extension during continental convergence, with application to the Tibetan Plateau, *J. Geophys. Res.*, **94**(B12), 17561-17579.

England, P. & Molnar, P., 1997. Active deformation of Asia: From kinematics to dynamics, *Science*, **278**(5338), 647-650.

Fleitout, L. & Froidevaux, C., 1982. Tectonics and topography for a lithosphere containing density heterogeneities, *Tectonics*, **1**(1), 21-56.

Fleitout, L. & Froidevaux, C., 1983. Tectonic stresses in the lithosphere, *Tectonics*, **2**(3), 315-324.

Flesch, L.M., Holt, E.W, Haines, A.J. & Shen-Tu, B.M., 2000. Dynamics of the Pacific-North American plate boundary in the western United States, *Science*, **287**, 834-836.

Flesch, L.M., Haines, A.J. & Holt, E.W., 2001. Dynamics of the India-Eurasia collision zone, *J. Geophys. Res.*, **106**(B8), 16435-16460.

Flesch, L.M., Holt, E.W, Silver, P., Stephenson, M., Wang, C.-Y. & Chan, W., 2005. Constraining the extent of crust-mantle coupling in central Asia using GPS, geologic, and shear wave splitting data, *Earth. Planet. Sci. Letts.*, **238**(1-2), 248-268.

Flesch, L.M., Holt, E.W, Haines, A.J., Wen, L.X. & Shen-Tu, B.M., 2007. The dynamics of western North America: stress magnitudes and the relative role of gravitational potential energy, plate interaction at the boundary and basal tractions, *Geophys. J. Int.*, **169**, 866-896.

Ghosh, A., Holt, E.W., Flesch, L.M. & Haines, A.J., 2006. Gravitational potential energy of the Tibetan Plateau and the forces driving the Indian plate, *Geology*, **34**(5), 321-324.

Ghosh, A., Holt, E.W., Wen, L., Haines, A.J. & Flesch, L.M., 2008. Joint modeling of lithosphere and mantle dynamics elucidating lithosphere-mantle coupling, *Geophys. Res. Letts.*, **35**(L16309), doi:10.1029/2008GL034365.

Ghosh, A., Holt, E.W., Flesch, L.M. & Haines, A.J., 2009. Contribution of gravitational potential energy differences to the global stress field, *Geophys. J. Int.*, **179**, 787-812.

Goes, S. & van der Lee, S. 2002. Thermal structure of the North American uppermost mantle inferred from seismic tomography, *J. Geophys. Res.*, **107**(B3), doi:10.1029/2000JB000049.

Gung, Y.C., Panning, M. & Romanowicz, B., 2003. Global anisotropy and the thickness of continents, *Nature*, **422**, 707-711.

Gurnis, M., 1993. Phanerozoic marine inundation of continents driven by dynamic topography above subducting slabs, *Nature*, **364**, 589-593.

Gurnis, M., Mitrovica, J.X., Ritsema, J. & Heijst, H.J., 2001. Constraining mantle density structure using geological evidence of surface uplift rates: The case of the African Superplume, *Geochem. Geophys. Geosyst.*, **1**, 1999GC000035.

Hager, B.H, Clayton, R.W., Richards, M.A., Comer, R.P. & Dziewonski, A.M., 1985. Lower mantle heterogeneity, dynamic topography and the geoid, *Nature*, **313**, 541-545.

Hartz, E.H. & Podladchikov, Y.Y., 2008. Toasting the jelly sandwhich: The effect of shear heating on lithospheric geotherms and strength, *Geology*, **36**(4), 331-334.

Haxby, W.F. & Turcotte, D.L., 1978. On isostatic geoid anomalies, *J. Geophys. Res.*, **83**, 5473-5478.

Hibbit & Sorenson 2002. ABAQUS, version 6.6, *J. Geophys. Res.*, Pawtucket, R.I.

Holt, W., 2000. Correlated crust and mantle strain fields in Tibet, *Geology*, **28**(1), 67-70.

Houseman, G. & England, P., 1986. Finite strain calculations of continental deformation I: methods and general results for convergent zones, *J. Geophys. Res., **91***, 3651-3663.

Houseman, G. & England, P. 1993. Crustal thickening versus lateral expulsion in the Indian-Asian Continental Collision, *Geology*, **98**(B7), 12233-12249.

Humphreys, E.D. & Coblentz, D.D., 2007. North American dynamics and Western US *Tectonics*, *Rev. Geophys.*, **45**, RG3001, doi:10.1029/2005RG000181.

Jackson, J., 2002. Strength of the continental lithosphere: Time to abandon the jelly sandwhich?, *GSA Today*, **12**, 1-4.

Jimenez-Munt, I., Garcia-Castellanos, D., & Fernandez, M., 2005. Thin-sheet modeling of lithospheric deformation and surface mass transport, *Tectonophysics*, **407**, 239-255.

Jimenez-Munt, I., Garcia-Castellanos, D., Negredo, A.M. & Platt, J.B., 2005. Gravitational and tectonic forces controlling postcollisional deformation and the present-day stress field of the Alps: Constraints from numerical modeling, *Tectonics*, **24**, TC5009, doi:10.1029/2004TC001754.

Jones, C.H., Unruh, J.R. & Sonder, L.J., 1996. The role of gravitational potential energy in active deformation in the southwestern United States, *Nature*, **381**, 37-41.

Jones, C.H., Unruh, J.R., & Sonder, L.J. 1998. Lithospheric gravitational potential energy and past orogenesis: Implications for conditions of initial basin and range and Laramide deformations, *Geology*, **26**(7), 639-642.

Jordan, T.H. 1975. The Continental Tectosphere, *Rev. Geophys.*, **13**(3), 1-12.

Jaupart, C. & Mareschal, J., 1999. The thermal structure and thickness of continental roots, *Lithos*, **48**, 93–114.

Kaban, M.K., Schwintzer, P., Artemieva, M., & Mooney, W.D. 2003. Density of the continental roots: compositional and thermal contributions, *Earth Planet. Sci. Letts.*, **209**(1-2), 53-69.

Klein, E. & Langmuir, C., 1987. Global correlations of ocean ridge basalt chemistry with axial depth and crustal thickness, *J. Geophys. Res.*, **92**(B8), 8089–8115.

Klein, E.C., Flesch, L.M., Holt, E.W. & Haines, A.J., 2009. Evidence of long-term weakness on seismogenic faults in western North America from dynamic modeling, *J. Geophys. Res.*, **114**, B03402, doi:10.1029/2007JB005201.

Kohlstedt, D.L., Evans, B. & Mackwell, D.J., 1995. Strength of the lithosphere – constraints imposed by laboratory experiments, *J. Geophys. Res.*, **100**(B9), 17587-17602.

De Koker, N.P., Lithgow-Bertelloni, C. & Stixrude, L., 2005. Dynamic Topography and the Density Structure of the Mantle Lithosphere, *EOS Trans. AGU*, **86**(52), Fall Meet. Suppl., Abstract T23A-0524 .

Kusznir, N.J. & Bott, M.H.P., 1977. Stress concentrations in the upper lithosphere caused by underlying visco- elastic creep, *Tectonophysics*, **43**, 247-256.

van der Lee, S., 2002. High-resolution estimates of lithospheric thickness from Missouri to Massachusetts, *Earth Planet. Sci. Letts.*, **203**, 15-23.

Levander, A., Niu, F. & Miller, M.S., 2008. The Moho and the Lithosphere-Asthenosphere Boundary under the western U.S. from USArray PdS Receiver Functions, *EOS Trans. AGU*, **89**(53), Fall Meet. Suppl., Abstract S31D-05.

Li, X., Yuan, X. & Kind, R., 2007. The lithosphere-asthenosphere boundary beneath the western United States, *Geophys. J. Int.*, **170**(2), 700-710.

Liu, M., Shen, Y. & Yang, Y., 2000. Gravitational collapse of orogenic crust: A preliminary three- dimensional finite element study, *J. Geophys. Res.*, **105**(B2), 3159-3173.

Liu, M. & Yang, Y., 2003. Extensional collapse of the Tibetan Plateau: Results of three-dimensional finite lement modeling, *J. Geophys. Res.*, **108**(B8), 2361, doi:10.1029/2002JB002248.

Lithgow-Bertelloni, C. & Richards, M.A., 1998. The Dynamics of Cenozoic and Mesozoic Plate Motions, *Rev. Geophys.*, **36**(1), 27-78.

Lithgow-Bertelloni, C. & Silver, P.G., 1998. Dynamic topography, plate driving forces and the African superswell, *Nature*, **395**, 269-272.

Lithgow-Bertelloni, C. & Guyn, J.H., 2004. Origin of the lithospheric stress field, *J. Geophys. Res.*, **109**, B01408, doi:10.1029/2003JB002467.

Lowry, A.R. & Smith, R.B., 1994. Flexural rigidity of the Basin and Range-Colorado Plateau-Rocky Mountain transition from coherence analysis of gravity and topography, *J. Geophys. Res.*, **99**(B10), 20,123-20,140.

Lowry, A.R. & Smith, R.B., 1995. Strength and rheology of the western U.S. Cordillera, *J. Geophys. Res.*, **100**(B9), 17,947-17,963.

Lowry, A.R., Ribe, N.M. & Smith, R.B., 2000. Dynamic elevation of the Cordillera, western United States, *J. Geophys. Res.*, **105**(B10), 23,371-23,390.

Masters, G. & Gubbins, D., 2003. On the resolution of density within the earth, *Phys. Earth Planet. Inter.*, **140**, 159–167.

Medvedev, S.E. & Podlacdchikov, Y. 1999. New extended thin-sheet approximation for geodynamic applications-I. Model formulation, *Geophys. J. Int.*, **136**, 567-585.

Michaut, C. & Jaupart, C., 2004. Nonequilibrium temperatures and cooling rates in thick continental lithosphere, *Geophys. Res. Lett.*, **31**, L24602.

Mitrovica, J.X., Beaumont, C. & Jarvis, G.T., 1989. Tilting of Continental Interiors by the Dynamical Effects of Subduction, *Tectonics*, **8**(5), 1079-1094.

Molnar, P. & Tapponier, P., 1978. Active *Tectonics* of Tibet, *J. Geophys. Res.*, **83**(B11), 5361-5375.

Molnar, P. & Lyon-Caen, H., 1988. Some simple physical aspects of the support, structure, and evolution of mountain belts, *Geol. Soc. Amer. Spec. Paper.*, **218**, 179-207.

Molnar, P., England, P. & Martinod, J. 1993. Mantle dynamics, uplift of the tibetan plateau, and the Indian monsoon, *Rev. Geophys.*, **31**(4), 357-396.

Moucha, R., Forte, A.M., Rowley, D.B., Mitrovica, J.X., Simmons, N.A. & Grand, S.P., 2008. Mantle convection and the recent evolution of the Colorado Plateau and the Rio Grande Rift valley, *Geology*, **36**(6), 439-442.

Muller, R., Roest, W., Royer, J.-Y., Gahagan, L. & Sclater, J., 1997. Digital isochrons of the world's ocean floor, *J. Geophys. Res.*, **102**, 3,211–3,214.

Pascal, C., 2006. On the role of heat flow, lithosphere thickness and lithosphere density on gravitational potential stresses, *Tectonophysics*, **425**(1-4), 83-99.

Pollack, H. & Chapman, D., 1977. On the regional variation of heat flow, geotherms, and lithospheric thickness, *Techtonophysics*, **38**, 279–296.

Pysklewec, R.N., Beaumont, C. & Fullsack, P., 2002. Lithospheric deformation during the early stages of continental collision: Numerical experiments and comparison with South Island, New Zealand, *J. Geophys. Res.*, **107**(B7), doi:10.1029/2001JB000252.

Regenauer-Lieb, KL., Weinberg, R. & Rosenbaum, G., 2006. The effect of energy feedbacks on continental strength, *Nature*, **442**, 67-70.

Richardson, R.M., 1992. Ridge Forces, Absolute Plate Motions, and the Intraplate Stress Field, *J. Geophys. Res.*, **97**(B8), 11,739-11,748.

Richardson, R.M., Solomon, S.C. & Sleep, N.H., 1978. Tectonic Stress in the Plates, *Rev. Geophys.*, **17**(5), 981-1019.

Richardson, R.M. & Redding, L.M., 1991. North-American plate dynamics, *J. Geophys. Res.*, **96**(B7), 12,201-12,223.

Royden, L., 1996. Coupling and decoupling of crust and mantle in convergent orogens: Implications for strain partitioning in the crust, *J. Geophys. Res.*, **101**(B8), 17,679-17,705.

Royden, L.H., Burchfiel, B.C., King, R.W., Wang, E., Chen, Z., Shen, F. & Liu, Y., 1997. Surface Deformation and Lower Crustal Flow in Eastern Tibet, *Science*, **276**, 788-790.

Rudnick, R.L., McDonough, W.F. & O'Connell, R.J., 1998. Thermal structure, thickness and composition of continental lithosphere, *Chem. Geo.*, **145**(3-4), 395-411.

Steinberger, B., Schmeling., H. & Marquart, G., 2001. Large-scale lithospheric stress field and topography induced by global mantle circulation, *Earth Planet. Sci. Letts.*, **186**(1), 75-91.

Stixrude, L. & Lithgow-Bertelloni, C., 2005. Thermodynamics of mantle minerals - I. Physical properties, *Geophys. J. Int.*, **162**(2), 610-632.

Thatcher, W. & Pollitz, F.F., 2008. Temporal evolution of continental lithospheric strength in actively deforming regions, *GSA Today*, **18**(4/5), 4-11, doi:10.1130/GSAT01804-5A.1

Thybo, H., Perchuc, E. & Zhou, S. 2000. Intraplate earthquakes and a seismically defined lateral transition in the upper mantle, Geophys. Res. Letts, **27**(23), 3953-3956.

Turcotte, D.L., 1983. Mechanisms of crustal deformation, *J. Geol. Soc.*, **140**(5), 701-724.

Turcotte, D.L. & Schubert, G., 2002. Geodynamics, *Copy-editing*:, 2nd edn, Cambride Univ. Press, Cambridge.

Xu, X., Lithgow-Bertelloni, C. & Conrad, C., 2006. Reconstructions of cenozoic seafloor ages: Implications for sealevel, *Earth Planet. Sci. Lett.*, **243**, 552-564.

Zandt, G., Myers, S.C. & Wallace, T.C., 1995. Crust and mantle structure across the Basin and Range- Colorado Plateau boundary at 37N latitude and implications for Cenozoic extensional mechanism, *J. Geophys. Res.*, **100**(B6), 10,529-10,548.

Zoback, M.L., 1992. 1st-Order and 2nd-Order Patterns of Stress in the Lithosphere - The World Stress Map Project, *J. Geophys. Res.*, **97**(B8), 11,703-11,728.

Zoback, M.L. & Mooney, W.D., 2003. Lithospheric Buoyancy and Continental Intraplate Stresses, *Int. Geol. Rev.*, **45**, 95-118.

CHAPTER III

The Contribution of Dynamic Topography to the Lithospheric Stress Field

3.1 Abstract

Surface topography supported by convective flow generates lithospheric stress patterns distinct from those balancing isostatically compensated topography and density variations. Here, we explore the contribution of dynamic topography to global stress patterns associated with the lithosphere's observed topography and density structure. Dynamic topography is determined through isostatic analysis of lithospheric structure or modeling of density-driven mantle flow. Lithospheric stress patterns balancing lateral gradients in gravitational potential energy exhibit globally averaged magnitude changes of 3-10 MPa when dynamic topography is removed from observed topography. These globally averaged changes in stress magnitude are only moderately sensitive to both mantle density structure and orders of magnitude variations in the lithosphere-asthenosphere contrast. On a regional basis, however, changes in stress magnitude often depend strongly on the assumed model of dynamic topography, although stress patterns in regions of prolonged subduction exhibit a strong dependence on dynamic topography regardless of the lithosphere-asthenosphere viscosity contrast. We also find that the magnitude of lithospheric membrane stresses generated by instantaneous dynamic uplift are comparable to the magnitude of stresses associated with variations in topography and

density, if the lithosphere exhibits significant elastic strength on the time scales over which dynamic topography is developed. The results presented here highlight the need to carefully assess the contribution of dynamic topography to regional stress patterns and consider the effects of variable lithospheric rheology.

3.2 Introduction

From the seminal works of Artyushkov (1973) to our recent detailed study of the influence of lithospheric structure on stresses (Chapter II, Naliboff et al., to be submitted) it is evident that topography at short and long wavelengths can have a dominant influence on the state of stress of the lithosphere, yet our understanding is hampered by incomplete knowledge of the origin of topography at a variety of length-scales. Far from solving the problem, new observations in our age of satellite altimetry have revealed our ignorance. What then determines Earth's topography and bathymetry?

Topography and bathymetry on Earth are an expression of the force balance acting on its free surface. This balance has an isostatic and a dynamic component on length scales exceeding the flexural strength of the lithosphere (~300 km, Watts 2001). The isostatic contribution arises from lateral variations in the density structure of the lithosphere and sub-lithospheric mantle, discussed at length in Chapter II, while the dynamic contribution is the displacement of Earth's surface in response to mantle flow. At long wavelengths, dynamic topography is the most important contributor to Earth's topography and it is the largest component of geoid anomalies (Ricard et al. 2006) as established in classic studies of the geoid (Richards & Hager 1984). Dynamic topography is important in continental (Lithgow-Bertelloni & Silver 1998; Daradich et al., 2003;

Gurnis et al. 2000; Conrad & Gurnis 2003) and oceanic regions (Cazenave & Thoraval 1994; Conrad et al. 2004) and can explain the anomalous depths of large sedimentary basins (Pysklywec & Mitrovica1999). Dynamic topography may cause tilting of entire continents (Mitrovica et al. 1989; Gurnis 1990, Sandiford 2007; DiCaprio et al. 2009) and influence the shape of the ocean surface via its effect on the geoid. The connection to continental flooding is immediate: as continents migrate over mantle upwellings (regions of positive dynamic topography) and downwellings (negative dynamic topography) the large vertical motions can lead to the emergence and submergence of entire regions (Figure 2) (Gurnis 1993; Lithgow-Bertelloni & Gurnis 1997). Indeed, time variations in dynamic topography can explain much of the Phanerozoic flooding record (Gurnis 1993). More recently, measures of dynamic topography have been used to constrain mantle dynamical models of inundation of North America (Liu et al. 2008; Spasojevic et al. 2008, 2009) and reconcile stratigraphically derived sea level curves (Miller et al. 2005), with sea level curves derived from changing mid-ocean ridge volume (Müller et al. 2008).

Of interest to us is that the presence of dynamic topography at long and short-wavelength may have a strong influence on the state of stress in areas of long-lived subduction such as Southeast Asia (Lithgow-Bertelloni & Guynn, 2004). By deflecting the Earth's surface, dynamic topography can give rise to regions of compression (over downwarps) and of extension (over uplifted regions) both by changing the gravitational potential and by the long-wavelength bending of the lithosphere (Lithgow-Bertelloni & Guynn, 2004). Because mantle flow gives rise to both radial and horizontal stresses that act on the bottom lithosphere, previous work on the effects of mantle flow on the state of

stress of either an elastic or viscous lithosphere had included the effects of dynamic topography (Bai et al. 1992; Steinberger et al. 2001). Its critical role however, was most emphasized in the study of Lithgow-Bertelloni & Guynn (2004), which realized that for an elastic shell, the presence of dynamic topography is determinant for the stress regime induced in the lithosphere by coupling with the mantle. Moreover, in areas of prolonged subduction such as SE Asia the coherency and azimuth of the compressive stress as seen by the World Stress Map (WSM) can only be reproduced by the stress response of the lithosphere to the dynamic topography predicted by mantle flow models for this region. This response is not altered dramatically by the presence of a low viscosity asthenosphere, as we expect normal stresses to be effectively transmitted across rheological boundaries (Chapter IV, Naliboff et al. 2009, in press). Therefore, areas of strong dynamic topography may also exhibit the strongest coupling between the lithosphere and mantle. As Earth's topography includes a dynamic component, studies of lithospheric sources of stress must account for dynamic topography (Steinberger et al. 2001; Lithgow-Bertelloni & Guynn 2004; Ghosh et al. 2009; Chapter II, Naliboff et al., submitted).

Yet despite the advances presented by these studies, the efforts cannot be considered definitive for two reasons: 1) while it is difficult to constrain uniquely from observations, indications are that observed dynamic topography on Earth has smaller amplitude than that predicted by mantle flow models (Colin & Fleitout 1990; Le Stunff & Ricard 1995; Wheeler & White 2000; Mooney & Vidale 2003; Winterbourne et al. 2009); 2) no study to date has presented a comprehensive quantitative analysis of the changes in

lithospheric stress magnitudes and patterns generated by dynamic topography as a function of the parameters that control it (mantle density and viscosity heterogeneity).

Indeed, mantle flow models commonly predict amplitudes of dynamic topography to be on the order of 1500 m, which is larger than expected given current estimates of the isostatic contribution (Colin & Fleitout 1990; Thoraval et al. 1995; Le Stunff & Ricard 1995; Panasyuk and Hager 2000a). Unequivocal signals of "observed" dynamic topography, measured as observed topography less the expected isostatic contribution, are rare and seemingly nonexistent at the expected amplitudes at regions of mantle downwelling (Wheeler & White, 2000; Winterbourne et al., 2009). At the global scale "observed" dynamic topography is problematic because removing the isostatic contribution depends on detailed knowledge of lithospheric structure.

A variety of studies have attempted to explain these discrepancies, exploring the effects of lateral viscosity variations in the mantle (Cadek & Fleitout 2003), barriers to flow at 660 km depth (Thoraval et al. 1995), the presence or absence of plates (Thoraval & Richards 1997), pressure-induced crystal phase transformations in the olivine component of the mantle (Thoraval et al. 1995; Christensen 1998; Steinberger 2007) and small scale convection under oceanic plates (Winterbourne et al. 2009). However, none have provided a satisfying resolution to the mismatch between observed and modeled global dynamic topography. It must always be remembered that the predicted amplitudes of the dynamic topography are what give rise to the excellent fits to observed geoid anomalies (Ricard et al. 1993; Forte & Mitrovica 2004).

The goal of this study is hence twofold. First, to comprehensively examine the sensitivity of global stress patterns and magnitudes to the presence of long- and medium-

wavelength dynamic topography using a wide array of dynamic topography predictions. These predictions are derived using a mantle flow model where dynamic topography is a function of mantle density and viscosity structure, or from a new complete model of lithospheric structure and the associated isostatic contribution to topography. Second, use the computed stress models to place an additional constraint on the likely amplitude of dynamic topography and set the stage for an examination of plate-mantle coupling due to viscosity heterogeneity in the mantle (Chapter III).

3.3 Theory and Methods

Dynamic topography is the deflection by radial stresses of any surface across which there is an inherent bulk compositional density difference, such as the crust-air(water) interface at the surface of our planet or the core-mantle boundary. The deflection redistributes mass (substituting air or water for rock in uplifted areas and vice versa in subsiding regions) affecting Earth's gravitational potential. Because dynamic topography is a result of Earth's viscous flow, the time-scales over which it is established (once the driving force is in place) is governed by the viscosity of the mantle and it is comparable to the time-scales of post-glacial rebound (10-100,000 years). Generally, the transient effects are ignored and we only consider the dynamic topography in the viscous limit. However, depending on load wavelength, elastic effects may be important for the total uplift and the evolution of the uplift (Barletta & Sabadini 2006).

The amplitude of the dynamic deflection is $h_{dyn}=-\tau_{rr}/\delta\rho g$, where τ_{rr} is the radial stress component produced by flow in the mantle, $\delta\rho$ is the density contrast between crust-air or crust-water and g is the gravitational acceleration. The stress response of the

lithosphere to dynamic topography can be illustrated by the simple carton in Figure 3.1 below. The radial stresses that give rise to dynamic topography produces two types of stresses: membrane stresses σ_{MEM} due to stretching of the lithosphere and gravitational stresses due to the topographic gradient. If we consider then the total topography (h_{tot}) and its stress response we can write in the terminology of Chapter II:

$$\sigma_{tot}(r) = \sigma_{ILS}\left(\frac{\partial\Omega(h_{iso})}{\partial r}\right) + \sigma_{ILS}\left(\frac{\partial\Omega(h_{dyn})}{\partial r}\right) + \sigma_{mem}(h_{dyn}) \tag{3.1}$$

where the different contributions to the stress σ are functions of the radial gradient in Ω (the integrated lithostatic stress from equation 2.4 in Chapter II) for both the isostatic (h_{iso})and dynamic (h_{dyn}) contributions to topography. It becomes clear from this equation that removing the dynamic component of the topography to examine the effects of lithospheric sources alone must be done carefully. The effects of dynamic topography on stress field patterns related to Ω can be examined by studying the effects of the radial stresses themselves (Lithgow-Bertelloni & Guynn 2004) or by subtracting different predictions and estimates of dynamic topography from a reference lithospheric structure (Ghosh et al. 2009). Here we take the latter approach.

To quantify the effects of dynamic topography on lithospheric stress patterns we perform four independent steps. The first three steps involve calculating dynamically supported surface topography, adjusting a reference lithospheric structure to remove the estimated dynamic topography and calculating the stress patterns associated with each lithospheric structure. The difference between the stress patterns associated with each lithospheric structure quantifies the effects of dynamic topography on the lithospheric stress field associated with variations in topography and density. We then separately

consider the membrane stresses generated by instantaneous dynamic displacement of the lithosphere.

3.4 Dynamic and Residual Topography

To calculate the magnitude of dynamically supported surface topography we either compute it directly from mantle flow or use a model of residual topography, which we describe below. To calculate radial stresses at the base of the lithosphere, we solve for instantaneous viscous flow induced by mantle density heterogeneity. Viscous flow is calculated by solving the equations of conservation of mass and momentum for an incompressible Newtonian fluid via propagator matrices (Hager & O'Connell 1981) up to spherical harmonic degree 20 (λ~2000 km). The density contrast between the surface (air ~ 0 kg m^{-3}, water 1020 kg m^{-3}) and lithosphere used to compute the dynamic deflection (h_{dyn}) is determined using the crustal density values from Crust 2.0 (Bassin et al. 2000) and a fixed mantle density of 3300 kg m^{-3}.

We use two different models of mantle density heterogeneity, one derived from subduction history (Lithgow-Bertelloni & Richards 1998), which has proven very successful at predicting geoid anomalies (Ricard et al. 1993) and plate driving forces (Lithgow-Bertelloni & Richards 1998) and the shear wave velocity tomography of Ritsema et al. (2004, s20rtsb). For the latter, seismic velocity is converted to density assuming that all heterogeneity is thermal in origin and using a constant velocity-density scaling factor of 0.15 g cm^{-3} km^{-1} s (Stixrude & Lithgow-Bertelloni 2007). Hence, for the seismic model the upper 325 km are excluded because we expect velocities at these

depths to be affected by lithospheric compositional variations, particularly under continents.

The viscosity structure is layered (radially symmetric) and consists of four distinct layers (lithosphere 0-120 km, asthenosphere 120 – 220 km, upper mantle 220 – 660 km, lower mantle 660 – 2900 km). The lithosphere and upper mantle are 10 and 50 times as viscous than the reference upper mantle viscosity, while the asthenospheric viscosity ranges from 1 to 1000 times less viscous than the upper mantle. The low viscosity of the lithospheric layer reflects the fact that the lithosphere is mobile and represents an approximate average over regions of high and very low viscosity. Varying the asthenospheric viscosity by 3 orders of magnitude impacts the amplitude of dynamic topography (Figure 3.2), but variations in the lower mantle viscosity within reasonable constraints (e.g. Mitrovica & Forte 2004) have relatively little impact on estimates of density-driven dynamic topography (e.g. Lithgow-Bertelloni & Richards 1998; Gurnis et al. 2000). This is not surprising as the dynamic topography kernels at all spherical harmonic degrees peak strongly in the upper mantle and decay quickly in the lower mantle (Hager & Richards 1989; Simmons et al. 2009). Lateral variations in asthenospheric thickness associated with different tectonic provinces have also been shown to have a negligible impact on radial traction magnitudes associated with density-driven flow (Gurnis et al. 2000; Chapter IV, Naliboff et al. 2009).

Numerous previous studies have similarly studied dynamic topography from flow induced by seismic heterogeneity at global (e.g. Steinberger 2006) and regional (Gurnis et al., 2000; Conrad et al. 2004; Moucha et al. 2008) scales, including the only unequivocal signal of dynamic topography (Lithgow-Bertelloni & Silver 1998). Because

dynamic topography kernels have greater sensitivity in the upper mantle, the dynamic topography signals from s20rtsb miss part of the signal arising from heterogeneity in the upper 300 km of the mantle, which may be important (e.g. Simmons et al. 2006; Simmons et al. 2009), although likely at length-scales much shorter than the flow analyzed here. We do not include the plate-driven convective flow to dynamic topography, due its strong dependence on absolute mantle viscosity (e.g. Cadek and Fleitout 2003; Conrad et al. 2007). In addition, imposing piece-wise continuous velocity boundary conditions on a viscous fluid leads to stress singularities, which give rise to artificially large stresses (and larger dynamic topography when plates move fast). This could be overcome by a complete knowledge of plate boundary rheology.

Nonetheless, the presence of very shallow mantle heterogeneity and contributions from plate flow in slow moving plates such as the Northern Atlantic may reconcile estimates of residual topography (observed dynamic topography) from lithospheric structure and dynamic topography from mantle flow models (Winterbourne et al. 2009). Because our focus is on the largest length-scales of the flow (> 2000 km) we expect that neither the absence of heterogeneity at the shallowest depths, nor the absence of plates will significantly affect the results shown here.

At the other end we consider a new estimate of global residual topography as "observed" dynamic topography (De Koker et al. 2005) derived from a 2^{o}x2^{o} lithospheric density model (hereby referred to with the acronym TDL). Crustal thickness and density is taken from Crust 2.0 (Bassin et al. 2000) and mantle densities are calculated using the thermodynamic approach of Stixrude & Lithgow-Bertelloni (2005), which determines equilibrium properties for a specified temperature, pressure and composition. The mantle

is divided into chemically depleted (harzburgite) and undepleted (lherzolite) layers, whose thickness and temperature varies according to the tectonic provinces in Crust 2.0. Specific details regarding the composition, temperature and thickness of the mantle were provided in Chapter II, section 2.4.2.2. The lithospheric model extends to 350 km depth, where the globally averaged pressure matches PREM. Global residual topography is determined by subtracting predicted isostatic topography (relative to a specified reference column) from observed topography, which gives the magnitude of non-isostatic (residual) surface topography, i.e. "observed" dynamic topography.

The inherent uncertainty associated with different estimates of lithospheric density structure often results in highly variable estimates of global residual topography (Forte et al. 1993; Le Stunff & Ricard 1995; Panasyuk & Hager 2000a, Kaban et al. 2003; Steinberger 2007). The different assumptions used in each study make it difficult to compare absolute magnitudes of residual topography, and it is beyond the scope of this study to analyze the origins of those differences. However, the TDL model made some considerable advances by treating the petrological origin of the mantle lithosphere and computing its physical properties (particularly density) with a self-consistent thermodynamic method for the first time. At length-scales shorter than 1000 km, careful regional analysis is often required to detect significant non-isostatic topographic signals, which would otherwise go undetected (Lowry et al. 2000; Artemieva 2007; Crosby and McKenzie 2009; Winterbourne et al. 2009).

For the long wavelengths of interest here (> 2000 km) our study should place some additional constraints on the likely magnitude of residual topography and illustrate

how stress patterns change when both deep and shallow sources of dynamic displacement are taken into account compared to the density-driven flow models.

3.5 Lithospheric Structure and Stress Patterns

We consider two sets of lithospheric structures for which stress patterns are calculated. The first set contains observed topography and crustal structure from Crust 2.0 (Bassin et al. 2000). The mantle densities are either adjusted to enforce isostatic compensation or taken from the TDL model. The thickness of the mantle lithosphere is the distance between the Moho and uniform global base depth. This set of lithospheric structures reflects the hypothesis that all topography reflects lithospheric processes and is not dynamically supported. The second set of lithospheric structures removes the calculated dynamic or residual topography from surface topography. For the case of dynamic topography, the mantle density structure is readjusted to enforce isostatic compensation at the selected base depth. For the case of residual topography, the thermodynamically determined mantle densities are unchanged.

Lithospheric stress patterns associated with variations in topography and density are computed with the assumption that the lithosphere behaves in a vertically coherent manner. Following this assumption, the lithostatic pressure is integrated over the thickness of each $2^{o}x2^{o}$ column from the specified global base depth. Dividing the integrated pressure by the global base depth gives the mean outward stress of each lithospheric column. Stresses balancing variations in mean outward stress are computed via the finite element method following the procedure of Lithgow-Bertelloni & Guynn (2004), which is outlined in detail in Chapter II. This procedure assumes a uniform

elastic rheology for the lithosphere, with a fixed Young's modulus of 10^{11} Pa and a Poisson's ratio of 0.3. The lithosphere consists of 100 km thick 2^{o}x2^{o} continuum shell elements and is underlain by a second layer of elements with a low Young's modulus (10^{6} Pa) and pinned basal nodes. The large strength contrast between the upper and lower element layers prevents the pinned basal nodes from modifying stresses patterns in the upper layer. A second type of model considers the membrane stresses generated by dynamic topography. In these models the upper (lithospheric) layer of elements are radially displaced according to the magnitude of dynamic topography. The resulting stresses in each element are isotropic (pure extension or compression) and depend only on the magnitude of radial displacement and the Young's modulus of the upper layer, which varies between 10^{11} and 10^{10} Pa. The magnitude of the membrane stresses is compared to the magnitude of stresses resulting from variations in lithospheric topography and density.

3.6 Results

Patterns of dynamic topography determined from density-driven mantle flow (Figure 3.2) depend almost entirely on the specified density heterogeneity and are affected minimally by the viscosity contrast across the lithosphere-asthenosphere boundary. This is what we expect, as the global low viscosity channel does not alter the pattern of flow only the ability of stresses to transmit effectively across the rheological boundary. Mantle densities determined from the seismic velocity model (Figure 3.2, left panel) generate dynamic topography lows and highs, respectively, along subduction zones and in regions associated with hotspot volcanism (i.e., Iceland, Central Pacific,

Eastern Africa) and large scale upwellings. Mantle densities determined from a history of slab subduction (Figure 3.2, right panel) generate strong dynamic lows over subduction zones and more distributed dynamics highs near mid-ocean regions that reflect counter flow from slab downwellings. The amplitudes of dynamic topography are larger for the subduction model, because slabs represent the largest source of buoyancy in the mantle and this amplitude is not captured in the highly damped shear wave tomographic models, which also tend not to properly image slabs in the upper mantle. Systematically decreasing the lithosphere-asthenosphere viscosity contrast from 10 (Figure 3.2, top row) to 10000 (Figure 3.2, bottom row) decreases the coupling between the convecting mantle and lithosphere, although the resulting decrease in dynamic topography is comparatively minor compared to the change in viscosity, a factor of ~0.6 when the contrast is 10000. Physically we expect that rheological boundaries will affect shear stresses more than radial stresses, which should still effectively transmit across them (Chapter IV, Naliboff et al. 2009, in press). This also implies that decoupling the lithosphere entirely from the mantle is not possible for lithosphere-asthenosphere viscosity contrasts within the range of geophysical observation and in line with previous results concerning the role of the mantle in driving plate motions (Lithgow-Bertelloni & Richards 1995).

Estimated residual topography from the TDL lithospheric structure contains many similar features to the convection driven dynamic topography patterns, with prominent residual topography along certain subduction boundaries, the central Pacific, Iceland, and Eastern Africa (Figure 3.3). Notably, the magnitude of residual topography in Eastern Africa is approximately a factor of 2 higher than for the convection driven model (Figure

3.2, top left panel). The residual topography model also contains multiple regions with strong amplitudes of positive (Antarctica, Tibet, Eastern Atlantic, Northernmost North America plate) and negative (Western Europe, Eastern North America) residual topography not present in either convection driven dynamic topography model. This reflects either uncertainty in the specified lithospheric structure or dynamic displacement driven by unaccounted for shallow heterogeneity.

On a regional basis, changes in stress patterns strongly depend on the magnitude of dynamic or residual topography. The removal of up to 2 km of dynamic subsidence in Southeast Asia (Figure 3.2, model SLB1000) generates strong extension throughout Indonesia and reduces compressional magnitudes associated with the elevated Tibetan Plateau (Figure 3.4). In Eastern Africa, removing up to 0.75 km of dynamic uplift has comparatively little impact on the stress patterns associated with the highest regions of uplift (Figure 3.5), although adjacent regions in the North Atlantic and India Ocean exhibit noticeable changes in stress patterns. In contrast, removing the calculated residual topography effectively eliminates the large topographic relief in Southern and Eastern Africa, and as a consequence significantly changes the stress patterns throughout Continental Africa and the Western Indian Ocean (Figure 3.6). The difference between the African stress patterns within dynamic or residual topography removed indicates that shallow upper mantle or deep lithospheric processes contribute significantly to the high elevation and extensional tectonics of Eastern Africa, as discussed by Zoback (1992) in relation to the world stress map.

On a global scale, we assess the effects of removing dynamic or residual topography by computing globally averaged changes in stress magnitude (Table 3.1).

The changes in stress magnitude generated by removing dynamic topography from the lithospheric structure is computed at each element between corresponding pairs of most extensional or most compressional principal stress values. The mean stress change of the two principal stress values is then averaged globally, which we find gives average changes in stress magnitude ranging between ~ 3-10 MPa. The higher changes in average stress magnitude correspond to models with larger amplitudes of dynamic topography.

The percentage of any given model (global histogram distribution) that has a specific percentage change in stress magnitude (Figure 3.7) illustrates this variability within each model. Peaks in the global distribution are centered over stress magnitude changes of 1 MPa for both dynamic and residual topography models (Figure 3.7, left panel). Notably, these peak values only account for 9-13% of the total model and the global distribution systematically decreases from the peak values (1 MPa) to higher changes in stress magnitude. The global distribution peak of the s20rtsb dynamic topography model is noticeably higher than the TDL and SLB models, which reflects the smaller dynamic topography amplitudes generated from the seismic velocity based model. Increasing the lithosphere-asthenosphere viscosity contrast decreases the magnitude of dynamic topography, thereby increasing height of the global distribution peak (Figure 3.6, right panel), although the character of the curve only changes dramatically at a contrast of 10000. In other words, decreasing the lithosphere-asthenosphere viscosity contrast increases the influence of dynamic topography on global lithospheric stress magnitudes, as shown in Table 1, because the radial stresses are transmitted more effectively when the viscosity contrast is lower

The magnitude of membrane stresses generated by instantaneous radial displacement depends directly on both the magnitude of displacement and the strength of the lithosphere (Figure 3.8). For a Young's modulus of 10^{11}, isotropic stress magnitudes (extensional or compressional) are on the order of 10's of MPa. Decreasing the Young's modulus by an order of magnitude results in a proportional decrease in the stress magnitudes, due to the choice of a linearly elastic rheology and because we specify the amount of displacement. As lithospheric stress magnitudes related to variations in topography and density are on the order of 10's of MPa, membrane stresses associated with dynamic uplift may control regional stress patterns if the magnitude of dynamic uplift is large.

3.7 Discussion and Conclusions

The results presented here demonstrate that the sensitivity of the lithospheric stress field to different estimates of dynamic topography largely depends on both the length-scale and specific region one considers. In Southeast Asia, prolonged subduction still promotes strong regional compression even with the presence of a 10000x viscosity jump across the lithosphere-asthenosphere boundary. In Eastern and Southern Africa, however, removing dynamic topography related to density-driven mantle flow with a much a stronger asthenosphere generates only minimal changes in regional stress patterns, while removing residual topography roughly a factor of 2 larger produces significant changes in regional stress patterns. In contrast, globally averaged changes in stress magnitude fall consistently between 3-10 Ma and are fairly insensitive to both mantle viscosity and density structure.

These findings illustrate a number of key points. First, it is clear that even for very large lithosphere-asthenosphere viscosity contrasts, stress patterns in regions associated with prolonged subduction will still be strongly coupled to radial mantle flow. Placing firm constraints on the stress patterns associated with dynamic topography, however, must be done very carefully as the example of Eastern and Southern Africa clearly demonstrates how different dynamic topography estimates can either have little effect or control regional dynamics. Considering this sensitivity, future calibrations of the contribution of dynamic topography to regional stress patterns should be done in regions where high resolution estimates of lithospheric structure are available. The topographically high and actively extending Western US may serve as an ideal location to perform such calibrations, as active uplift related to upper mantle processes may support some areas of high topography (e.g. Lowry et al. 2000) and the availability of new seismic (USArray) and gravity (GRACE and GOCE) data is likely to significantly improve estimates of lithospheric density structure. The neighboring Colorado Plateau may also serve as an ideal location based on the recent proposal of large-scale mantle flow contributing to its anomalous topography (Moucha et al. 2008, 2009).

As discussed in Chapter II, future models of lithospheric stress patterns related to variations in topography and density must transition from depth-independent to three-dimensional in order to account for the effects of variable lithospheric rheology on controlling stress distributions. Indeed, strongly depth-dependent rheological profiles are likely to generate strongly depth-dependent lithospheric responses to dynamic topography, as illustrated by recent convection models examining the interaction of mantle plumes with the lithosphere (Burov & Guillou-Frottier 2005; Burov & Cloetingh

2009). Again, the Western US appears to be an ideal location to test the sensitivity of stress patterns to dynamic topography, based on extensive previous work examining regional variations in elastic thickness and the associated implications for lithospheric strength (Lowry and Smith 1994; 1995; Lowry et al. 2000).

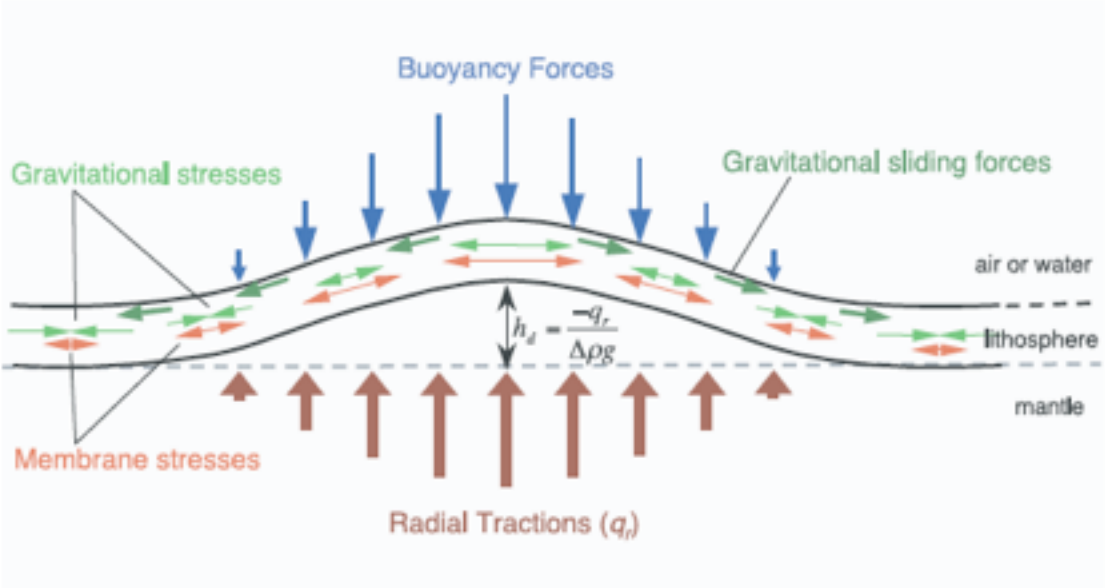

Figure 3.1: Modified from Lithgow-Bertelloni and Guynn (2004). Radial tractions are opposed by gravity; the balance between these two forces yields a dynamic topography h_{dyn}, which produces membrane stresses due to stretching and gravitational stresses due to the topographic gradient.

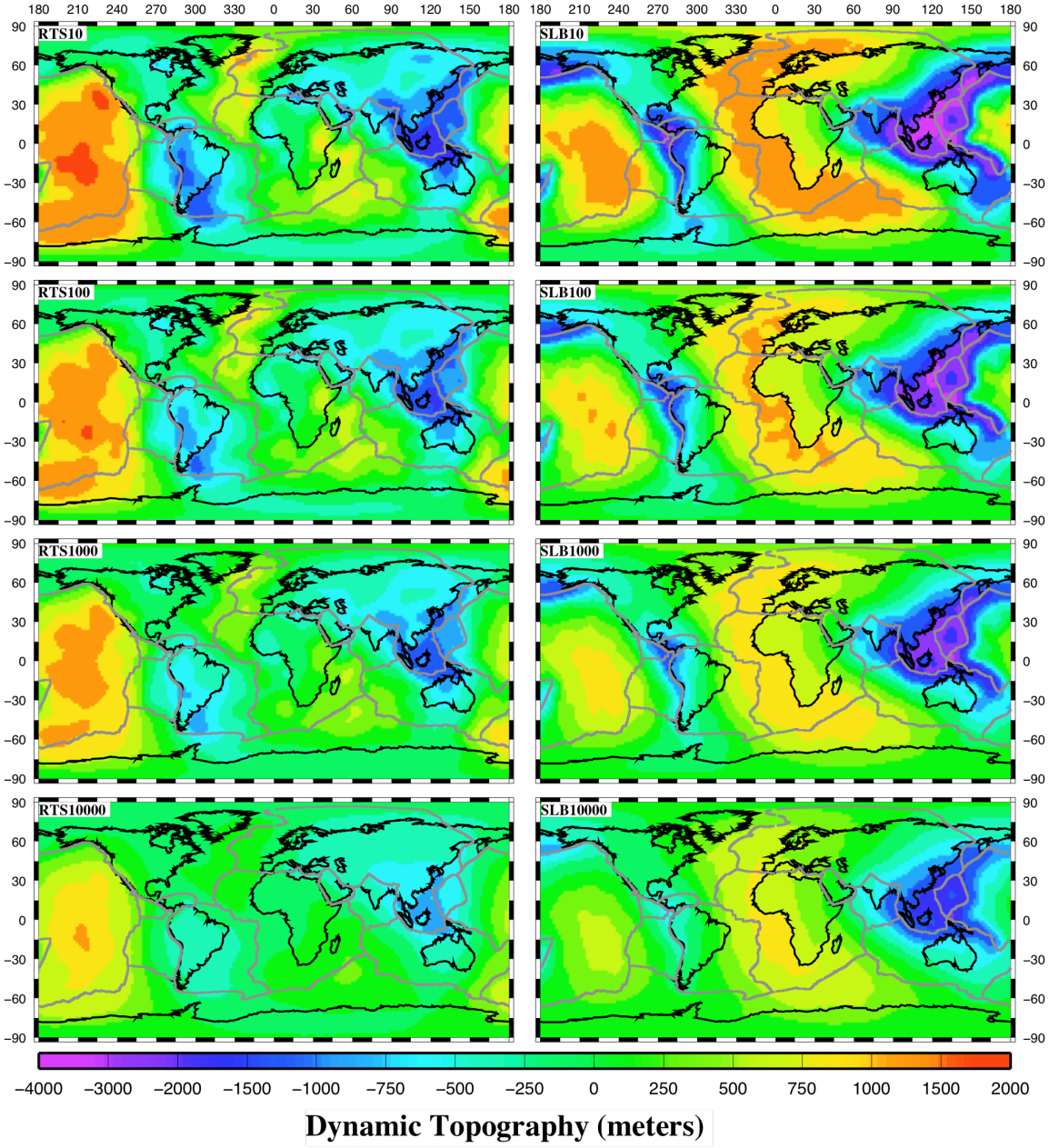

Figure 3.2: Dynamic topography produced by density-driven mantle flow. Mantle density structure is derived from a seismic velocity ('RTS', left panels) or subduction history model ('SLB', right panels). The lithosphere-asthenosphere viscosity contrast ranges from 10-10,000x and is indicated next to the mantle density model acronym (RTS10: seismic velocity model, 10x viscosity contrast across lithosphere-asthenosphere boundary).

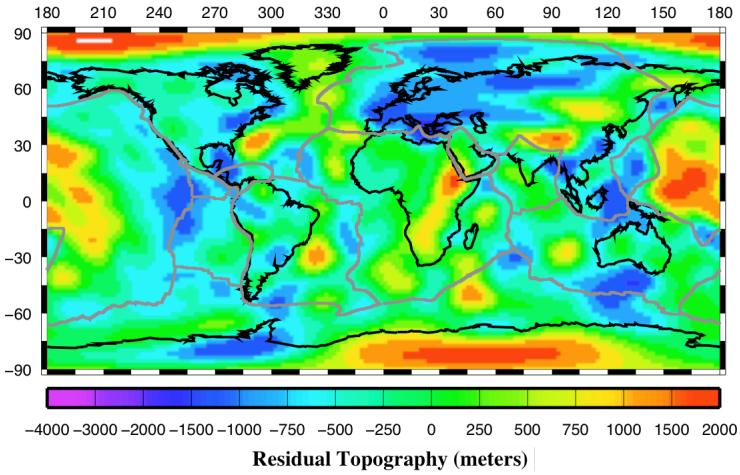

Figure 3.3: Residual topography determined from the TDL lithospheric structure model and expanded to spherical harmonic degree 12. The residual topography represents the difference between the predicted isostatic surface topography relative to a reference column and the observed topography.

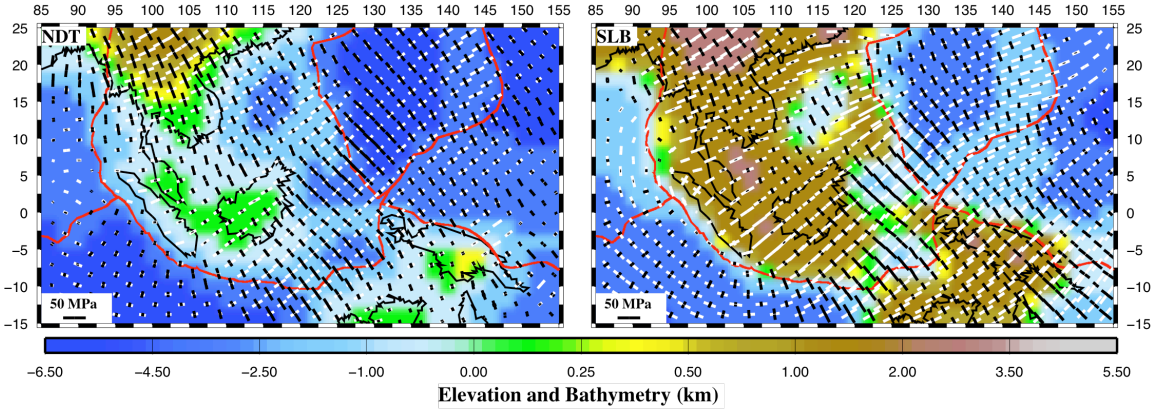

Figure 3.4: Elevation, bathymetry and the associated lithospheric stress patterns in Southeast Asia. Elevation and bathymetry represent observed topography (left panel,'NDT' ~ no dynamic topography) and observed topography minus calculated dynamic topography (right panel). The subtracted dynamic topography is derived from a convection model with a 1000x viscosity contrast across the lithosphere-asthenosphere boundary and subduction history (SLB) based mantle density model. White and black bars, respectively, represent extensional and compressional principal stresses.

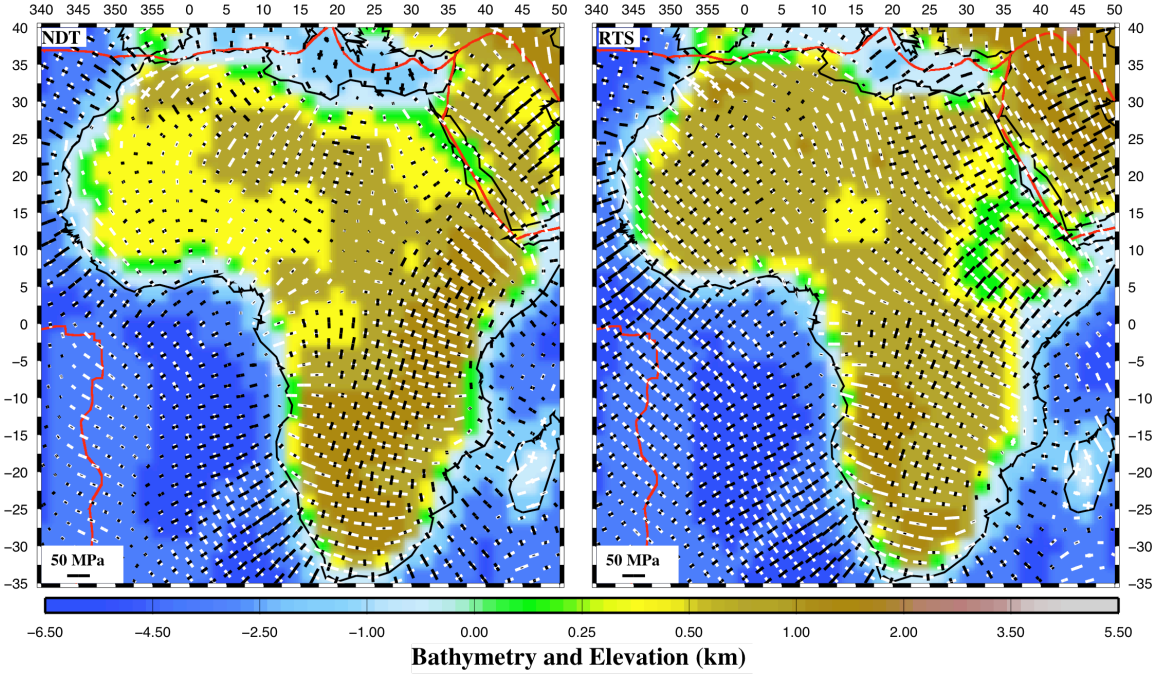

Figure 3.5: Elevation, bathymetry and the associated lithospheric stress patterns in Africa. Elevation and bathymetry represent observed topography (left panel,'NDT' ~ no dynamic topography) and observed topography minus calculated dynamic topography (right panel). The subtracted dynamic topography is derived from a convection model with a 10x viscosity contrast across the lithosphere-asthenosphere boundary and seismic velocity (RTS) based mantle density model.

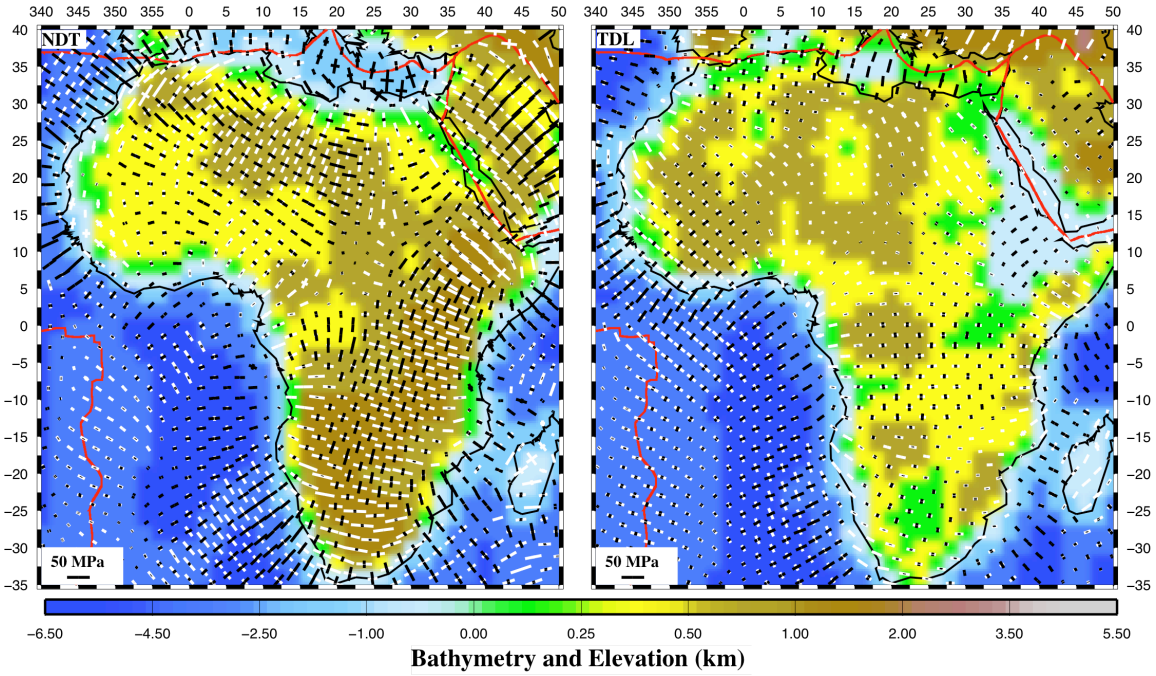

Figure 3.6: Same as figure 3.5, except residual topography (TDL) is removed from observed topography (right panel).

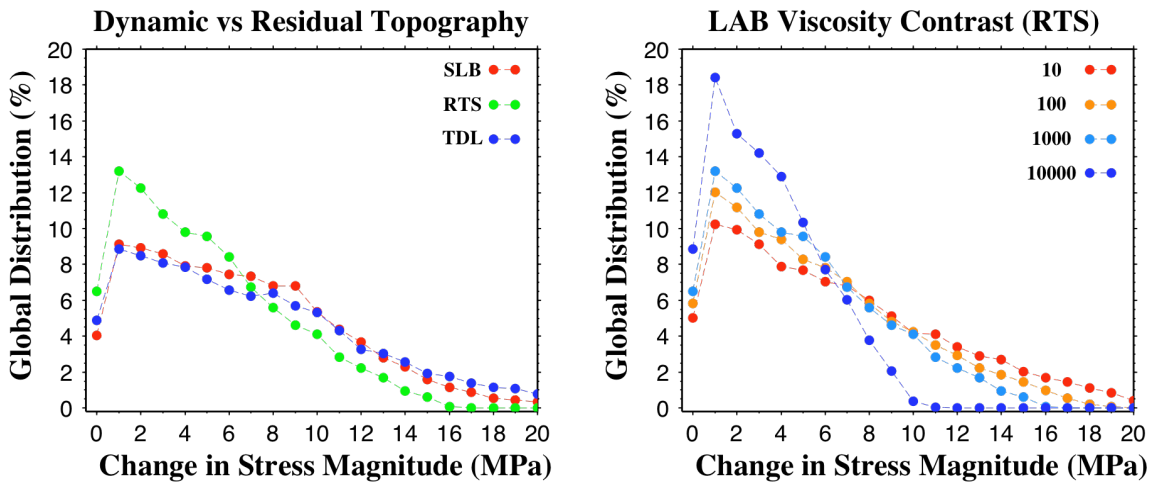

Figure 3.7: Global histogram distribution of changes in principal stress magnitudes. The change in principal stress magnitude is defined as (abs($SPCO_{ref}$ – $SPCO_{dyn}$)) + abs($SPEX_{ref}$ – $SPEX_{dyn}$))/2. SP_{ref} and SP_{dyn}, respectively, are the principal stress magnitudes tied to lithospheric structures without or with dynamic topography removed. SPEX and SPCO, respectively, refer to the most extensional and compressional principal stresses. The global distribution illustrates the percentage of each model that contains a specific change in stress magnitude. Left panel: global distributions associated with subduction history (SLB), seismic velocity (RTS) and lithospheric structure (TDL) based dynamic topography estimates. The lithosphere-asthenosphere viscosity contrast is 100x for both convection based dynamic topography estimates (SLB, RTS). Right panel: global distributions associated with seismic velocity (RTS) based dynamic topography estimates and a range of lithosphere-asthenosphere (LAB) viscosity contrasts.

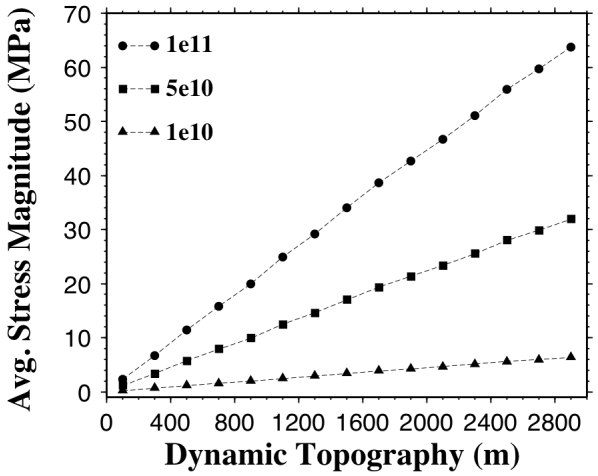

Figure 3.8: Absolute stress magnitudes (isotropic extension or compression) due instantaneous radial displacement. Stress magnitudes are plotted as a function of dynamic topography (magnitude of radial displacement) and Young's modulus (10^{10} – 10^{11} MPa).

Table 1.

Model Description	Change in Stress Magnitude (MPa)
TDL	7.33
RTS10	6.48
RTS100	5.51
RTS1000	4.86
RTS10000	3.37
SLB10	9.88
SLB100	7.85
SLB1000	6.75
SLB10000	4.73

Table 3.1. Globally averaged changes in stress magnitude between models tied to lithospheric structures without or with dynamic topography removed. TDL refers to the model of residual topography, while RTS and SLB, respectively, refer to seismic or subduction history based estimates of mantle density structure. The lithosphere-asthenosphere contrast is indicated by the number following RTS or SLB.

3.8 References

Artemieva, I.M., 2007. Dynamic topography of the East European craton: Shedding light upon lithospheric structure, composition and mantle dynamics, *Global Planet. Change*, **58**, 411-434.

Bai,W., Vigny, C., Ricard, Y. & Froidevaux, C., 1992. On the origin of deviatoric stresses in the lithosphere, *J. Geophys. Res.*, **97**(B8), 11729-11737.

Bassin, C., Laske, G. & Masters, G., 2000. The Current Limits of Resolution for Surface Wave Tomography in North America, *EOS Trans. AGU*, **81**, F897.

Burov, E. & Guillou-Frottier, L., 2005. The plume head-continental lithosphere interaction using a tectonically realistic formulation for the lithosphere, *Geophys. J. Int.*, **161**, 469-490.

Burov, E. & Cloetingh, S., 2009. Controls of mantle plumes and lithospheric folding on modes of intraplate continental tectonics: differences and similarities, *Geophys. J. Int.*, **178**, 1691-1722.

Cadek, O. & Fleitoux, L., 2003. Effects of lateral viscosity variations in the top 300 km on the geoid and dynamic topography, *Geophys. J. Int.*, **152**, 566-580.

Cazenave, A. & Lago, B., 1991. Long wavelength topography, sea floor subsidence and flattening, *Geophys. Res. Lett.*, **18**, 1257-1260.

Cazenave, A. & Thoraval, C., 1994. Mantle dynamics constrained by degree 6 surface topography, seismic tomography and geoid: Inference on the origin of the South Pacific Superswell, *Earth Planet. Sci. Lett.*, **122**, 207-219.

Christensen, U., 1998. Dynamic phase boundary topography by latent heat effects, *Earth Planet. Sci. Lett.*, **154**, 295-306.

Colin, P. & Fleitout, L., 1990. Topography of the ocean floor: Thermal evolution of the lithosphere and interaction of the deep mantle heterogeneity with the lithosphere, *Geophys. Res. Lett.*, **17**, 1961-1964.

Corrieu, V., Thoraval, C. & Ricard, Y., 2007. Mantle dynamics and geoid green functions, *Geophys. J. Int.*, **120**, 516-523.

Conrad, C.P. & Gurnis, M., 2003. Seismic tomography, surface uplift, and the breakup of Gondwanaland: Integrating mantle convection backwards in time, *Geochem. Geophys. Geosyst.*, **4**(3), 1031, doi: 0.1029/2001GC000299.

Conrad, C.P., Lithgow-Bertelloni, C. & Louden, K.E., 2004. Iceland, the Farallon slab,

and dynamic topography of the North Atlantic, *Geology*, **32**(3), 177-180, doi: 10.1130/G20137.1

Crosby, A.G. & McKenzie, D., 2009. An analysis of young ocean depth, gravity and global residual topography, *Geophys. J. Int.*, **178**, 1198-1219.

Daradich, A., Mitrovica, J.X., Pysklywec, R.N., Willet, S.D. & Forte, A.M, 2003. Mantle flow, dynamic topography, and rift-flank uplift of Arabia, *Geology*, **31**, 901-904.

DiCaprio, L., Gurnis, M. & Müller, R.D., 2009. Long-wavelength tilting of the Australian continent since the Late Cretaceous. *Earth Planet. Sci. Lett.*, **278**, 175-185.

Forte, A.M., Pettier, W.R., Dziewonski, A.M. & Peltier, W.R., 1993. Dynamic topography: a new interpretation based upon mantle flow models derived from seismic tomography, *Geophys. Res. Lett.*, **20**, 225-228.

Ghosh, A., Holt, E.W., Flesch, L.M. & Haines, A.J., 2009. Contribution of gravitational potential energy differences to the global stress field, *Geophys. J. Int.*, **179**, 787-812.

Gurnis, M., 1990. Bounds on global dynamic topography from Phanerozoic flooding of continental platforms, *Nature*, **344**, 754-756, doi: 10.1038.344754a0.

Gurnis, M., 1993. Phanerozoic marine inundation of continents driven by dynamic topography above subducting slabs, *Nature*, **364**, 589-593.

Gurnis, M., Mitrovica, J.X., Ritsema, J. & Heijst, H.J., 2001. Constraining mantle density structure using geological evidence of surface uplift rates: The case of the African Superplume. *Geochem. Geophys. Geosyst.*, **1**, 1999GC000035.

Hager, B.H. & O'Connell, J., A simple global model of plate dynamics and mantle Convection, *J. Geophys. Res.*, **86**, 4843-4867.

Hager, H.B., Clayton, R.W., Richards, M.A., Comer, R.P. & Dziewonski, A.M., 1985. Lower mantle heterogeneity, dynamic topography and the geoid, *Nature*, **313**, 541-545.

Hager, B. H. & Richards, M.A., 1989. Long-wavelength variations in Earth's geoid: Physical models and dynamical implications, *Phil. Trans. R. Soc. Lond.*, **328**, 209-327.

Heine, C., Müller, R.D., Steinberger, B. & Torsvik, T.H., 2008. Subsidence in intracontinental basins due to dynamic topography, *Phys. Earth Planet. Inter.*, **171**, 252-264.

Kaban, M.K., Schwintzer, P., Artemieva, I.A. & Mooney, W.D., 2003. Density of the continental roots: compositional and thermal contributions, *Earth Planet. Sci. Lett.*, **209**, 53-69.

De Koker, N.P., Lithgow-Bertelloni, C. & Stixrude, L. 2005. Dynamic Topography and the Density Structure of the Mantle Lithosphere, EOS Trans. AGU, **86**(52), Fall Meet. Suppl., Abstract T23A-0524 .

Le Stunff, Y. & Ricard, Y., 1995. Topography and geoid due to lithospheric mass anomalies, *Geophys. J. Int.*, **122**(3) 982-990.

Le Stunff, Y. & Ricard, Y., 1997. Partial advection of equidensity surfaces: A solution for the dynamic topography problem, *J. Geophys. Res.*, **102**, 24,655-24,667.

Lithgow-Bertelloni, C. & Richards, M.A., 1995. Cenozoic Plate Driving Forces, *Geophys. Res. Lett.*, **22**(11), 1317-1320.

Lithgow-Bertelloni, C. & Gurnis, M., 1997. Cenozoic subsidence and uplift of continents from time-varying dynamic topography, *Geology*, **25**(8), 735-738.

Lithgow-Bertelloni, C. & Richards, M.A., 1998. The Dynamics of Cenozoic and Mesozoic Plate Motions, *Rev. Geophys.*, **36**(1), 27-78.

Lithgow-Bertelloni, C. & Silver, P.G., 1998. Dynamic topography, plate driving forces and the African superswell, *Nature*, **395**, 269-272.

Lithgow-Bertelloni, C. & Guynn, J.H., 2004. Origin of the lithospheric stress field, *J. Geophys. Res.*, **109**, B01408, doi: 10.1029/2003JB002467.

Liu, L. & Gurnis, M., 2008. Simultaneous inversion of mantle properties and initial conditions using an adjoint of mantle convection, *J. Geophys. Res.*, **113**(B08405), doi:10.1029/2008JB005594.

Liu, L., Spasojevic, S. & Gurnis, M., 2008. Reconstructing Farallon Plate Subduction Beneath North America Back to the Late Cretaceous, *Science*, **322**, 934-938.

Lowry, A.R. & Smith, R.B. 1994. Flexural rigidity of the Basin and Range-Colorado Plateau-Rocky Mountain transition from coherence analysis of gravity and topography, *J. Geophys. Res.*, **99**(B10), 20,123-20,140.

Lowry, A.R. & Smith, R.B. 1995. Strength and rheology of the western U.S. Cordillera, *J. Geophys. Res.*, **100**(B9), 17,947-17,963.

Lowry, A.R., Ribe, N.M. & Smith, R.B., 2000. Dynamic elevation of the Cordillera, western United States, *J. Geophys. Res.*, **105**(B10), 23,371-23,390.

Miller, K.G., Kominz, M.A., Browning, J.V., Wright, J.D., Mountain, G.S., Katz, M.E., Sugarman, P.J., Cramer, B.S., Christie-Black, N. & Pekar, S.F., 2005. The Phanerozoic record of global sea level change, *Science*, **310**, 1293-1298.

Mitrovica, J.X., Beaumont, C. & Jarvis, G.T., 1989. Tilting of the continental interiors by the dynamical effects of subduction, *Tectonics*, **8**(5), 1079-1094.

Mitrovica, J.X. & Forte, A.M., 2004. A new inference of mantle viscosity based upon joint inversion of convection and glacial isostatic adjustment data, *Earth Planet. Sci. Lett.*, **115**, 177-189.

Mooney, W.D. & Vidale, J.E., 2005. Thermal and chemical variations in subcrustal cratonic lithosphere: evidence from crustal isostasy, *Lithos*, **71**, 185-193.

Moucha, R., Forte, A.M., Rowley, D.B., Mitrovica, J.X., Simmons, N.A. & Grand, S.P., 2008. Mantle convection and the recent evolution of the Colorado Plateau and the Rio Grande Rift valley, *Geology*, **36**(6), 439-442, doi: 10.1130/G24577A.1

Moucha, R., Forte, A.M., Rowley, D.B., Mitrovica, J.X., Simmons, N.A. & Grand, S.P., 2009. Deep mantle forces and the uplift of the Colorado Plateau, *Geophys. Res. Lett.*, **36**, L19310, doi:10.1029/2009GL039778

Müller, R.D., Sdrolias, M., Gaina, C., Steinberger, B. & Heine, C., 2008. Long-Term Sea-Level Fluctuations Driven by Oceanic Basin Dynamics, *Science*, **319**, 5868, 1357-1362.

Panasyuk, S.V. & Hager, B.H., 2000a. Models of isostatic and dynamic topography, geoid anomalies and their uncertainties, *J. Geophys. Res.*, **105**(B12), 28199-28209.

Panasyuk, S.V. & Hager, B.H., 2000b. Inversion for mantle viscosity profiles constrained by dynamic topography and the geoid, and their estimated errors, *Geophys. J. Int.*, **143**, 821-836.

Pari, G., 2001. Crust 5.1-based inference of the Earth's dynamic surface topography: geodynamic implications, *Geophys. J. Int.*, **144**, 501-516.

Pysklywec, R. & Mitrovica, J., 1999. The role of subduction-induced subsidence in the evolution of the Karoo Basin, *J. Geology*, **107**, 155-164.

Ricard, Y., Chambat, F. & Lithgow-Bertelloni, C., 2006. Gravity observations and 3D structure of the Earth, *Comptes Rendus GeoScience*, **338**, 992-1001.

Ricard, Y., Richards, M., Lithgow-Bertelloni, C. & LeStunff, Y., 1993. A geodynamic

model of mantle density heterogeneity, *J. Geophys. Res.*, **98**, 21895-21909.

Richards, M.A. & Hager, B.H., 1984. Geoid Anomalies in a Dynamic Earth, *J. Geophys. Res*., **89**(B7), 5987-6002.

Ritsema, J., van Heijst, H. & Woodhouse, J., 2004. Global transition zone tomography, *J. Geophys. Res.*, **109**, B02302, doi:10.1029/2003JB002610.

Sandiford, M., 2007. The tilting continent: A new constraint on the dynamic topographic field from Australia, *Earth Planet. Sci. Lett.*, **261**(1-2), 152-163.

Simmons, N.A., Forte, A.M. & Grand, S.P., 2006. Constraining mantle flow with seismic and geodynamic data: a joint approach, *Earth. Planet. Sci. Lett.*, 242(1-2), 109-124.

Simmons, N.A., Forte, A.M. & Grand, S.P., 2009. Joint, seismic, geodynamic and mineral physical constraints on three-dimensional mantle heterogeneity: Implications for the relative importance of thermal versus compositional heterogeneity. *Geophys. J. Int.*, **177**, 1284-1304.

Smith, W. & Sandwell, D., 1997. Global sea floor topography from satellite altimetry and ship depth soundings, *Science*, **277**, 1956-1962.

Steiner, S.A. & Conrad, C.P., 2007. Does active mantle upwelling help drive plate motions? Phys. Earth Planet. Int., **161**, 103-114.

Spasojevic, S., Liu, L., Gurnis, M. & Müller, R.D., 2008. The case for dynamic subsidence of the U.S. east coast since the Eocene, *Geophys. Res. Lett.*, **35**, L08305, doi:10.1029/2008GL033511.

Spasojevic, S., Liu, L. & Gurnis, M., 2009. Adjoint models of mantle convection with seismic, plate motion, and stratigraphic constraints: North America since the Late Cretaceous, *Geochem. Geophys. Geosyst.*, **10**(5), Q05W02, doi:10.1029/2008GC002345.

Steinberger, B., Schmeling., H. & Marquart, G., 2001. Large-scale lithospheric stress field and topography induced by global mantle circulation, *Earth Planet. Sci. Lett.*, **186**(1), 75-91.

Steinberger, B. & Calrderwood, A.R., 2006. Models of large-scale viscous flow in the Earth's mantle with constraints from mineral physics and surface observations, *Geophys. J. Int.*, **167**, 1461-1481.

Steinberger, B., 2007. Effects of latent heat release at phase boundaries on flow in the Earth's mantle, phase boundary topography and dynamic topography at the Earth's surface, *Phys. Earth Planet. Inter.*, **164**, 2-20.

Stixrude, L. & Lithgow-Bertelloni, C., 2005. Thermodynamics of mantle minerals - I. Physical properties, *Geophys. J. Int.*, **162**(2), 610-632.

Stixrude, L. & Lithgow-Bertelloni, C., 2007. Influence of phase transformations on lateral heterogeneity and dynamics in Earth's mantle. *Earth Planet. Sci. Lett.*, **263**, 45-55.

Thorval, C., Machetel, P. & Cazenave, A., 1995. Effects of an endothermic phase transition at 670 km Locally layered convection inferred from dynamic models of the Earth's mantle, *Nature*, **375**, 777-780.

Thorval, C. & Richards, M., 1997. The geoid constraint in global geodynamics: viscosity structure, mantle heterogeneity models and boundary conditions, *Geophys. J. Int.*, **131**, 1-8.

Watts, A.B., 2001. Isostasy and Flexure of the Lithosphere, Cambridge, U.K.: Cambridge University Press.

Wheeler, P. & White, N., 2000. Quest for dynamic topography: Observations from Southeast Asia, *Geology*, **28**(11), 963-966.

Winterbourne, J., Crosby, A. & White, N., 2009. Depth, age and dynamic topography of oceanic lithosphere beneath heavily sedimented Atlantic margins, *Earth Planet. Sci. Lett.,* **287**, 137-151.

Zoback, M.L., 1992. First- and Second-Order Patterns of Stress in the Lithosphere: the World Stress Map Project, *J. Geophys. Res.*, **97**(B8), 11,703-11,728.

CHAPTER IV

Modification of the Lithospheric Stress Field by Lateral Variations in Plate-Mantle Coupling

4.1 Abstract

The presence of deeply penetrating continental roots may locally increase the magnitude of basal shear tractions by up to a factor of 4 compared to a layered viscosity structure. Here we examine how these increases in mantle-lithosphere coupling influence stress patterns in the overlying elastic lithosphere. By coupling a mantle flow model to a model for the elastic lithosphere, we show that the amplification of mantle tractions beneath cratons increases elastic stress magnitudes by at most a factor of only 1.5 in a pattern not correlated to local basal traction changes. This disconnect is explained by both the integration of basal tractions over plate-scale wavelengths and the effective transmission of stress within a homogenous elastic lithosphere, which makes elastic stress patterns sensitive to regionally-averaged changes in basal tractions, but not local variations. Our results highlight the importance of regional variations in lithospheric strength, which could allow stress patterns to more closely match regional changes in basal shear.

4.2 Introduction

The relationship between mantle flow and the lithospheric stress field depends strongly on the rheological structure of the convecting mantle, asthenosphere and overlying lithosphere. Previous work has demonstrated that the presence of a laterally-varying viscosity structure in mantle flow models significantly enhances mantle-lithosphere coupling beneath deeply penetrating continental roots (Zhong 2001; Conrad & Lithgow-Bertelloni 2006; Becker 2006) as thicker lithosphere comes into closer contact with deeper and more viscous mantle. In the case of flow driven by mantle density variations, the magnitude of shear tractions at the base of deep continental roots increase by a factor of 2-5 when laterally-varying and layered viscosity structures are compared (Conrad & Lithgow-Bertelloni 2006). Here, we look at how increases in shear tractions acting at the base of plates affect the stress field in the elastic lithosphere for a range of continental structures and different combinations of mantle flow fields driven by mantle density heterogeneity and plate motions.

4.3 Combined Modeling of Viscous Flow and Elastic Deformation

Because it is not yet possible to compute both mantle flow and lithospheric deformation within a single calculation at the global scale, we first calculate viscous shear stresses acting on the base of the lithosphere using a global flow model (Conrad & Lithgow-Bertelloni 2006; Conrad et al. 2007) and then separately calculate the lithospheric response to these basal tractions (Bai et al. 1992; Bird 1998; Steinberger et al. 2001; Lithgow-Bertelloni & Guynn 2004; Ghosh et al. 2008) using a model for the elastic lithosphere (Lithgow-Bertelloni & Guynn 2004). First, we compute the viscous flow field driven by density variations or surface plate motions for a given viscosity

structure and extract the horizontal and radial tractions that these flows exert on the base of the lithosphere. These tractions are in turn applied to the base of an elastic lithospheric model. This lithospheric model assumes a vertically and horizontally homogenous lithosphere in order is to isolate the relative effects of lateral variations in the depth of the lithosphere-asthenosphere boundary on lithospheric stresses.

4.3.1 Viscous Flow

We compute global viscous flow using the finite element code CitcomS (Zhong et al. 2000; Tan et al. 2006) with details as described in Conrad et al. (2007). To resolve basal tractions, we use horizontal and vertical resolutions of 105 and 17 km, respectively, in the lithospheric and asthenospheric layers, and 100 km vertical resolution in the lower mantle. Flow is driven by internal density heterogeneity below 325 km (density-driven) determined from seismic tomography (Ritsema et al. 2004) (0.15 g cm^{-3} km^{-1} s (Karato & Karki 2001) velocity to density conversion) or NUVEL-1A surface plate motions (plate-driven) (DeMets et al. 1994). As in numerous previous studies the upper 325 km of the seismic model are excluded because they are partially affected by lithospheric compositional variations. For a Newtonian rheology we may add the density- and plate-driven flow fields to give the net tractions acting at the base of the lithosphere (e.g. Lithgow-Bertelloni & Guynn 2004; Conrad et al. 2007), which are responsible for surface deformation. However, for the purpose of illustration we show the individual contributions of plate- and density-driven flow models separately. While density-driven flow tractions do not depend on the absolute mantle viscosity, plate-driven flow tractions depend on both imposed plate motion rates and the absolute mantle viscosity Conrad et

al. (2007). As a result, scaling the magnitude of plate-driven tractions in effect adjusts the assumed absolute mantle viscosity (i.e., the choice of μ_{um} in Figure 4.1b). Due to the uncertainty associated with the absolute upper mantle viscosity, we examine cases where plate-driven tractions assume an absolute upper mantle viscosity of 10^{21} Pa s, or a value half as large (i.e., scaled by 0.5), which Conrad et al. (2007) found provided the best fit to anisotropy observations.

Following our previous work we compare, for each flow model, a layered (radially symmetric) and a series of laterally-varying lithospheric viscosity structures (Figure 4.1b). For the layered case, the lithosphere, asthenosphere and lower mantle are 30, 0.1 and 50 times as viscous as the upper mantle, respectively. The lithospheric thickness is set to 50 km or 100 km, and the asthenosphere extends from the lithospheric base to 300 km. In models driven by surface plate motions, asthenospheric viscosities are assigned to points within 300 km of plate boundaries in order to dampen artificially high stress magnitudes associated with a singularity arising from the piecewise velocity boundary condition. Models with laterally-varying viscosity structures assign an error function profile above 300 km using a length scale consistent with half-space cooling for oceanic regions (with a maximum thickness of 100 km corresponding to seafloor older than ~80 Ma) and the maximum depth of the 1.5% S_v anomaly isosurface from the Gung et al. (2003) velocity model for continental regions (Figure 4.1a). The resulting temperature profile is converted to a viscosity structure using a temperature-dependent Arrhenius model with an activation energy of 200 kJ mol^{-1}. Assigning different maximum (H_{max}) and minimum (H_{min}) continental lithospheric thicknesses modifies the viscosity structure (Figure 4.1b) and consequently changes traction magnitudes at the

base of the lithosphere. Horizontal and radial tractions are extracted at the base of the lithosphere, defined by the viscosity contour $\mu = \mu_{um}$, as indicated by the point along each curve in Figure 4.1b.

4.3.2 Elastic Deformation

The elastic lithosphere's response to radial and horizontal basal tractions is computed using the finite element code ABAQUS v6.6 (Hibbitt & Sorenson 2005) for a 3D linearly elastic spherical shell (Lithgow-Bertelloni & Guynn 2004). The elastic shell is composed of two layers, each consisting of a single layer of 8 node continuum shell elements (for all models) with a horizontal resolution of 110 km. The upper and lower layers are, respectively, 50 km and 100 km thick. Stress magnitudes scale inversely with the elastic layer thickness at these flow wavelengths. The Young's moduli of the upper and lower layers are 10^{11} Pa and 10^{6} Pa, respectively, while Poisson's ratio remains fixed at 0.3 for both layers. The bottom nodes of the basal layer are pinned to prevent translation of the model. The low Young's modulus of the basal layer prevents stresses associated with the pinned basal nodes from affecting stresses in the stiffer upper element layer, where stresses are analyzed based on the applied loads.

We compute the response of the elastic lithosphere to the radial tractions by separately computing the membrane stresses associated with dynamic topographic deflection and the gravitational sliding effect (gravitational potential energy) from the uplift and subsidence caused by the topography (Lithgow-Bertelloni & Guynn 2004). Dynamic deflections are given by $\tau_r/(\Delta\rho g)$, where τ_r is the radial stress at the base of the lithospheric mantle, $\Delta\rho$ is the density contrast between the lithosphere (3200 kg m^{-3}) and surface (air ~ 0 kg m^{-3}, water 1020 kg m^{-3}) and g is the gravitational acceleration.

Combining the elastic stresses related to basal shear, dynamic topography deflections and gravitational sliding give the total elastic stress response to the basal tractions.

4.4 Results

4.4.1 Laterally-Varying vs. Layered Viscosity

Horizontal tractions on base of the lithosphere (density- + 0.5*plate-driven) for a layered viscosity structure (50 km thick lithosphere) and the resulting elastic stresses exhibit long-wavelength patterns (Figure 4.1c and 4.1d) similar to those shown in previous work. Elastic stress magnitudes reflect integration of the basal horizontal tractions over plate-scale wavelengths and as a result are on average ~1-2 orders of magnitude higher than basal traction magnitudes. This is not surprising, as an examination of Love's thin shell equations reveals that the magnitude of stress resultants should be higher than applied tractions by a factor proportional to the ratio of the shell thickness to the radius of the sphere. Replacing the layered viscosity structure with a laterally-varying viscosity (H_{max} = 250 km, H_{min} = 50 km) magnifies the tractions in regions with deeply penetrating continental roots by up to a factor of 5 (Figure 4.1e) compared to the layered case. This is because the mantle tractions are transmitted more effectively to the overlying lithosphere if the asthenosphere is thin (Cooper & Conrad 2009). Variations greater than a factor of 5 only occur in regions with near zero traction magnitudes for the layered case. In contrast, changes in elastic stress magnitudes show little correlation with increases in the horizontal traction magnitude beneath thick continental lithosphere, and on average only change by a factor between 0.8 and 1.5 (Figure 4.1f). Although not shown, only minor variations in the orientation of the most

compressive principal stress direction occur, as changes in the lithospheric viscosity structure strongly affect the magnitude but not direction of basal shear (Conrad & Lithgow-Bertelloni 2006). The stress regimes, which are largely controlled by radial traction patterns (e.g. Lithgow-Bertelloni & Guynn 2004), also show insignificant variations because radial tractions are largely insensitive to viscosity structure (Figure 4.2a).

4.4.2 Plate-Driven vs. Density-Driven Flow

Global averages of the ratio of basal tractions (Figure 4.2a) with and without laterally-varying viscosity for given lithospheric thicknesses (H_{max} = 250 km, H_{min} = 50 km) show how increases in basal tractions with increasing lithospheric thickness vary for different combinations of density- and plate-driven flow. Flow driven by only density variations shows the smallest increase of the average horizontal traction magnitude ratios with increasing lithospheric thickness. This is due to the decrease in flow speed as coupling increases beneath thickened lithosphere for density-driven flow, while models that impose plate motions lack such a feedback mechanism because the strain rate is specified. Traction magnitude ratios increase as the component of plate-driven flow increases relative to the density-driven flow component (red through dark blue lines, Figure 4.2a). By contrast, average ratios of the elastic principal stress magnitude remain roughly constant between 1.0 and 1.25 (Figure 4.2b), with the exception of pure plate-driven flow. This difference between patterns of basal tractions and elastic principal stresses reflects the integration of the basal tractions over plate-scale distances and effective transmission of stresses across these distances within a homogenous elastic

lithosphere. As a result, the stress magnitude ratio for the elastic lithosphere represents an average of the basal traction ratios across plate-scale distances. Ratios of radial tractions (density-driven flow only) and the resulting elastic stresses show essentially no variation between layered and laterally-varying viscosity models (green lines, Figure 4.2a-b) because normal stresses are effectively transmitted across rheological boundaries, while shear stresses are not.

4.4.3 Continental Lithospheric Thickness

Varying the maximum and minimum thickness of the continental lithosphere illustrates relations between global peaks in basal traction ratios (Figure 4.2c) and the associated elastic stress magnitude ratios (Figures 4.2d). For example, as the minimum thickness of the continental lithosphere increases from 50 km to 100 km (orange and red vs. light blue and dark blue curves, Figure 4.2c-d), peaks in the distribution of both the basal horizontal tractions (Figure 4.2c) and the corresponding elastic stresses (Figure 4.2d) shift from ratio values of ~ 1.2 for 50 km to 1.3-1.4 for 100 km. For tractions, we have shown above that this amplification is due to the deeper average penetration of the lithosphere for thicker lithosphere. Significantly, this amplification occurs even when the continental thickness is fixed (orange and light blue curves) and equal to the lithospheric thickness in the layered viscosity model. For these cases, the tractions are amplified for the smoothly-varying viscosity structures (light red and yellow curves, Figure 4.1b) because these profiles reach the asthenospheric viscosity at a greater depth than the layered case (dark red curve, Figure 4.1b). In other words, the laterally-varying viscosity model has a higher "effective" lithospheric thickness than the corresponding layered case,

which amplifies the tractions that mantle flow exerts on it. This amplified average traction magnitude is reflected in the average elastic stress magnitude.

A restricted distribution of possible continental lithosphere thicknesses causes the peaks of the traction magnitude ratios to become higher and more laterally-restricted (orange and light blue curves compared to the red and dark blue curves, Figure 4.2c), reflecting the lithosphere thickness distribution that governs the traction magnitudes. However, the amplification of peaks for the elastic lithosphere stress distribution (Figure 4.2d) is not as large as it is for tractions (Figure 4.2c). This is because elastic stress magnitudes reflect an integration and subsequent homogenization of the basal tractions, which tends to narrow and amplify the magnitude of the peak in the distribution of lithospheric stress ratios. Indeed, for any given continental structure, the peak of the elastic stress curve (Figure 4.2d) is higher and narrower than the corresponding peak of the traction ratio curve (Figure 4.2c) due to the integration, transmission and resulting homogenization of the elastic stresses over large distances. Thus, the magnitude distribution of elastic stresses primarily reflects the average tractions applied to the lithosphere, rather than the variability in these tractions.

4.5 Discussion and Conclusions

This study shows that amplification of lithosphere-mantle coupling beneath deeply penetrating continental roots is not accompanied by an equivalent amplification of stresses within the elastic lithosphere above continental roots, and produces no significant changes in stress regimes or orientations. Instead, the integration of basal tractions and transmission of elastic stresses across large distances in the homogenous elastic

lithosphere spreads any stress amplification over a wider area. Changes in elastic stress magnitudes centered over thick cratonic roots reflect both amplification of basal shear tractions beneath the thick roots, as well as changes in basal tractions over much thinner lithosphere, which constitute a much larger percentage of the model. Comparisons with stress observations (Lithgow-Bertelloni & Guynn 2004) are unlikely to change significantly if variable plate-mantle coupling beneath thick continental lithosphere is taken into account.

We note that the asthenospheric layer in all our models is only a factor of 10 less viscous than the upper mantle, smaller than some current estimates (e.g. Mitrovica & Forte 2004). Reducing the viscosity of the asthenosphere more than one order of magnitude would reduce the amplitude of plate-mantle coupling at deep continental roots slightly (Conrad & Lithgow-Bertelloni 2006), yielding a small decrease in lithospheric stresses and deformation, when averaged globally. Larger lithosphere-asthenosphere viscosity contrasts are thus not likely to affect the observed relationship between changes in basal tractions and elastic stresses in any particular location. Large ($> 10^2$) viscosity contrasts between the lithosphere and asthenosphere, however, may play an important role in plate boundary regions where Ghosh et al. (2008) found that lithosphere-asthenosphere viscosity contrasts of three orders of magnitude or greater provided the best fit to observed strain rate data.

The minor changes in elastic stresses induced by more significant enhancements of mantle-lithosphere coupling at deep continental roots could change significantly if lateral variations in lithospheric strength prevented transmission of stresses across tectonic provinces. Previous work has shown that cratonic lithosphere can be effectively

shielded from mantle-related stresses if it is bordered by weaker tectonic provinces that decouple the cratonic lithosphere from external stresses (Lenardic et al. 2000, 2003). If in fact lateral changes in mechanical strength prevented transmission of stresses across some tectonic provinces, the lithosphere above thick continental roots would be much more sensitive to changes in mantle-lithosphere coupling because the elastic stress field would reflect only the stresses at the base of the thick roots. Modeling of the Australian continent (Dyksterhuis et al. 2005) and plate boundary regions (Ghosh et al. 2008) demonstrated that lateral changes in lithospheric strength can indeed have a large effect on stress patterns in vertically homogenous models. Thus, future studies should incorporate these variations where possible in order to accurately determine the length-scales over which basal stresses are integrated and transmitted. Similarly, vertical changes in the strength of the lithosphere (e.g. Kohlstedt 1995) may play a strong role in decoupling basal shear from the upper parts of the lithosphere, as horizontal shear is transmitted much less effectively than radial stresses across rheological boundaries. Lithospheric models containing lateral and vertical variations in rheology and thickness are likely required to properly asses the relationship between mantle flow and lithospheric stress patterns. In that event, observations of stress and deformation patterns may provide new constraints on mantle viscosity structure and strength variations between lithospheric provinces, which are otherwise difficult to constrain (e.g. Paulson et al. 2007).

4.6 Acknowledgements

All figures were prepared using GMT version 4.2.0 by P. Wessel and W.F. Smith. This work was supported by NSF grants EAR-0914712 (C.P.C.) and EAR-0609553 (C.L.-B.).

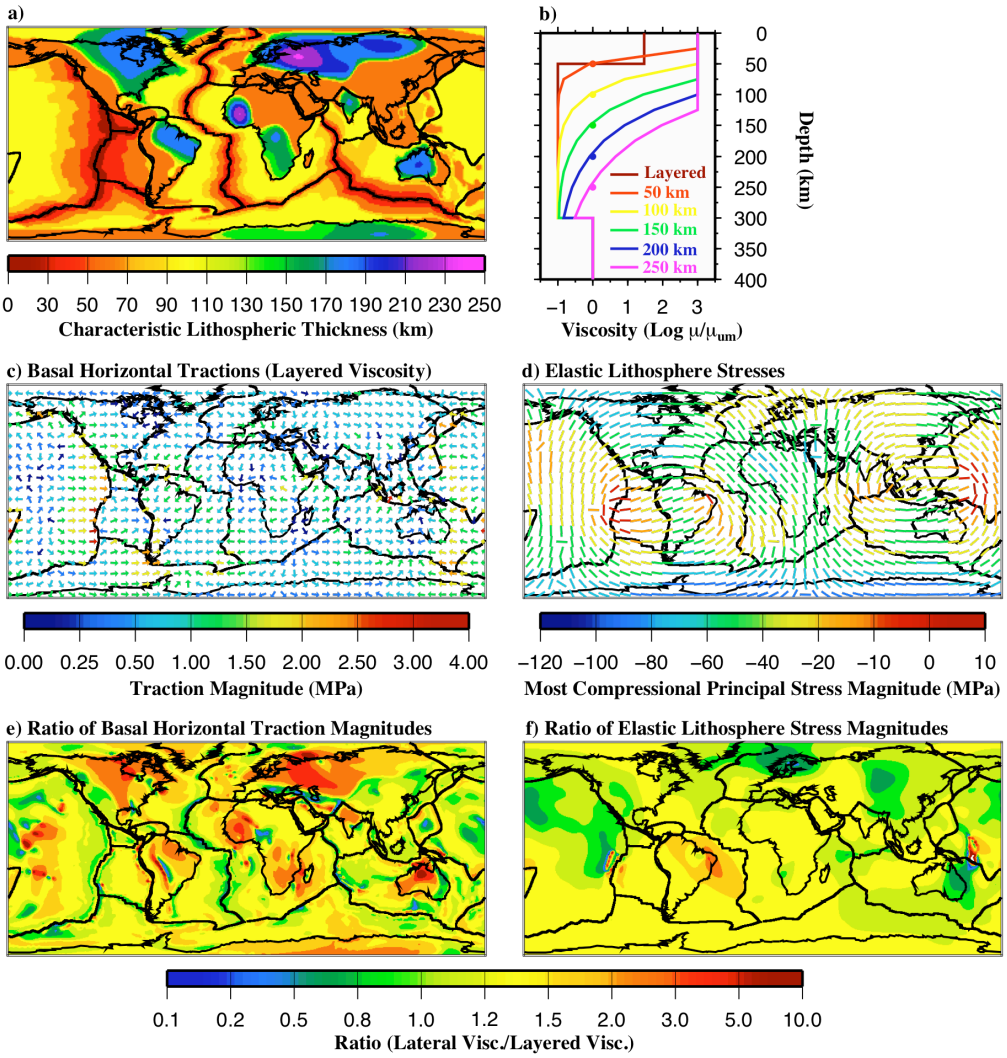

Figure 4.1: Lithospheric thickness determined with a half-space cooling model for oceanic lithosphere and from the 1.5% S_v contour (anomaly isosurface) from *Gung et al.* (2003) for continental lithosphere (a). Depth versus log of the viscosity divided by the reference upper mantle viscosity (μ_{um}) for layered and temperature-dependent viscosity structures (b). The maximum viscosity cutoff is set to $10^3*\mu_{um}$ and the dots in (b) indicate the depth at which basal tractions were measured for lithosphere of a given viscosity profile. Orientation and magnitude of horizontal tractions measured at the base of the lithosphere for a layered viscosity structure (c) and the resulting most compressive elastic principal stress directions and magnitudes (d). The horizontal basal tractions are extracted from combined density- and plate-driven*0.5 flow fields. In the elastic models compressive stresses are defined as negative. Ratio of the magnitude of horizontal basal tractions (e) and related elastic most compressive principal stress (f) between layered and laterally-varying (temperature-dependent) viscosity structures. The laterally-varying viscosity model contains minimum and maximum continental lithospheric thickness values of, respectively, 50 km and 250 km.

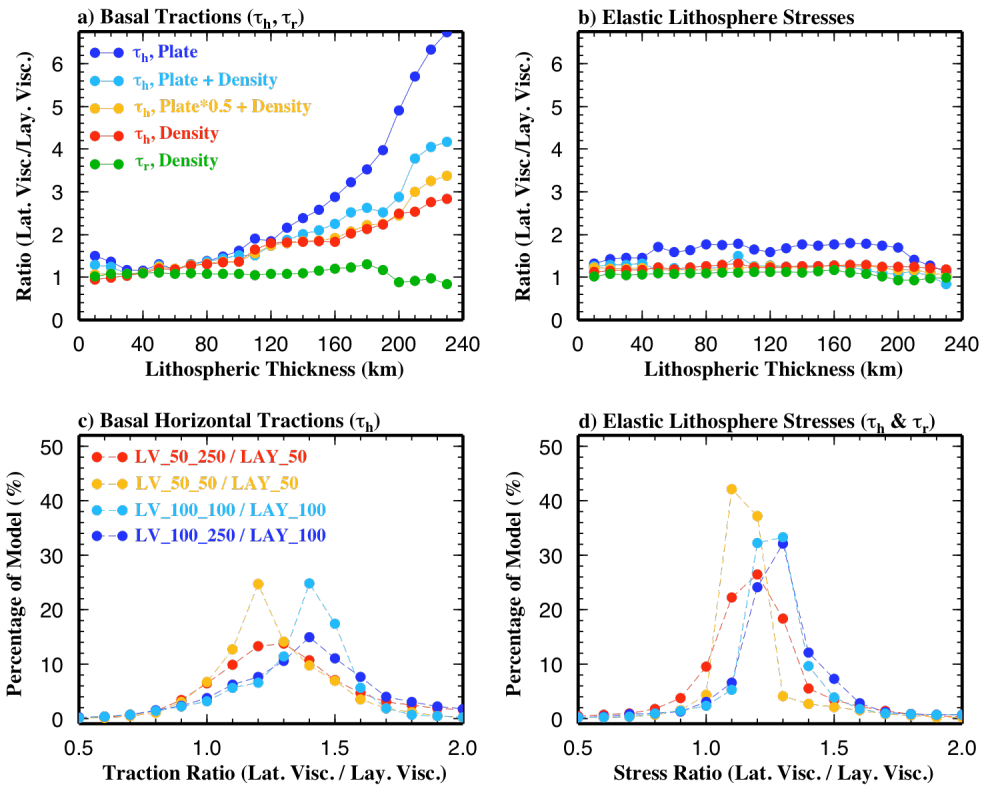

Figure 4.2: Ratio (laterally-varying/layered viscosity) of horizontal (τ_h) and radial (τ_r) basal tractions magnitudes (a) and the most compressive elastic principal stress magnitudes (b) as a function of lithospheric thickness. Curves are shown for plate-driven flow, density-driven flow and combinations of density- and plate-driven flow. The layered viscosity thickness is 50 km and the laterally-varying viscosity models contain minimum and maximum continental lithospheric thickness values of, respectively, 50 km and 250 km. Regions where the elastic stress magnitude is less than 3% of the maximum value are not included in order to eliminate the influence of high ratio values associated with low absolute stress magnitudes. Percentage of a model with a given ratio (laterally-varying/layered viscosity) for (c) net horizontal basal tractions (Density- + 0.5*Plate-Driven) and (d) associated elastic lithosphere stresses (including the stresses generated by radial basal tractions, although tests show that the inclusion of radial tractions does not affect the percentage distributions significantly). Legend symbols describe the continental lithospheric structure associated with each percentage-ratio curve: $LV\_H_{min}\_H_{max}$ ~ laterally-varying viscosity (LV), minimum continental lithospheric thickness (H_{min}) (note that when H_{min}=H_{max} the continental thickness is constant but the oceanic thickness is not), maximum continental lithospheric thickness (H_{max}); LAY_H ~ layered viscosity (LAY) and lithospheric thickness (H).

4.7 References

Bai, W., Vigny, C., Ricard, Y. & Froidevaux, C., 1992. On the origin of deviatoric stresses in the lithospheres, *J. Geophys. Res.*, **97**(B8), 11,729–11,737.

Becker, T. W., 2006. On the e ect of temperature and strain-rate dependent viscosity on global mantle flow, net rotation, and plate-driving forces, *Geophys. J. Int.*, **167**(2), 943–957.

Bird, P., 1998. Testing hypotheses on plate-driving mechanisms with global lithosphere models including topography, thermal structure, and faults, *J. Geophys. Res.*, **103** (B5), 10,115–10,129.

Conrad, C.P. & Lithgow-Bertelloni, C., 2006. Influence of continental roots and asthenosphere on plate-mantle coupling, *Geophys. Res. Lett.*, **33**, L05312, doi:10.1029/2005GL025621.

Conrad, C.P., Behn, M., & Silver, P., 2007. Global mantle flow and the development of seismic anisotropy: Di erences between the oceanic and continental upper mantle, *J. Geophys. Res.*, **112**, B07317, doi:10.1029/2006JB004608.

Cooper, C.M. & Conrad, C.P., 2009. Does the mantle control the maximum thickness of cratons?, *Lithosphere*, **1**(2), 67-72.

DeMets, C., Ordon, R., Argus, D. & Stein, S., 1994. E ect of recent revisions to the geomagnetic reversal time scale on estimates of current plate motions, *Geophys. Res. Lett.*, **21**(20), 2191–2194.

Dyksterhuis, S., Muller, R. & Albert, R., 2005. Paleostress field evolu-tion of the australian continent since the eocene, *J. Geophys. Res.*, **110**, B05102, doi:10.1029/2003JB002728.

Ghosh, A., Holt, W.E., Wen, L., Haines, A.J. & Flesch, L.M., 2008. Joint modeling of lithosphere and mantle dynamics elucidating lithosphere-mantle coupling, *Geophys. Res. Lett.*, **35**, L16309, doi:10.1029/2008GL034365.

Gung, Y.C., Panning, M. & Romanowicz, B., 2003. Global anisotropy and the thickness of continents, *Nature*, **422**, 707–711, doi:10.1038/nature01559.

Hibbitt, K. & Sorensen, I., 2005. Abaqus analysis manual, version 6.6, Pawtucket, RI.

Karato, S.-I. & Karki, B.B., 2001. Origin of lateral variation of seismic wave velocities and density in the deep mantle, *J. Geophys. Res.*, **106**, 21,771-21,783.

Kohlstedt, D.L., Evans, B. & Mackwell, S.J., 1995. Strength of the lithosphere - constraints imposed by laboratory experiments, *J. Geophys. Res.*, **100**(B9), 17,587–17,602.

Lenardic, A., Moresi, L.-N. & Muhlhaus, H., 2000. The role of mobile belts for the longevity of deep cratonic lithosphere: The crumple zone model, *Geophys. Res. Lett.*, **27**(8), 1235–1238.

Lenardic, A., Moresi, L.-N. & Muhlhaus, H., 2003. Longevity and stability of cratonic lithosphere: Insights from numerical simulations of coupled mantle convection and continental tectonics, *J. Geophys. Res.*, **108**(B6), doi:10.1029/2002JB001859.

Lithgow-Bertelloni, C. & Guynn, J.H., 2004. Origin of the lithospheric stress field, *J. Geophys. Res.*, **109**, B01408, doi:10.1029/2003JB002467.

Mitrovica, J.X. & Forte, A.M., 2004. A new inference of mantle viscosity based upon joint inversion of convection and glacial isostatic adjustment data, *Earth Planet. Sci. Lett.*, **225**(1-2), 177-189.

Paulson, A., Zhong, S. & Wahr, J., 2007. Inference of mantle viscosity from GRACE and relative sea level data, *Geophys. J. Int.*, **171**(2), 497-508, doi:10.1111/j.1365-246X.2007.03556.x.

Ritsema, J., van Heijst, H. & Woodhouse, J., 2004. Global transition zone tomography, *J. Geophys. Res.*, **109**, B02302, doi:10.1029/2003JB002610.

Steinberger, B., Schmeling, H. & Marquart, G., 2001. Large-scale lithospheric stress field and topography induced by global mantle circulation, *Earth Planet. Sci. Lett.*, **186**(1), 75–91.

Tan, E., Choi, E., Thoutireddy, P., Gurnis, M. & Aivazis, M., 2006. Geoframework: Coupling multiple models of mantle convection within a computational framework, *Geochem. Geophys. Geosyst.*, **7**, Q06001, doi:10.1029/2005GC001155.

Zhong, S., 2001. Role of ocean-continent contrast and continental keels on plate motion, net rotation of lithosphere, and the geoid, *J. Geophys. Res.*, **106**(B1), 703–712.

Zhong, S., Zuber, M., Moresi, L.-N. & Gurnis, M., 2000. Role of temperature-dependent viscosity and surface plates in spherical shell models of mantle convection, *J. Geophys. Res.*, **105**(B5), 11,063–11,082.

CHAPTER V

Conclusions

At the onset, the primary goal of this thesis was to reexamine the forces acting on and within the lithosphere in order to provide better constraints on the processes controlling the total lithospheric stress field. The motivation for this reexamination was largely based on the results of Lithgow-Bertelloni & Guynn (2004), who found large discrepancies between observed (Zoback 1992) and predicted global stress patterns in many regions. Lithgow-Bertelloni & Guynn (2004) largely attributed the discrepancies to 1) oversimplification of the lithosphere's density structure and isostatic state, 2) enhanced plate-mantle coupling at the base of thick continental roots and 3) the assumption of strong mechanical coupling throughout the entire lithosphere. While maintaining the assumption of mechanical coherence throughout the thickness of the lithosphere (i.e. thin elastic shell), Chapters II/III and IV, respectively, explored the effects variable lithospheric structure and enhanced plate-mantle coupling beneath thick continental roots on global stress patterns.

The results from Chapter II reveal that lithospheric thickness, composition and isostatic state strongly influence stress patterns related to gradients in integrated lithostatic pressure. As lithospheric thickness varies significantly across tectonic provinces, the required assumption of a uniform base depth brings into question whether

the integrated lithostatic pressure method is appropriate for determining stress patterns in the lithosphere. Although this method is also used to examine the influence of dynamic topography on lithospheric stress patterns (Chapter III), the results clearly demonstrate that on a regional basis stress patterns are highly sensitive to the amplitude of dynamic topography. On a global basis, however, changes in stress magnitude when dynamic topography is subtracted from surface topography are relatively consistent for different estimates of dynamic topography, with orders of magnitude variation in the lithosphere-asthenosphere viscosity contrast having a relatively moderate influence. This indicates that no reasonable variation in the viscosity of the asthenosphere or lithosphere will reduce the presence of dynamic topography enough to remove its influence, which is logical as the radial component of stress is efficiently transmitted across rheological boundaries. Last, we demonstrate that when long-wavelength basal shear patterns are applied to a homogenous elastic lithosphere, increases in plate-mantle coupling beneath thick continental roots do not produce an associated large increases in local stress magnitudes, but rather regionally distributed changes in stress magnitude (Chapter IV).

The common theme that emerges from the results of each chapter is the critical importance of transitioning from depth-independent models to models incorporating both lateral and vertical variations in lithospheric rheology. The results presented in this thesis, particularly those in Chapters II and IV, strongly suggest that this transition to 3D models with variable lithospheric rheology is necessary in order to calibrate how different sources of stress contribute to the total lithospheric stress field. Indeed, previous work has shown how using even simplified first-order depth-dependent material properties leads to stress distributions that deviate from the solutions obtained by depth-independent

studies (Kusznir and Bott 1977; Bott and Kusznir 1979 ; Liu et al. 2000). Considering the strong dependence of the depth-independent stress field on the assumed lithospheric density structure and thickness (Chapter II), incorporating such first-order variations in lithospheric strength (i.e. asthenosphere vs. lithosphere, mantle vs. crustal lithosphere) will allow a self-consistent determination of how stresses are distributed between regions with large variations in lithospheric structure. Likewise, first-order variations in both vertical and lateral strength are likely to strongly control how the lithosphere responds to enhanced plate-mantle coupling beneath thick continental roots, which for long-wavelength loads and a homogenous elastic lithosphere is a regionally distributed response rather than enhanced local deformation (Chapter IV; Naliboff et al. 2009). Although controversial (e.g. Jackson 2002; Burov & Diamont 2006; Regenauer-Leib *et al.* 2006; Hartz & Podloadchikov 2008; Thatcher & Pollitz 2008; Burgmann and Dresen 2008), more complicated strength profiles can lead to strongly depth-dependent deformation (Pysklewec *et al.* 2002; Beaumont *et al.* 2004; for example), in which case the results from depth-independent models will no longer have any significant meaning.

Although the primary conclusion of this thesis is that depth-independent models of lithospheric stress are not suitable for determining the origins of the lithospheric stress field, it is important to note that counter arguments do exist for coherent deformation through the lithosphere. In particular, observations of seismic anisotropy have been used to argue for vertically coherent deformation through the Australian lithosphere (Simons et al. 2003) and between the crust and mantle in Tibet (Holt 2000; Flesch et al. 2005). These findings for Tibet are seemingly at odds with observations of lower crustal flow (e.g. Royden et al. 1997, Clark and Royden 2000), which suggest that significant

variations in lithospheric strength occur as a function depth. Notably, observations of seismic anisotropy provide no information regarding the magnitude of stress, but rather provide information regarding the alignment of olivine crystal axis, which is inferred to coincide with the orientation of maximum strain. Perhaps a strongly-depth dependent stress field may in fact be compatible with correlations between surface deformation and anisotropy in the lithospheric mantle, or alternatively the seismic anisotropy observations simply reflect rheological processes that are not relevant at tectonic time scales. Future work should focus on regions where high-resolution estimates of lithospheric structure are available.

In particular, the Western United States may serve as an ideal laboratory to test how regional depth-independent stress patterns (e.g. Jones et al. 1996; Flesch et al. 2000) compare with models of 3D lithospheric deformation. Although the crustal structure of the Western US is comparatively well known, recent high-resolution seismic (USArray) and gravity (GRACE) data is likely to significantly improve estimates of both lithospheric thickness (e.g. Li et al. 2007) and strength (e.g. Lowry et al. 1994, 1995, 2000). Thus, future studies of the Western US may provide the unique opportunity to both understand how rheology controls the distribution of stress within the lithosphere and calibrate the relative contribution of lithostatic pressure variations, plate boundary forces and mantle flow to the total lithospheric stress field.

5.1 References

Bott, M.H.P., & Kusznir, N.J, 1979. Stress distributions associated with compensated plateau uplift structures with application to the continental splitting mechanism, *Geophys. J. R. Astr. Soc.*, **56**, 451-459.

Bürgmann, R. & Dresen, G., 2008. Rheology of the lower crust and upper mantle: Evidence from rock mechanics, geodesy and field observations, *Ann. Rev. Earth Plan. Sci.*, **36**, 531-567, doi:10.1146/annurev.earth.36.031207.124326.

Burov, E.B. & Watts, A.B., 2006. The long-term strength of continental lithosphere: "jelly sandwhich" or "creme brulee"?, *GSA Today*, **16**(1), 4-10.

Clark, M. K. & Royden, L. H., 2000. Topographic ooze: Building the eastern margin of Tibet by lower crustal flow, *Geology*, **28**, 703–706.

Flesch, L.M., Holt, E.W, Haines, A.J. & Shen-Tu, B.M., 2000. Dynamics of the Pacific-North American plate boundary in the western United States, *Science*, **287**, 834-836.

Flesch, L.M., Holt, E.W, Silver, P., Stephenson, M., Wang, C.-Y. & Chan, W., 2005. Constraining the extent of crust-mantle coupling in central Asia using GPS, geologic, and shear wave splitting data, *Earth. Planet. Sci. Letts.*, **238**(1-2), 248-268.

Holt, W., 2000. Correlated crust and mantle strain fields in Tibet, *Geology*, **28**(1), 67-70.

Jackson, J., 2002. Strength of the continental lithosphere: Time to abandon the jelly sandwhich?, *GSA Today*, **12**, 1-4.

Jones, C.H., Unruh, J.R., & Sonder, L.J. 1996. The role of gravitational potential energy in active deformation in the southwestern United States, *Nature*, **381**, 37-41.

Kusznir, N.J. & Bott, M.H.P., 1977. Stress concentrations in the upper lithosphere caused by underlying visco- elastic creep, *Tectonophysics*, **43**, 247-256.

Li, X., Yuan, X. & Kind, R., 2007. The lithosphere-asthenosphere boundary beneath the western United States, *Geophys. J. Int.*, **170**(2), 700-710.

Lithgow-Bertelloni, C. & Guynn, J.H., 2004. Origin of the lithospheric stress field, *J. Geophys. Res.*, **109**, B01408, doi:10.1029/2003JB002467.

Liu, M., Shen, Y. & Yang, Y., 2000. Gravitational collapse of orogenic crust: A preliminary three- dimensional finite element study, *J. Geophys. Res.*, **105**(B2), 3159-3173.

Lowry, A.R. & Smith, R.B., 1994. Flexural rigidity of the Basin and Range-Colorado Plateau-Rocky Mountain transition from coherence analysis of gravity and topography, *J. Geophys. Res.*, **99**(B10), 20,123-20,140.

Lowry, A.R. & Smith, R.B., 1995. Strength and rheology of the western U.S. Cordillera, *J. Geophys. Res.*, **100**(B9), 17,947-17,963.

Lowry, A.R., Ribe, N.M. & Smith, R.B. 2000. Dynamic elevation of the Cordillera, western United States, *J. Geophys. Res.*, **105**(B10), 23,371-23,390

Regenauer-Lieb, KL., Weinberg, R. & Rosenbaum, G., 2006. The effect of energy feedbacks on continental strength, *Nature*, **442**, 67-70.

Royden, L.H., Burchfiel, B.C., King, R.W., Wang, E., Chen, Z., Shen, F. & Liu, Y., 1997. Surface Deformation and Lower Crustal Flow in Eastern Tibet, *Science*, **276**, 788-790.

Simons, F.J., van der Hilst, R.D. & Zuber, M.T., 2003. Spatiospectral localization of isostatic coherence anisotropy in Australia and its relation to seismic anisotropy: Implications for lithospheric deformation, *J. Geophys. Res.*, **108**(B5), 2250, doi:10.1029/2001JB000704.

Thatcher, W. & Pollitz, F.F., 2008. Temporal evolution of continental lithospheric strength in actively deforming regions, *GSA Today*, **18**(4/5), 4-11, doi:10.1130/GSAT01804-5A.1

Zoback, M.L., 1992. 1st-Order and 2nd-Order Patterns of Stress in the Lithosphere - The World Stress Map Project, *J. Geophys. Res.*, **97**(B8), 11,703-11,728.

APPENDIX

APPENDIX A

Numerical Method and Validation

The numerical methods used in Chapters II-IV closely follow the methods outlined in Lithgow-Bertelloni & Guynn (2004). The model geometry is defined as a spherical shell, whose thickness (10's – 100's of km) and circumference (~ 40,030 km) matches the geometry of the solid earth's uppermost boundary layer. The spherical shell is discretized into sub-domains (Figure A.1) defined by 8-node equal area elements (Figure A.2), whose length on each side is either 2^o (~ 220 km) or 1^o (~ 110 km). Radially, the shell is divided into two element layers (Figure A.2), where the mechanically strong (Young's modulus - 10^{11} Pa) upper element layer represents the lithosphere and the mechanically weak (Young's modulus – 10^6 Pa) lower element layer acts to prevent the pinned basal nodes from affecting stresses patterns in the upper layer. Although a thin (1 km) element layer is depicted in Figure A.2 between the upper and lower element layers, this layer was not used utilized in this thesis due to expanded element capabilities in the selected finite element solver. The thickness of the lower element layer is fixed at 100 km, while the thickness of the upper layer varies between chapters according to different estimates of lithospheric thickness and structure. Loads are applied directly to the upper element layer (Figure A.2) and all analyzed stress patterns are extracted from this layer.

Throughout the thesis, all results are obtained using continuum shell elements although using continuum elements provides nearly identical solutions. Stress and deformation patterns are calculated using the commercial finite element package ABAQUS (Hibbit & Sorenson 2002). Although Lithgow-Bertelloni & Guynn (2004) performed extensive validation of the numerical setup, we provide further numerical validation here by comparing calculated stress patterns to the analytical solution of a pressure vessel. In the pressure vessel scenario, a uniform radial load is applied to the base an elastic shell, which results in outward expansion of the shell. The resulting stress patterns in the expanded shell are dominated by 'hoop stresses', or stresses acting parallel to the plane of the shell. Inherently, the radial stresses are significantly smaller than the in-plane stresses and decrease linearly from the base of the shell, where the stress is equal to the applied pressure, to the free surface where the radial stress is zero. The in-plane stress magnitudes within the shell are equal to $(P*r)/(2*t)$, where P is the radial basal pressure, r is the spherical radius and t is the shell thickness. For a basal pressure of 10^6 Pa, a radius of 6271000 meters and a shell thickness of 100000 meters, the in-plane stress magnitudes within the pressure vessel are 31.355 MPa. Applying the radial basal pressure of 1 MPa to the base of the upper element layer with a horizontal element resolution of 2^o gives in-plane stress values between 31 and 32 MPa, which closely matches the analytical solution for the pressure vessel.

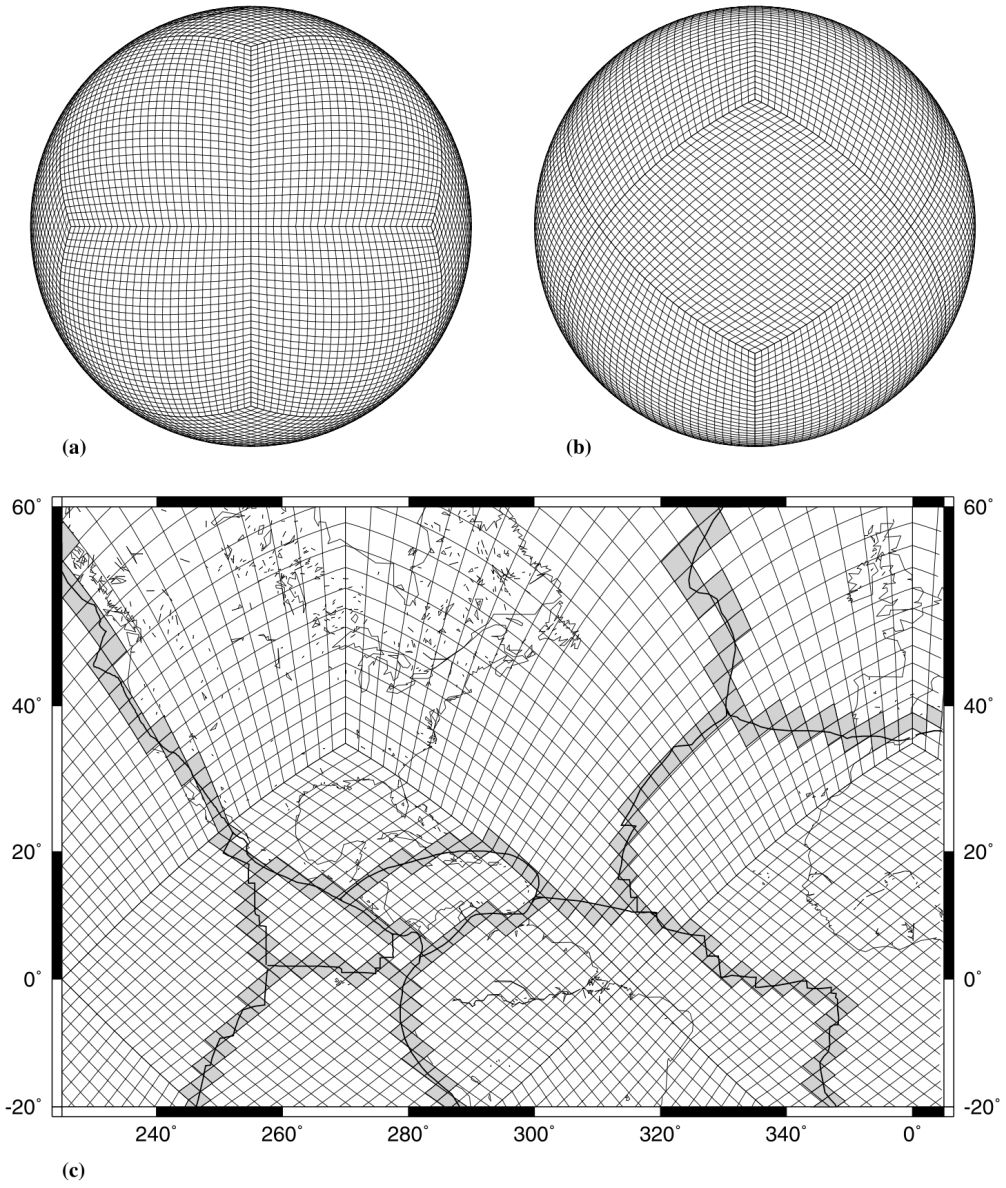

Figure A.1: Illustration of 2^{o}x2^{o} global mesh from Lithgow-Bertelloni & Guynn (2004, Figure 4). Global mesh is shown from the perspective of a polar view (a), intersection of the prime meridian and equator (b) and map view including continents and plate-boundary regions (c).

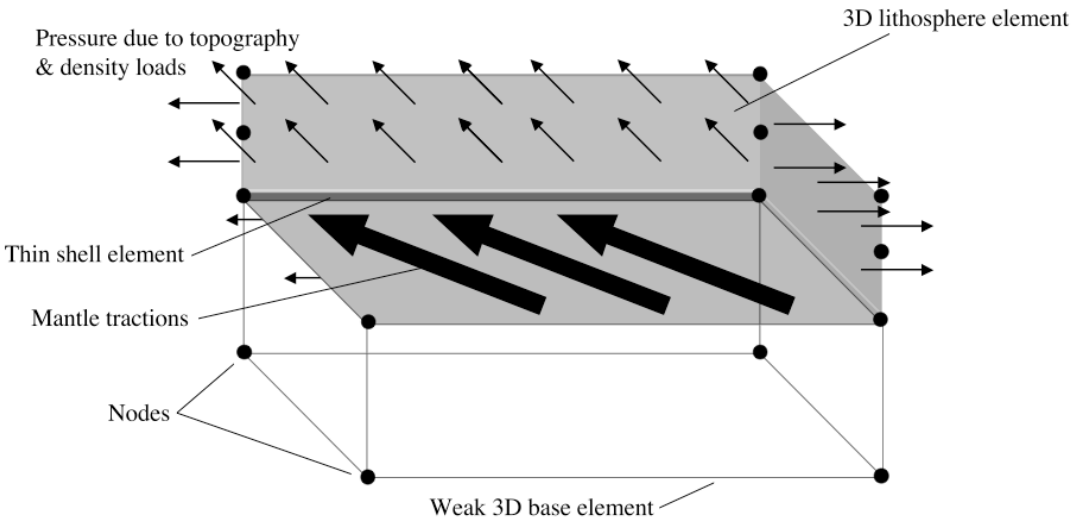

Figure A.2: Illustration of numerical model element geometry and applied loads from Lithgow-Bertelloni & Guynn (2004, Figure 5). Note that in this thesis the middle thin shell element layer is not included as mantle tractions are applied directly to the base of the upper element layer.

A.1 References

Hibbit & Sorenson 2002. ABAQUS, version 6.6, *J. Geophys. Res.*, Pawtucket, R.I.

Lithgow-Bertelloni, C. & Guynn, J.H., 2004. Origin of the lithospheric stress field, *J. Geophys. Res.*, **109**, B01408, doi:10.1029/2003JB002467.